

Published in final edited form as:

J Med Chem. 2010 October 14; 53(19): 6867–6888. doi:10.1021/jm1001748.

Structure-Based Design and Synthesis of Potent, Ethylenediamine-Based, Mammalian Farnesyltransferase Inhibitors as Anticancer Agents

Steven Fletcher^{#,†}, Erin Pusateri Keaney^{#,†}, Christopher G. Cummings[†], Michelle A. Blaskovich[‡], Michael A. Hast[§], Matthew P. Glenn[†], Sung-Youn Chang[†], Cynthia J. Bucher[‡], Ryan J. Floyd[‡], William P. Katt[†], Michael H. Gelb^{||}, Wesley C. Van Voorhis[⊥], Lorena S. Beese[§], Said M. Sebti[‡], and Andrew D. Hamilton^{*,†}

[†]Department of Chemistry, Yale University, 225 Prospect Street, New Haven, Connecticut 06511

[‡]Department of Drug Discovery, H. Lee Moffitt Cancer Center and Research Institute and Department of Molecular Medicine, University of South Florida, Tampa, Florida 33612

[§]Department of Biochemistry, Duke University Medical Center, Box 3711, Durham, North Carolina 27710

^{||}Department of Chemistry and Biochemistry, University of Washington, Seattle, Washington 98195

[⊥]Department of Medicine, University of Washington, Seattle, Washington 98195

Abstract

A potent class of anticancer, human farnesyltransferase (hFTase) inhibitors has been identified by “piggy-backing” on potent, antimalarial inhibitors of *Plasmodium falciparum* farnesyltransferase (PfFTase). On the basis of a 4-fold substituted ethylenediamine scaffold, the inhibitors are structurally simple and readily derivatized, facilitating the extensive structure–activity relationship (SAR) study reported herein. Our most potent inhibitor is compound **1f**, which exhibited an in vitro hFTase IC₅₀ value of 25 nM and a whole cell H-Ras processing IC₅₀ value of 90 nM. Moreover, it is noteworthy that several of our inhibitors proved highly selective for hFTase (up to 333-fold) over the related prenyltransferase enzyme geranylgeranyltransferase-I (GGTase-I). A crystal structure of inhibitor **1a** co-crystallized with farnesyl pyrophosphate (FPP) in the active site of rat FTase illustrates that the *para*-benzonitrile moiety of **1a** is stabilized by a π – π stacking interaction with the Y361 β residue, suggesting a structural explanation for the observed importance of this component of our inhibitors.

Introduction

As the successful treatment of cancer remains a challenging goal, research into novel, selective, and less toxic chemotherapeutic agents is gathering pace.^{1–3} Indeed, increasing understanding of the cellular processes that lead to cancer has identified additional targets for the design of such chemotherapeutics. Ras, the protein product of the *ras* oncogene, is a small GTPase that is important in signal transduction, cell growth, and cell proliferation.⁴ Mutations in Ras, which cause the protein to persistently bind GTP and thus become

constitutively active, can lead to unregulated cell division; such Ras mutants are found in approximately 30% of human tumors.^{5,6} In the 1980s, it was reported that Ras required farnesylation to enhance its hydrophobicity and thereby facilitate its anchorage to the plasma membrane, a process necessary for its signaling function.^{7,8} Accordingly, it was envisioned that inhibition of the enzyme that performs this post-translational modification, protein farnesyltransferase (FTase^a), would offer an indirect method of blocking the function of Ras oncoproteins. Indeed, in addition to inhibiting FTase in vitro,⁹⁻¹² farnesyltransferase inhibitors (FTIs) have demonstrated anti-tumor activity in several animal models.^{2,9} Clinically, however, the results are mixed. For example, a lack of activity was reported when Tipifarnib¹³ (R115777) was used against advanced colorectal and pancreatic cancers.^{14,15} In contrast, extremely encouraging results were observed when Tipifarnib was used against breast cancer in combination with cytotoxic agents.^{16,17} In recent years, it has become clear that aberrant Ras activity is not the only target for FTIs, and it is likely that other FTase substrates, such as Rheb, are also involved in oncogenesis.¹⁸⁻²¹ Nonetheless, despite the now-apparent complexity of this system and the unclear molecular mechanisms by which FTIs operate, the past decade has seen many FTIs established as antiproliferative agents of high efficacy and low toxicity, validating the continued research into more drug-like FTIs as alternative chemotherapeutics for cancer.¹⁻³

The prenyltransferases are a family of zinc metalloenzymes that catalyze the prenylation (addition of a prenyl group through a thioether linkage) of a particular set of proteins, many of which are crucial to signal transduction pathways, causing their localization to the plasma membrane and other cellular compartments and so rendering them biologically active.²² There are three members of the prenyltransferase family: farnesyltransferase (FTase), geranylgeranyltransferase I (GGTase-I), and geranylgeranyltransferase II (GGTase-II). FTase catalyzes the transfer of a farnesyl (C₁₅ isoprenoid) group from the cosubstrate farnesyl pyrophosphate (FPP) to the cysteine residue within the C-terminus Ca₁a₂X tetra-peptide sequence of the target protein (including Ras and Rheb), where C = cysteine, a = an aliphatic amino acid, and X = methionine (M), serine (S), alanine (A), or glutamine (Q).²³ Likewise, GGTase-I catalyzes the corresponding S-geranylgeranylation by accelerating the transfer of the geranylgeranyl group (C₂₀ isoprenoid) from geranylgeranyl pyrophosphate (GGPP) to the cysteine within the C-terminus Ca₁a₂X sequence of the substrate protein (including Rho, Rap, and Ral),²⁴ where this time X is usually leucine (L), isoleucine (I), or phenylalanine (F).²³ It is the identity of the X residue that dictates if a target protein is farnesylated or geranylgeranylated, and is so-called the specificity residue. Finally, in a similar fashion, GGTase-II transfers two geranylgeranyl groups to protein trafficking Rab proteins that contain Cys-Cys or Cys-Ala-Cys sequences at the C-terminus.²³

Previous research within our laboratories has focused on the design of peptidomimetic inhibitors of FTase based on the Ca₁a₂X tetrapeptide substrate.²⁵⁻²⁸ Herein we describe a novel series of ethylenediamine-based, mammalian FTase inhibitors as anticancer compounds that were discovered by a “piggy-back” approach after the success of the core scaffold in a series of antimalarial plasmodial FTase inhibitors.²⁹ We present an extensive structure–activity relationship (SAR) study of these inhibitors with both in vitro and whole cell data, including relative activities against FTase and GGTase-I. Additionally, we discuss our efforts to improve inhibitor potency against mammalian FTase, and we present crystallographic data that reveals the actual binding mode of our inhibitors within the active site of the enzyme.

^aAbbreviations: FTase, farnesyltransferase; hFTase, human FTase; rFTase, rat FTase; PfFTase, *Plasmodium falciparum* FTase; FTI, farnesyltransferase inhibitor; FPP, farnesyl pyrophosphate; GGTase-I, geranylgeranyltransferase-I; IC₅₀, inhibitor concentration that inhibits 50% of enzyme activity; rt, room temperature.

Results and Discussion

Design

We have previously reported on the design and synthesis of inhibitors of *Plasmodium falciparum* farnesyltransferase (*Pf*FTase).^{29,30} An homology model of the active site of *Pf*FTase suggests the presence of four sub-pockets.³¹ By employing the computational modeling program GOLD,³² we identified that an ethylenediamine scaffold with both nitrogens doubly substituted in order to gain simultaneous access to these four subpockets might furnish inhibitors of *Pf*FTase. Indeed, compounds based on this scaffold, including **1a** (Figure 1), in which the choice of the four substituents (*para*-benzonitrile, imidazolylmethyl, arylmethyl, and heterocycle-substituted sulfonyl) was influenced by the BMS series of tetrahydrobenzodiazepine-based³³ and tetrahydroquinoline (THQ)-based³⁴ FTase inhibitors, proved particularly potent inhibitors of *Pf*FTase, both in vitro and in infected erythrocytes.^{29,30} Although *Pf*FTase is significantly larger than rat FTase (rFTase) in both the α - (472 vs 379 residues) and β -subunits (923 vs 437 residues), the differences are mainly due to insertions in the *Pf*FTase protein sequence, and overall there is minimal difference in the residues that form the active site.^{29,31} Of the sequence segments in the model of *Pf*FTase, there is 23% identity (53% similarity) for the α -subunit between *Pf*FTase and rFTase isoforms and 37% (56%) for the β -subunit. Therefore, we anticipated that our *Pf*FTase inhibitors may also inhibit mammalian FTase, binding in the same sub-domains but, in certain instances, to differing active site residues (i.e., *Pf*FTase³¹ \rightarrow rFTase (PDB ID: 1JCR³⁵): S150 \rightarrow N165 α , F151 \rightarrow Y166 α , N317 \rightarrow H201 α), providing a route to inhibitor selectivity for the mammalian isoform of the enzyme.

Specifically, as with an almost identical analogue of **1a** in the homology model of the active site of *Pf*FTase (Figure 2 in ref ^{29b}), we hypothesized that the more basic of the two imidazoles, the 1-methyl-1*H*-imidazol-5-ylmethyl substituent of **1a**, would bind the zinc ion (itself held in place by D297 β (D659), C661 β (C299), and H362 β (H838), where the labels in parentheses represent the corresponding residues in *Pf*FTase³¹). In addition, we envisioned that the *para*-benzonitrile moiety would bind in the mostly hydrophobic pocket constructed from the tetramethylene portion of the side chain of K164 α (K149) and Y166 α (F151) and whose deepest point forms a hydrophilic domain (H201 α (N317) and N165 α (S150)). We considered that the benzyl moiety would bind in the hydrophobic pocket comprising W102 β (W452), W106 β (W456), and Y361 β (Y837), and finally that the sulfonylimidazole would bind in the hydrophilic domain formed by R202 β (R564) and three water molecules participating in a hydrogen-bonded network between S99 β (S449) and Q167 α (Q152).

To maintain consistency with the GOLD docking experiments of our ethylenediamine-based inhibitors in the homology model of the active site of *Pf*FTase,^{29,30} the only constraint imposed in the flexible ligand GOLD docking with compound **1a** in the active site of rFTase (PDB ID: 1JCR) was that the more basic, non-sulfonylated imidazole should again bind the Zn²⁺ ion. Due to the flexible nature of the ethylenediamine scaffold in **1a**, we did not want to bias the docking results any further and used no additional constraints. Moreover, despite the similarities of the pendant groups in **1a** and the former clinical candidate (*R*)-7-cyano-2,3,4,5-tetrahydro-1-(1*H*-imidazol-4-ylmethyl)-3-(phenylmethyl)-4-(2-thienylsulfonyl)-1*H*-1,4-benzodiazepine (BMS-214662, **2**³³), we elected not to use the knowledge of the crystal structure of **2**³⁶ given its more rigid tetrahydrobenzodiazepine scaffold. As was anticipated owing to the similarities in the active sites of *Pf*FTase and rFTase, several low energy GOLD docked poses of compound **1a** in rFTase demonstrated an almost identical binding mode to that observed with a very close analogue of **1a** in *Pf*FTase, with the biggest difference being that the benzyl group, rather than binding in the W102 β , W106 β , Y361 β sub-pocket, is engaged in a π - π stacking interaction with Y361 β (compare

Figure 2 in ref ^{29b} with Figure **1a** above). Figure 1A illustrates one such high scoring (low energy) docked pose of compound **1a** in green and colored by atom type, using the graphical representation (Connolly analytical surface, PyMOL³⁷) and orientation employed in previous publications.^{29,30} The binding surface of rFTase shown incorporates the cosubstrate farnesyl pyrophosphate (FPP: farnesyl, red; pyrophosphate, blue). This binding mode of **1a** overlays well with the tetrapeptide inhibitor CVFM from the rFTase crystal structure as shown in Figure 1B, in which we have used an alternative graphical representation (“cartoon”, PyMOL³⁷) and orientation that have also been presented by us recently.³⁸ For simplicity, the latter graphical representation shall be used throughout the remainder of this manuscript. Given the highly flexible nature of the ligand, coupled with the fact that the other high scoring poses from our studies (data not shown) were generally those in which the scaffold projected functionalities to positions similar to those seen in Figure 1, we feel that it is likely that the molecule, in solution, would occupy pockets as previously predicted as part of an ensemble of binding motifs.

Initially, we selected a focused set of our *Pj*FTase inhibitors and analyzed their abilities to inhibit human FTase (hFTase), as well as GGTase-I, both in vitro and in whole cells (Table 1). The amino acid sequences of rat and human FTase are 95% identical with complete sequence and structural conservation around the active site,³⁵ so it is reasonable to analyze inhibition of hFTase with respect to docking studies in rFTase. Briefly, in vitro inhibition assays for hFTase and GGTase-I were carried out by measuring the incorporation of [³H]FPP and [³H]GGPP into recombinant H-Ras-CVLS and H-Ras-CVLL, respectively, as described previously.³⁹ Whole cell inhibition of farnesylation and geranylgeranylation were determined based on the level of inhibition by synthetic compounds of H-Ras and Rap1A processing, respectively.⁴⁰ In all cases, IC₅₀ data represent the average of three independent assays (*n* = 3), unless otherwise stated, and errors are given as standard deviations. The importance of both the *para*-substitution of the aniline component and *N*^π-methylation (R¹ = Me) of the imidazole that we observed in the inhibition of *Pj*FTase²⁹ was reflected in the mammalian isoform of the enzyme. Unsubstituted aniline **3** exhibited little activity toward the inhibition of hFTase. Incorporation of bromine into the *para* position of the aniline ring, however, led to an order of magnitude increase in potency with in vitro IC₅₀s for hFTase improving from 6300 ± 360 nM for **3** to 730 ± 20 nM for **4**. Additionally, H-Ras processing IC₅₀s of the FTIs were enhanced from > 10 μM to 5.7 ± 1.2 μM. A further order of magnitude increase in FTase inhibition in vitro was achieved upon *N*^π-methylation of the imidazole, with **5** exhibiting an IC₅₀ of 79 ± 30 nM, and an associated increase in whole cell activity (H-Ras processing IC₅₀ = 1.6 ± 1.3 μM) was also observed. Even greater hFTase inhibitory activity was achieved by the replacement of bromine with cyano in the *para* position of the aniline ring (**1a**: IC₅₀ = 56 ± 29 nM). It is interesting to note that a considerable improvement in selectivity for hFTase over GGTase-I was also observed; **1a** was approximately 7-fold more selective for hFTase than was **5**. In addition, the trends observed here in the inhibition of the mammalian isoform of FTase are mirrored by those observed in the disruption of the plasmodial isoform.²⁹ Given these very encouraging data, we embarked on an SAR study of our ethylenediamine-based inhibitors in order to optimize the inhibitory activity of **1a** against hFTase.

Crystal Structure

We recently reported the crystal structure of the **1a**:FPP:rFTase ternary complex (Figure 2A; PDB ID: 3E32).³⁸ As a comparison, in Figure 2B we have superimposed the crystal structure of **1a** with that of the tetrapeptide substrate CVFM (PDB ID: 1JCR). Interestingly, the crystal structure shows that the ethylenediamine-based FTIs actually adopt a different binding mode to that predicted (Figure 1B). Figure 2A illustrates that the *para*-benzonitrile substituent of **1a** is oriented toward the product exit groove and is partially stabilized by a

stacking interaction with Y361 β . The rings are approximately 30° offset from parallel, with the distance between them ranging from 3.8 to 4.9 Å. The binding pocket also consists of F360 β (not shown in Figure), Y93 β , L96 β , and W106 β , creating a generally hydrophobic environment for this moiety. Inhibitor **1a** possesses two *N*-methylimidazole groups: one coordinates the catalytic zinc ion (2.0 Å distance) through its nonmethylated τ -nitrogen in place of the Ca₁a₂X box cysteine residue, while the second (at the sulfonamide position) is stacked between the first *N*-methylimidazole (3.7 Å distance) and the first isoprene of FPP (4.1 Å distance). The non-methylated τ -nitrogen of the 1-methyl-1*H*-imidazole-4-sulfonyl group also makes a single, weak polar contact (3.7 Å distance) to the side chain hydroxyl of Y361 β . The phenyl substituent of **1a** binds in a pocket formed by W106 β , W102 β , and L96 β , essentially the a₂ residue binding site of the Ca₁a₂X substrate, and occupying almost exactly the same space as the phenylalanine side chain of CVFM (Figure 2B).

Several similarities exist between the chemical substituents and binding mode of the ethylenediamine inhibitor **1a** with tetrahydrobenzodiazepine **2**; their crystal structures are overlaid in Figure 3. The binding modes of the *para*-benzonitrile group and the non-sulfonylated *N*-methylimidazole group of the ethylenediamine inhibitor **1a** are nearly indistinguishable from the similar substituents in **2**, with the imidazole of **2** coordinating the catalytic zinc ion like the non-sulfonylated *N*-methylimidazole in **1a**. The scaffold nitrogen atoms bearing these substituents in both **1a** and **2** occupy similar locations. The *para*-benzonitrile groups extend into the exit groove, with the positions of the cyano group nitrogen atoms from the two molecules differing by only ~0.4 Å, a value close to the estimated error in crystallo-graphic coordinates. Finally, the phenyl substituents of both compounds take advantage of the aromatic character of the Ca₁a₂Xa₂ residue site, interacting with tryptophan residues 102 β and 106 β . The sulfonamide positions of both compounds exhibit the greatest differences in binding modes. As a consequence, the scaffold nitrogen bearing this group in the tetrahydrobenzodiazepine ring of **2** is not oriented in a spatially similar location to the nitrogen bearing the sulfonylated *N*-methylimidazole of **1a**, which is sandwiched between the first isoprene of the lipid substrate and the zinc-coordinating *N*-methylimidazole moiety. By contrast, the thienyl group of **2** is largely solvent-exposed and binds in a manner resembling the a₁ residue of the Ca₁a₂X motif. This ring is primarily stabilized by stacking on the tetrahydrobenzodiazepine ring scaffold itself, as opposed to interacting with the enzyme active site or lipid substrate.

The crystal structure of the ternary complex of **1a**:FPP: rFTase was solved toward the end of this research; the medicinal chemistry research program reported herein was actually driven by piggy-backing on our inhibitors of *Pf*FTase and, to a lesser extent, the GOLD docking result presented in Figure 1. At the end of the SAR discussion, the FTase inhibition data will be evaluated in the context of both this crystal structure and the GOLD docking models.

Chemistry

“Piggy-back” mammalian FTase inhibitors (FTIs) were prepared as described previously,²⁹ with new FTIs furnished by synthetic routes depicted in Schemes 1–3. Inhibitors incorporating the *para*-benzonitrile moiety were accessed by the route in Scheme 1. Briefly, mono-*N*-Bocethylenediamine (**6**) was arylated with *para*-fluorobenzonitrile at 120 °C for 48 h in DMSO, affording secondary aniline **7**.^{29b} Installation of the imidazole was achieved by double deprotonation of **7** with LDA at –78 °C and subsequent chemo-selective alkylation with 5-chloromethyl-1-methyl-1*H*-imidazole 3 HCl,^{29b} affording **8**^{29b} in a moderate yield. After Boc deprotection, completion of the syntheses of FTase inhibitors **1** was conducted in one of two ways: either sulfonylation of **9**^{29b} followed by alkylation of the resultant sulfonamide, or reductive amination of **9**, and then sulfonylation of the resultant secondary amine. Finally, purification of the FTIs was achieved by silica gel flash column

chromatography, followed by rpHPLC. Full details can be found in the Experimental Section.

Sulfonyl R² SAR

With R¹ constrained as methyl and R³ as benzyl, a series of eight R² sulfonyl groups was surveyed (Table 2), all of which proved potent inhibitors of hFTase. The largest and most basic 5-dimethylamino-naphthalene-1-sulfonyl derivative **1h** was the least active inhibitor (hFTase IC₅₀ = 160 ± 110 nM) of this series, with the most potent being the pyridine-2-sulfonyl compound **1f** (hFTase IC₅₀ = 25 ± 20 nM). Additionally, these inhibitors were more selective for hFTase over GGTase-I, with selectivities ranging from around 8-fold to 333-fold. Many of these compounds also demonstrated very good whole cell activity, with pyridine-2-sulfonyl derivative **1f** proving one of the most effective inhibitors (H-Ras processing IC₅₀ = 0.09 ± 0.06 μM). Despite its potency in vitro (hFTase: IC₅₀ = 56 ± 29 nM), 1-methyl-1*H*-imidazole-4-sulfonyl derivative **1a** had the poorest H-Ras processing IC₅₀ (1.9 ± 1.2 μM). This might be a consequence of the basicity of imidazole, and its protonation could hinder cellular entry. Regardless of this, the potent in vitro activity of **1a** against hFTase, coupled with the fact that we already had several inhibitors functionalized with the 1-methyl-1*H*-imidazole-4-sulfonyl group in-house from the related *Pj*FTase project,²⁹ led us to retain this particular sulfonyl group as a benchmark while varying other parts of the molecule. Selectivity of these FTIs for the hFTase isoform over the *Pj*FTase isoform might then later be achieved by taking advantage of the previously mentioned three amino acid differences in the subpocket that is predicted to bind the *para*-benzotrile ring.

Sulfonamide R³ SAR

Thus, constraining R² as 1-methyl-1*H*-imidazole-4-sulfonyl, the R³ group was next investigated with a broad series of derivatives, which included previously reported²⁹ and novel inhibitors (Table 3). Replacement of benzyl in the parent inhibitor **1a** with a propargyl group (**1aa**) led to a reduction in both in vitro activity (IC₅₀ = 720 ± 200 nM cf. 56 ± 29 nM) and whole cell activity, as well as in GGTase-I/FTase selectivity. However, the unsubstituted allyl derivative (**1ab**) was tolerated in vitro (IC₅₀ = 54 ± 30 nM), although not in whole cells (H-Ras processing IC₅₀ > 10 μM). Substitution of the allyl moiety with a methyl group at position-2 (**1ac**) led to a reduction in hFTase in vitro activity and, at the same time, afforded an improvement in GGTase-I, resulting in a reduced GGTase-I/FTase selectivity of about 5-fold. Again, whole cell activity was poor but this was recovered somewhat by replacement of the methyl in **1ac** with a bromine atom, giving an H-Ras processing IC₅₀ of 5.7 ± 1.5 μM for inhibitor **1ad**. Extension of this *sp*²-hybridized series to the bulky *tert*-butylacetamido derivative **1ae** was not tolerated, neither in vitro nor in whole cells. Incorporation of nitrogen into the *para* position of benzyl to give pyridine derivative **1af** maintained activity in vitro (IC₅₀ = 72 ± 20 nM), although it showed little activity in whole cells. Nonetheless, **1af** exhibited substantially improved selectivity toward hFTase, with a GGTase-I/FTase selectivity of > 139-fold.

We next examined a focused set of five-membered heteroaromatics **1ag–1an**. Pyrrole **1ag** was around twice as active as the parent inhibitor **1a**, disrupting hFTase with an IC₅₀ value of 30 ± 33 nM. Conversely, the series of furans and thiophenes typically proved much poorer inhibitors, although interestingly FTase inhibitory activity was found to be sensitive to heteroatom position. Furan **1ah** was more than twice as potent as isomeric **1aj**, and thiophene **1ai** was more than 34 times as potent as isomeric **1ak** and approximately as active as **1a**. Despite these moderate to poor in vitro data for hFTase (except for **1ai**) all members of this series exhibited reasonable H-Ras processing whole cell data and in all cases the IC₅₀ values were more potent than **1a**. The remaining heteroaromatics (**1al–1an**) containing two heteroatoms were poor inhibitors of hFTase.

Introduction of a methyl group on the benzyl ring of **1a** was tolerated in the *ortho* (**1ao**) and *meta* (**1ap**) positions (in vitro hFTase IC₅₀s of 51 ± 26 nM and 54 ± 30 nM, respectively) but not in the *para* (**1aq**) position (IC₅₀ = 370 ± 210 nM). A similar trend was observed in whole cell activity, with *meta*-derivative **1ap** the most potent (H-Ras processing IC₅₀ = 0.3 ± 0.2 μM). The members of this series demonstrated GGTase-I IC₅₀ values between 580 and 780 nM, considerably reducing the GGTase-I/hFTase selectivities, relative to that of the parent benzyl inhibitor **1a**. The greater potency of meta-substituted benzyl groups over their *para* counterparts was also observed for the cyano derivatives **1ar** and **1as** and for the phenyl derivatives **1at** and **1au**, a finding that was reflected in their corresponding H-Ras processing whole cell activities. Additionally, the same trend was noticed in the in vitro data of GGTase-I inhibition. The poor in vitro inhibition of hFTase by *para*-phenyl derivative **1au** (IC₅₀ = 1700 ± 900 nM) was improved by approximately 4-fold by replacement of the terminal phenyl group with the smaller pyrrole heterocycle (**1av**; IC₅₀ = 390 ± 210 nM), which was also reflected in the whole cell assays (IC₅₀ = 5 ± 1 μM (**1au**) vs 4 ± 1 μM (**1av**)).

The small cyclopropylmethyl derivative **1aw** was less active than the parent benzyl inhibitor **1a**, but the larger cyclohexylmethyl derivative **1ax**, a closer match to benzyl, proved a potent inhibitor in vitro (hFTase IC₅₀ = 60 ± 10 nM) and was one of our most potent inhibitors in whole cells (H-Ras processing IC₅₀ = 0.1 ± 0.07 μM). However, inhibitor **1ax** was also quite active toward GGTase-I (IC₅₀ = 530 ± 120 nM), giving a much-reduced hFTase/GGTase-I selectivity of about 9-fold. We envisaged probing deeper into the binding pocket that was predicted to bind the R³ group by modifying the cyclohexylmethyl substituent to a 4-piperidinylmethyl group; the piperidine nitrogen provided a handle from which to achieve further functionalization. Accordingly, *N*-Boc-piperidin-4-ylmethyl derivative **1ay** and *N*-(2-pyrimidinyl)-4-ylmethyl derivative **1az** were synthesized. Introduction of the *N*-Boc group at the 4 position of the cyclohexyl group (**1ay**) caused more than a 60-fold drop in hFTase inhibition relative to **1ax**. Activity was recovered by more than 7-fold through replacement of the bulky *tert*-butoxycarbonyl group with the planar 2-pyrimidinyl group (**1az**; IC₅₀ = 510 ± 62 nM; cf. **1ay**: IC₅₀ = 3700 ± 790 nM) although both piperidinylmethyl derivatives exhibited poor whole cell activities.

Aniline R⁴ SAR: The *para*-Position (X)

At the deepest point of the predominantly hydrophobic pocket of rFTase in which GOLD docking studies consistently predicted the *para*-benzotrile moiety (the aniline “R⁴ group”) of our inhibitors would bind, there is a hydrophilic domain formed by N165 α , Y166 α , and H201 α . To probe this site further, we replaced the cyano group (X) of the *para*-benzotrile moiety with alternative polar groups, such as a carboxylic acid or a carboxamide, in the anticipation that such groups might be able to participate in additional hydrogen-bonding interactions and so furnish more potent hFTase inhibitors. We also investigated nonpolar substituents in the *para* position, such as Br, Ph and CO₂*t*-Bu, which, provided the aniline group binds as predicted, would be expected to inhibit hFTase less well. Accordingly, *para*-(*tert*-butyl ester) derivative **11** was prepared in a similar manner to the synthetic route in Scheme 1 but employing *tert*-butyl *para*-fluorobenzoate in place of *para*-fluorobenzotrile (see Experimental Section for full details). As shown in Scheme 2, treatment of **11** with TFA furnished the *para*-carboxylic acid **12**, which was then converted to *para*-carboxamide **13** using HBTU and ammonium chloride. *para*-Phenyl derivative **14** was prepared from the previously reported intermediate 1-*tert*-butoxycarbonylamino-2-[biphenyl-4-yl-(3-methyl-3*H*-imidazol-4-ylmethyl)amino]-ethane (compound **9a** in ref ^{29b}; see Experimental Section for full details). As illustrated in Table 4, all replacements for the cyano group afforded compounds that were poorer inhibitors of hFTase in vitro. Interestingly, FTIs with bulky X groups (**11**: X = CO₂*t*-Bu; **14**: X = Ph) exhibited a reversed selectivity for GGTase-

I over hFTase, suggesting the aniline-binding domain may be larger in GGTase-I than in hFTase.

Aniline R⁴ SAR: The Aromatic Ring

In addition to the *para*-substituent of the aniline affecting inhibitor activity, GOLD docking studies suggested that two of the polar amino acids within the *para*-benzotrile-binding pocket might influence binding of the aniline ring itself. Specifically, Y166 α could make contact with hydrogen bonding acceptor or donor groups in the *ortho* and *meta* positions of the aniline to improve inhibitor binding in mammalian FTase, and likewise, H201 α might be exploited with an appropriate group in the *meta* position. Accordingly, a series of FTase inhibitors was prepared in which the *para*-benzotrile portion was modified in an attempt to target these two amino acids; the synthetic route that was pursued is shown in Scheme 3. We selected compound **1az** bearing the *N*-(2-pyrimidinyl)-piperidin-4-ylmethyl R³ group as the benchmark, anticipating that its moderate activity would better highlight the effects of modifying the *para*-benzotrile component. Again, with the only constraint being that the non-methylated τ -nitrogen of the 1-methyl-1*H*-imidazol-5-ylmethyl group should bind the active site Zn²⁺ ion, several GOLD docking experiments of compound **1az** were performed. While the R³ = *N*-(2-pyrimidinyl)-piperidin-4-ylmethyl and the 1-methyl-1*H*-imidazole-4-sulfonyl groups in **1az** bound differently to the corresponding groups in **1a**, the R⁴ = *para*-benzotrile group under investigation bound in the same subpocket (tetramethylene side chain of K164 α and side chain of Y166 α) as the corresponding motif in **1a** in four out of the five highest scoring (lowest energy) docking solutions (for example, Figure 4A). Furthermore, in most of those cases, the *para*-benzotrile moieties of **1a** and **1az** overlaid excellently, as illustrated in Figure 4B. Thus, we were confident the SAR data that would be acquired by varying the R⁴ aniline component of **1az** would be directly translatable to **1a** and related inhibitors.

As depicted in Scheme 3, mono-*N*-Boc-ethylenediamine (**6**) was sulfonylated with 1-methyl-1*H*-imidazole-4-sulfonyl chloride to give **15** in 95% yield. Chemoselective alkylation of the more acidic and less hindered sulfonamide NH was then readily accomplished by treatment of **15** with *N*-(2-pyrimidinyl)-piperidin-4-ylmethyl bromide in the presence of cesium carbonate in DMF. After TFA-mediated Boc deprotection of **16**, arylation of the resultant primary amine was achieved by heating **17** at 120 °C in DMSO with a series of aryl fluorides, giving the secondary anilines **18** in a range of yields from 48 to 97%. Finally, these secondary anilines were then smoothly alkylated in good to excellent yields by deprotonation with NaH in DMF, followed by reaction with 5-chloromethyl-1-methyl-1*H*-imidazole · HCl^{29b} to furnish the FTase inhibitors **19a–19h** (Table 5).

Positioning a chlorine (**19a**) at the *ortho* position had little effect relative to the parent compound **1az** on the inhibition of hFTase. Conversely, replacement of an *ortho*-CH unit with nitrogen to give pyridine **19c** conferred approximately 4-fold improvement in hFTase enzymatic inhibitory activity (**19c** 110 ± 26 nM vs **1az** 510 ± 320 nM), while *meta*-substituted pyridine **19b** offered no enhancement in activity, suggesting an important role for a hydrogen-bonding acceptor group in the *ortho* position. However, incorporation of nitrogens at both *ortho* positions, as in pyrimidine **19d**, caused a reduction in the IC₅₀ value back to approximately the same as that exhibited by the parent compound **1az**. Inhibitor **19e** with a fluorine at one of the *meta* positions was around twice as potent as **1az**, while a fluorine at the *ortho* position led to an especially potent inhibitor (**19f**) with an hFTase IC₅₀ of 64 ± 8.6 nM, approximately 8-fold as active as **1az** and twice as potent as the *ortho*-pyridine **19c**. Introduction of a second fluorine atom at the other *ortho* position (inhibitor **19g**) caused a reduction in inhibition potency relative to the singly *ortho*-substituted inhibitor **19f**, as was observed with the pyridine derivatives **19c** and **19d** (pyrimidine), respectively. Replacement of all four ring hydrogens in **19h** offered no benefit to hFTase

inhibition, relative to parent **1az**. Finally, it is noteworthy that all derivatives based on the parent compound **1az** generally exhibited very good to excellent selectivity for inhibition of hFTase over GGTase-I, particularly for *ortho*-pyridine **19c** and *ortho*-fluoride **19f**.

Scaffold Optimization

After optimizing the R¹, R², R³, R⁴, and X groups, we next investigated modifying the ethylenediamine core with a variety of alternative diamino-based scaffolds, whose structures are depicted in Table 6 and whose syntheses have been described elsewhere.³⁰ 1,3-Diaminopropane-based inhibitor **20a** has increased conformational flexibility relative to the corresponding ethylenediamine-based inhibitor **1a**. The data in Table 6 suggest that increasing the flexibility in this way caused more than a 7-fold drop in hFTase inhibitory activity. Likewise, reducing the conformational flexibility of the scaffold with the 1,2- and 1,3-diaminocyclopentyl derivatives **20b–20e** also led to a decrease in hFTase inhibitor potency, with the *cis*-configurations exhibiting half the potencies of their *trans*-counterparts. Similar trends were observed in *Pf*FTase.³⁰ Of all the different scaffolds examined, the ethylenediamine unit was found to be optimal at delivering the four substituents into the proposed subpockets as well as furnishing the greatest GGTase-I/hFTase selectivity.

Optimization of FTIs

Finally, we designed three ethylenediamine-based inhibitors incorporating optimized R¹, R², R³, R⁴, and X substituents that were identified from our SAR studies, as illustrated by compounds **21a–21c** in Table 7. Primary data considered in the selection of moieties that we hoped would furnish optimized inhibitors were in vitro FTase inhibition, whole cell H-Ras processing data, and to a lesser extent, GGTase-I/hFTase selectivity. The R¹ group selected was methyl (Table 1), R² was 2-pyridinesulfonyl (Table 2), R³ was cyclohexylmethyl (Table 3), R⁴ was *para*-benzointrile (Table 4) substituted at the *ortho* position (Table 5), and the core scaffold incorporated was the simple ethylenediamine unit (Table 6), leading to inhibitors **21a**, **21b**, and **21c** in Table 7. As a comparison, we have also included in Table 7 three of our most potent “unoptimized” FTIs: **1a**, **1ax**, and **1f**. The trend observed in Table 5 upon varying the *ortho*-CH unit to CF and to N was reproduced with these optimized inhibitors, however none of compounds **21a–21c** exhibited improved activity over the leads **1a**, **1ax**, and **1f**, possibly due to the adoption of different binding geometries. Much reduced selectivities for hFTase over GGTase-I were also observed. Nonetheless, **21b** was equipotent with **1ax** in whole cells, whereby both inhibitors disrupted H-Ras processing with IC₅₀ values of about 90 nM.

Discussion of SAR Data in the Context of the Crystal Structure of **1a** and the GOLD

Docking of **1a**

Figure 5 shows the crystal structure of **1a** (yellow; taken from Figure 2A) overlaid with the flexible ligand GOLD docking of **1a** (green; taken from Figure 1B). We correctly predicted that the more basic imidazole 1-methyl-1*H*-imidazol-5-ylmethyl would bind the zinc ion (which was the only constraint implemented in the GOLD docking experiments), and GOLD subsequently correctly placed the benzyl moiety of **1a** in very close proximity to the subpocket formed by W102 β , W106 β , and Y361 β . However, as Figure 5 illustrates, the *para*-benzointrile and the sulfonylimidazole substituents were found to bind in different manners to those predicted. Specifically, the *para*-benzointrile moiety was predicted to bind in the subpocket created by K164 α , N165 α , H201 α , Y166 α , but was actually found engaged in a weak π - π interaction with Y361 β in the product exit groove, F360 β , Y93 β , L96 β , W106 β , while the sulfonylimidazole group was predicted to bind the Arg202 β , yet was found stacked between the Zn-binding imidazole and the first isoprene of FPP.

Despite the GOLD prediction of a very different binding mode for the *para*-benzotrile moiety, several potent inhibitors (e.g., **19f**, Table 5) were serendipitously identified as a consequence of the *para*-benzotrile making alternative but still significant contacts. The observed π - π stacking of the *para*-benzotrile moiety against the Y361 β residue suggests an explanation for the observed in vitro SAR data for the modifications made to the *para*-benzotrile ring of **1a** (Tables 1 and Table 4) and **1az** (Table 5). π - π Stacking interactions are known to be energetically more favorable between an electron-rich arene, here Y361 β , and an electron-poor arene, here the *para*-benzotrile of inhibitor **1a**. For the series of inhibitors in Table 4, substitution of the *para* position of the aniline with a strongly electron-withdrawing cyano group led to the most potent inhibitor (**1a**) while eliminating all substitution from the aniline ring of **1a** and with R¹ = H essentially abolished activity (compound **2**, Table 1). Additionally, the product exit groove where the *para*-benzotrile binds is of limited size and mostly hydro-phobic, suggesting that substituents larger than the linear cyano unit, such as the bulky *tert*-butyl ester in **11** or the phenyl ring in **14**, and more polar than the cyano group, such as the acid in **12** and the carboxamide in **13**, would be poorly tolerated. This was confirmed experimentally (Table 4). For the series of inhibitors in Table 5, replacement of the *ortho* (with respect to the aniline nitrogen) CH (**1az**) with either N (**19c**) or CF (**19f**) led to an approximate 5-fold or 8-fold improvement in inhibitor activity, respectively. This may be due to the introduced electron-withdrawing groups that render the aniline even more electron-poor, thereby enhancing its interaction with Y361 β . On the other hand, replacement of the *meta*-CH (**1az**) with N (**19b**) resulted in no improvement in activity, while substitution of the *meta*-CH with a CF group (**19e**) led to only a 2-fold increase in inhibitor potency, as opposed to the 8-fold enhancement achieved by *ortho*-fluoride **19f**. The crystal structure of **1a** suggests that the incorporation of electronegative groups in the *meta* position might be poorly tolerated due to a clash with the anionic side chain of D359 β , explaining the reduced enhancement in potency of inhibitors **19b** and **19e** (as a means of avoiding this unfavorable interaction, 180° rotation about the N-C aniline bond would direct the introduced N or CF group into a hydrophobic domain comprising L96 β , W102 β and W106 β and would therefore also be unfavorable). Replacement of both *ortho*-CH groups with either two nitrogens (**19d**) or two CF groups (**19g**) was not tolerated relative to the mono-*ortho*-substituted inhibitors (**19b** and **19e**, respectively). This observation may be a consequence of one of the electronegative groups being forced into the hydrophobic L96 β , W102 β and W106 β region in order that the energetically favorable π - π stacking between the aniline ring of the inhibitor and Y361 β is maintained.

Generally, there was little variation in activity among the R² sulfonyl derivatives shown in Table 2, which may be a consequence of this moiety exhibiting insignificant interactions with the protein itself, being found stacked between the zinc-binding imidazole and FPP. However, there were clear trends in the hFTase inhibition data for the R³ series of sulfonamide analogues (Table 3). The crystal structure of **1a** illustrates that the R³ phenyl ring can access the a₂ residue binding site (L96 β , W102 β and W106 β) of the Ca₁a₂X substrate. For the most part, small, hydrophobic R³ groups afforded potent hFTase inhibitors, likely due to the R³ group making van der Waals contacts with L96 β , W102 β and/or W106 β . Within a particular series of R³ substituents, for example the *ortho*-, *meta*-, and *para*-tolyl derivatives **1ao**, **1ap**, and **1aq**, respectively, *ortho*- and *meta*-functionalized compounds were tolerated, whereas *para*-functionalization was not. This may be a consequence of the *para* derivative being too large to access the a₂ residue binding site. Indeed, the crystal structure of **1ay** shows that the large *N*-Bocpiperidin-4-ylmethyl group traverses, rather than binds in, the a₂ residue binding site and instead reaches into the X residue binding site.³⁸ We have previously reported on the relative selectivities of our ethylenediamine-based inhibitors for the *Plasmodium* isoform of FTase over the mammalian isoform.^{29,30} With this crystal structure data in hand, along with several others,³⁸ it should

now be possible to tailor these compounds to become more selective for one enzyme isoform over the other.

Conclusions

In summary, we have developed a potent series of mammalian farnesyltransferase inhibitors (FTIs) based on an ethylenediamine scaffold. This class of compounds was identified by a “piggy-back” approach on our potent antimalarial inhibitors of plasmodium FTase. The simple and cost-effective ethylenediamine core allowed facile access to a diverse array of inhibitors, greatly facilitating lead inhibitor optimization. We have identified several inhibitors with double-digit nano-molar inhibition of hFTase in vitro, the most potent compound being **1f** ($IC_{50} = 25$ nM). In most cases, potent inhibition of hFTase in vitro was accompanied by potent whole cell data (inhibition of H-Ras processing); for example, inhibitor **1f** displayed a whole cell IC_{50} of 90 nM, one of the most active of the entire series. Moreover, in all but two cases inhibitors were selective for hFTase over GGTase-I, with the greatest selectivity (333-fold) exhibited by inhibitor **1g**. Finally, we have solved the crystal structure of one of our ethylenediamine-based FTIs (**1a**) in the active site of rFTase, and this will assist in the future design of more potent and isoform-selective mammalian farnesyltransferase inhibitors.

Experimental Section

Ligand Docking Studies

Ligand energy minimization was performed with the CVFF force field in InsightII on an SGI O2. Flexible ligand docking studies were subsequently performed with GOLD, version 3.0,³² on a Linux PC. Default GOLD parameters were utilized with the following exceptions: (i) maximal ligand flexibility was allowed; (ii) the affinity of nitrogen for zinc ion was increased in the GOLD parameters file to better reflect the ability of an imidazole ring to bind to the active site metal ion. Each ligand was used to seed the genetic algorithm 10 times.

Chemistry: General Methods

Solvents CH_2Cl_2 , CH_3CN , and DMF were dried on an Innovative Technology SPS-400 dry solvent system. Anhydrous MeOH and DMSO were purchased from Sigma-Aldrich and used directly from their Sure-Seal bottles. Molecular sieves were activated by heating to 300 °C under vacuum overnight. All reactions were performed under an atmosphere of dry nitrogen in oven-dried glassware and were monitored for completeness by thin-layer chromatography (TLC) using silica gel (visualized by UV light, or developed by treatment with $KMnO_4$ stain or Hanessian's stain). 1H and ^{13}C NMR spectra were recorded on Bruker AM 400 MHz and Bruker AM 500 MHz spectrometers in either $CDCl_3$, $MeOH-d_4$, or $DMSO-d_6$. Chemical shifts (δ) are reported in parts per million after calibration to residual isotopic solvent. Coupling constants (J) are reported in Hz. Mass spectrometry was performed using electrospray ionization on either a Varian MATCH-5 (HRMS) or Waters Micromass ZQ (LRMS). Before biological testing, all new target molecules (**1b**, **1c**, **1ah–1an**, **1aw**, **11–14**, **19a–19h**, **21a–21c**) were subjected to further purification by reversed-phase HPLC (rpHPLC). Analysis and purification by rpHPLC were performed using either a Phenomenex Luna 5 μm C18 (2) 250 mm \times 21 mm column run at 15 mL/min (preparative) or a Microsorb-MV 300 A C18 250 mm \times 4.6 mm column run at 1 mL/min (analytical), using gradient mixtures of (A) water with 0.1% TFA and (B) 10:1 acetonitrile/water with 0.1% TFA. Appropriate product fractions were pooled and lyophilized to dryness, affording the inhibitors as fluffy, white powders as their TFA salts. Inhibitor purity was confirmed by analytical rpHPLC using linear gradients from 100% A to 100% B, with changing solvent

composition of either (I) 4.5% or (II) 1.5% per min after an initial 2 min of 100% A. For reporting HPLC data, percentage purity is given in parentheses after the retention time for each condition. FTase inhibitors **1a**, **1d–1h**, **1aa–1ag**, **1ao–1av**, **1ax–1az**, **3–5**, and **20a–20e** have been previously reported in ref ^{29b}.

General Procedure A (Reaction of Amines with Sulfonyl Chlorides)

The appropriate sulfonyl chloride (1.2 equiv) was added to a solution of the amine (1 equiv) and DIPEA (2 equiv) in anhydrous CH₃CN (0.1 M) at 0 °C. The reaction was warmed to room temperature and stirred for 16 h, at which time the solvent was evaporated. The residue was redissolved in CH₂Cl₂, washed with 5% NaHCO₃, water, brine, dried (Na₂SO₄), filtered, and concentrated.

General Procedure B (Alkylation of Sulfonamides)

To a solution of the sulfonamide (1 equiv) and Cs₂CO₃ (2 equiv) in DMF (0.1 M) at 0 °C was added the appropriate alkyl bromide or chloride (1.1 equiv). The resulting mixture was stirred at room temperature overnight. The reaction was diluted with water, then extracted into EtOAc (×3). The combined EtOAc extractions were washed with 5% NaHCO₃ (×3), brine, dried (Na₂SO₄), filtered, and concentrated.

General Procedure C (Reductive Amination of Primary Amines)

To a solution of **9** (1 equiv) in dry methanol (0.2 M) with 4 Å molecular sieves was added the appropriate aldehyde (1.1 equiv) and acetic acid (1.3 equiv). The reaction was stirred under nitrogen at room temperature for 30 min. Sodium cyanoborohydride (1.5 equiv) was added, and the resulting suspension was stirred at room temperature overnight. The reaction mixture was decanted, washing thoroughly with further MeOH, and then dry-loaded onto silica gel.

General Procedure D (Arylation of Primary Amines)

To a stirring solution of the primary amine (1 equiv) in DMSO (0.2 M) were added the aryl fluoride (1.2 equiv) and DIPEA (3 equiv). The reaction mixture was heated to 120 °C for 48 h. After allowing the reaction to cool, H₂O was added, and the crude product was extracted with EtOAc (×3). The EtOAc extractions were combined, washed with water (×3), brine, dried (Na₂SO₄), filtered, and concentrated.

General Procedure E (Alkylation of Secondary Anilines)

The secondary aniline (1 equiv) was dissolved in DMF (0.07 M), and then the reaction was cooled to 0 °C. After 15 min, NaH (3 equiv) was added in one portion. After a further 15 min, 5-chloromethyl-1-methyl-1*H*-imidazole-3 HCl³¹ (1.1 equiv) was added. The reaction was allowed to stir at 0 °C from 2–3 h, when TLC indicated the reaction was complete or had stalled. Upon quenching the reaction with brine (approximately 1 mL for 1 mmol scale), the reaction was diluted with water and extracted with EtOAc (×3). The EtOAc extractions were combined, and washed with 5% NaHCO₃ (×3), brine, dried (Na₂SO₄), filtered, and concentrated.

General Procedure F (Cyanation of Aryl Bromides)

A stirring solution of the aryl bromide (1 equiv) in DMF (0.1 M) was degassed, and then Zn(CN)₂ (0.6 equiv), Pd(PPh₃)₄ (0.1 equiv), Zn dust (0.05 equiv), and Zn(OAc)₂ (0.05 equiv) were added. The mixture was heated to 120 °C for 2 h, after which time the reaction was allowed to cool, diluted with water, and extracted into EtOAc (×3). The EtOAc extractions were combined and washed with 5% NaHCO₃ (×3), brine, dried (Na₂SO₄), filtered, and concentrated.

4-[(2-Aminoethyl)-(3-methyl-3H-imidazol-4-ylmethyl)-amino]-benzotrile (9)

To a solution of 4-[(2-*N*-*tert*-butoxycarbonyl)-aminoethyl)-(3-methyl-3*H*-imidazol-4-ylmethyl)-amino]-benzotrile (compound **9c** in ref ^{29b}) (8.0 g, 30.6 mmol) in CH₂Cl₂ (75mL) cooled to 0 °C was added TFA (75mL). The reaction was warmed to room temperature and stirred for 30 min, after which time the solvent was concentrated *in vacuo*, and then the crude material was repeatedly re-dissolved in CHCl₃ and re-evaporated until a constant weight was achieved, to afford the ditrifluoroacetic acid salt of **9** as a light-brown solid (14.8 g, 100%): δ_{H} (500 MHz, MeOH-*d*₄) 3.20(t, *J* = 7.1 Hz, 2H, CH₂CH₂NH₂), 3.81 (t, *J* = 7.1 Hz, 2H, CH₂CH₂NH₂), 3.87 (s, 3H, CH₃ (Im)), 4.82 (s, 2H, CH₂Im), 6.96 (d, *J* = 9.0 Hz, 2H, 2 CH(Ar)), 7.19 (s, 1H, CH (Im)), 7.56 (d, *J* = 9.0 Hz, 2H, 2 CH (Ar)), 8.88 (s, 1H, CH (Im)); δ_{C} (125 MHz, MeOH-*d*₄) 33.9, 37.1, 45.3, 48.2, 100.8, 114.0, 118.4, 120.4, 132.3, 134.6, 137.5, 151.0; HRMS (ESI) *m/z* calcd for [C₁₄H₁₇N₅ + H] 256.1562, obsd 256.1559. Subsequently, the free base form of **9**, which is the form used for all subsequent reactions, was furnished by passing the di-TFA salt through a short pad of silica gel (eluent CH₂Cl₂/MeOH/NH₄OH, 92:7:1).

N-Benzyl, *N*-{2-[(4-Cyanophenyl)-(3-methyl-3H-imidazol-4-ylmethyl)-amino]-ethyl} Propane-1-sulfonamide (1b)

Compound **9** was treated with propane-1-sulfonyl chloride, according to general procedure A, on a 0.15 mmol scale. The crude material was purified by silica gel flash column chromatography (eluent CH₂Cl₂/MeOH/NH₄OH, 92:7:1) to give *N*-{2-[(4-cyanophenyl)-(3-methyl-3*H*-imidazol-4-ylmethyl)-amino]-ethyl} propane-1-sulfonamide as a colorless film (46 mg, 85%): δ_{H} (500 MHz, MeOH-*d*₄) 0.98 (t, *J* = 7.5 Hz, 3H, CH₂CH₂CH₃), 1.71 (sextet, *J* = 7.5 Hz, 2H, CH₂CH₂CH₃), 2.96 (m, 2H, NHCH₂CH₂N), 3.21–3.26 (m, 2H, CH₂CH₂CH₃), 3.61 (t, *J* = 6.5 Hz, 2H, NHCH₂CH₂N), 3.84 (s, 3H, CH₃ (Im)), 4.79 (s, 2H, CH₂Im), 6.91 (d, *J* = 9.1 Hz, 2H, 2CH (Ar)), 7.20 (s, 1H, CH (Im)), 7.47 (d, *J* = 9.1 Hz, 2H, 2 CH (Ar)), 8.82 (s, 1H, CH (Im)); δ_{C} (125 MHz, MeOH-*d*₄) 11.7, 16.9, 32.8, 39.7, 44.4, 50.6, 53.2, 98.9, 112.6, 117.7, 119.4, 131.5, 133.3, 136.2, 150.4; LRMS (ESI) *m/z* 384.2 [C₁₇H₂₃N₅O₂S+Na]. Subsequently, the sulfonamide (36 mg, 0.1 mmol) was treated with benzyl bromide according to general procedure B. After the usual workup and flash chromatography over silica gel (eluent CH₂Cl₂/MeOH/NH₄OH, 192:7:1), the title compound **1b** was furnished as a glassy film (37 mg, 82%): δ_{H} (400 MHz, MeOH-*d*₄) 1.20(t, *J* = 7.4 Hz, 3H, CH₂CH₂CH₃), 1.99 (m, 2H, CH₂CH₂CH₃), 3.24 (t, *J* = 7.8 Hz, 2H, N(Bn)CH₂CH₂N), 3.40 (obscured, 4H, NHCH₂CH₂N, CH₂CH₂CH₃), 3.94 (s, 3H, CH₃ (Im)), 4.52 (s, 2H, CH₂Ph), 4.65 (s, 2H, CH₂Im), 6.75 (d, *J* = 8.9 Hz, 2H, 2 CH (Ar)), 7.25 (s, 1H, CH (Im)), 7.55 (m, 7H, 5 CH (Ph), 2 CH (Ar)), 9.00 (s, 1H, CH (Im)); δ_{C} (125 MHz, MeOH-*d*₄) 13.7, 18.6, 34.6, 45.4, 46.8, 51.6, 53.4, 55.1, 100.3, 114.1, 119.6, 121.2, 129.8, 130.7, 133.1, 135.1, 138.2, 138.7, 151.9, 152.9; HRMS (ESI) *m/z* calcd for [C₂₄H₂₉N₅O₂S + H] 452.2120, obsd 452.2108; HPLC (I) *t*_R = 13.45 min (100%), (II) *t*_R = 19.72 min (100%).

N-Benzyl, *N*-{2-[(4-Cyanophenyl)-(3-methyl-3H-imidazol-4-ylmethyl)-amino]-ethyl} Cyclopropanesulfonamide (1c)

First, amine **9** was reacted with cyclopropanesulfonyl chloride, according to general procedure A, on a 0.15 mmol scale. After workup and flash column chromatography (eluent CH₂Cl₂/MeOH/NH₄OH, 92:7:1), *N*-{2-[(4-cyanophenyl)-(3-methyl-3*H*-imidazol-4-ylmethyl)-amino]-ethyl} cyclopropanesulfonamide was yielded as a colorless film (44 mg, 82%): δ_{H} (500 MHz, MeOH-*d*₄) 0.98 (m, 4H, 2 CH₂ (cyclopropyl)), 2.51 (m, 1H, CH (cyclopropyl)), 3.33 (t, *J* = 5.8 Hz, 2H, NHCH₂CH₂N), 3.67 (t, *J* = 5.8 Hz, 2H, NHCH₂CH₂N), 3.88 (s, 3H, CH₃ (Im)), 4.76 (s, 2H, CH₂Im), 6.95 (d, *J* = 8.83 Hz, 2H, 2 CH (Ar)), 7.25 (s, 1H, CH (Im)), 7.53 (d, *J* = 8.84 Hz, 2H, 2CH (Ar)), 8.86 (s, 1H, CH (Im)); δ_{C} (125 MHz, MeOH-*d*₄) 4.1, 29.0, 32.8, 39.9, 44.5, 50.5, 99.1, 112.7, 117.8, 119.4, 131.6,

133.4, 136.3, 150.4; LRMS (ESI) m/z 382.1 [C₁₇H₂₁N₅O₂S + Na]. Subsequently, the sulfonamide (36 mg, 0.1 mmol) was treated with benzyl bromide, according to general procedure B. The crude material was dry-loaded onto silica gel and purified by flash column chromatography (eluent CH₂Cl₂/MeOH/NH₄OH, 192:7:1) to give **1c** as a white foam (40 mg, 89%): δ_{H} (500 MHz, MeOH-*d*₄) 0.95 (m, 4H, 2 CH₂ (cyclopropyl)), 2.55 (m, 1H, CH (cyclopropyl)), 3.31 (m, 4H, NCH₂CH₂N), 3.71 (s, 3H, CH₃ (Im)), 4.32 (s, 2H, CH₂Ph), 4.43 (s, 2H, CH₂Im), 6.51 (d, $J = 8.89$ Hz, 2H, 2 CH (Ar)), 7.02 (s, 1H, CH (Im)), 7.26–7.33 (m, 7H, 5 CH (Ph), 2 CH (Ar)), 8.76 (s, 1H, CH (Im)); δ_{C} (125 MHz, MeOH-*d*₄) 5.3, 28.1, 34.3, 45.1, 46.3, 51.1, 54.9, 100.3, 113.7, 119.1, 120.8, 129.4, 129.9, 130.3, 132.7, 134.7, 137.8, 138.2, 151.5; HRMS (ESI) m/z calcd for [C₂₄H₂₇N₅O₂S + H] 450.1964, obsd 450.1985; HPLC (I) $t_{\text{R}} = 12.70$ min (100%), (II) $t_{\text{R}} = 18.99$ min (100%).

[*N*-(Furan-3-ylmethyl), *N*-{2-[(4-Cyanophenyl)-(3-methyl-3*H*-imidazol-4-ylmethyl)-amino]-ethyl}] 1-Methyl-1*H*-imidazole-4-sulfonamide (1ah**, 4.38)**

Furan-3-carbaldehyde was reductively aminated with amine **9** according to general procedure C, on a 0.15 mmol scale. Purification by flash column chromatography (eluent CH₂Cl₂/MeOH/NH₄OH, 92:7:1) then gave 4-[[2-[(furan-3-ylmethyl)-amino]-ethyl]-[3-methyl-3*H*-imidazol-4-ylmethyl)-amino]-benzotrile as a film (39 mg, 78%): δ_{H} (400 MHz, MeOH-*d*₄) 3.24 (obscured t, 2H, NHCH₂CH₂N), 3.78 (m, 5H, NHCH₂CH₂N, CH₃ (Im)), 4.07 (s, 2H, CH₂-furan), 4.75 (s, 2H, CH₂Im), 6.50 (s, 1H, CH (furan)), 6.88 (d, $J = 9.0$ Hz, 2H, 2 CH (benzotrile)), 7.11 (s, 1H, CH (furan)), 7.42–7.53 (m, 3H, 2 CH (benzotrile), CH (Im)), 7.62 (s, 1H, CH (furan)), 8.82 (s, 1H, CH (Im)); δ_{C} (100 MHz, MeOH-*d*₄) 34.5, 43.5, 44.7, 45.9, 47.7, 101.7, 111.9, 114.5, 117.3, 119.0, 120.8, 132.9, 135.2, 138.2, 145.1, 146.0, 151.5; LRMS (ESI) m/z 358.2 [C₁₉H₂₁N₅O + Na]. This secondary amine (34 mg, 0.1 mmol) was reacted with 1-methyl-1*H*-imidazole-4-sulfonyl chloride according to general procedure A to yield the title compound **1ah** as a white foam (43 mg, 90%): δ_{H} (500 MHz, MeOH-*d*₄) 3.38 (obscured t, 2H, ((furan-3-ylmethyl)-NHCH₂CH₂N)), 3.56 (t, $J = 7.0$ Hz, 2H, ((furan-3-ylmethyl)-NHCH₂CH₂N)), 3.81 (s, 3H, CH₃ (Im)), 3.89 (s, 3H, CH₃ (Im)), 4.19 (s, 2H, CH₂-furan), 4.70 (s, 2H, CH₂Im), 6.57 (s, 1H, CH (furan)), 6.77 (d, $J = 8.94$ Hz, 2H, 2 CH (benzotrile)), 7.25 (s, 1H, CH (furan)), 7.46–7.52 (m, 4H, 2 CH (benzotrile), 2 CH (Im)), 7.78 (s, 1H, CH (furan)), 7.81 (s, 1H, CH (Im)), 8.91 (s, 1H, CH (Im)); δ_{C} (125 MHz, MeOH-*d*₄) 34.3, 34.4, 45.3, 45.5, 45.9, 51.0, 100.4, 111.9, 113.8, 119.3, 120.8, 122.0, 126.8, 132.9, 134.8, 137.9, 139.1, 141.5, 143.2, 145.3, 151.7; HRMS (ESI) m/z calcd for [C₂₃H₂₅N₇O₃S + H] 480.1818, obsd 480.1809; HPLC (I) $t_{\text{R}} = 12.62$ min (100%).

[*N*-(Thiophen-3-ylmethyl), *N*-{2-[(4-Cyanophenyl)-(3-methyl-3*H*-imidazol-4-ylmethyl)-amino]-ethyl}] 1-Methyl-1*H*-imidazole-4-sulfonamide (1ai**, 4.39)**

Thiophene-3-carbaldehyde was reductively aminated with amine **9** (38 mg, 0.15 mmol) according to general procedure C to give, after flash column chromatography (eluent CH₂Cl₂/MeOH/NH₄OH, 92:7:1), 4-((3-methyl-3*H*-imidazol-4-ylmethyl)-{2-[(thiophen-3-ylmethyl)-amino]-ethyl)-amino)-benzotrile as a glassy film (40 mg, 76%): δ_{H} (400 MHz, MeOH-*d*₄) 3.20 (obscured t, 2H, NHCH₂CH₂N), 3.70–3.75 (m, 5H, NHCH₂CH₂N, CH₃ (Im)), 4.16 (s, 2H, CH₂-thiophene), 4.69 (s, 2H, CH₂Im), 6.74 (d, $J = 9.0$ Hz, 2H, 2 CH (benzotrile)), 7.06 (s, 1H, CH (Im)), 7.09 (d, $J = 3.9$ Hz, 1H, CH (thiophene)), 7.41–7.48 (m, 4H, 2CH (benzotrile), 2 CH (thiophene)), 8.77 (s, 1H, CH (Im)); δ_{C} (100 MHz, MeOH-*d*₄) 34.7, 45.0, 46.1, 47.4, 47.9, 102.0, 114.7, 119.2, 120.9, 129.0, 129.1, 129.5, 133.1, 133.2, 135.4, 138.4, 151.6; LRMS (ESI) m/z 374.2 [C₁₉H₂₁N₅S + Na]. This secondary amine (35 mg, 0.1 mmol) was then reacted with 1-methyl-1*H*-imidazole-4-sulfonyl chloride according to general procedure A to give, after purification by silica gel flash column chromatography (eluent CH₂Cl₂/MeOH/NH₄OH, 192:7:1), compound **1ai** as a white foam (46 mg, 93%): δ_{H} (400 MHz, MeOH-*d*₄) 3.29 (obscured t, 2H, ((thiophen-3-ylmethyl)NCH₂CH₂N)), 3.39 (t, $J = 6.9$ Hz, 2H, ((thiophen-3-ylmethyl)NCH₂CH₂N)), 3.69

(s, 3H, CH₃ (Im)), 3.75 (s, 3H, CH₃ (Im)), 4.20 (s, 2H, 2 CH (CH₂-thiophene)), 4.50 (s, 2H, CH₂Im), 6.57 (d, *J* = 9.1 Hz, 2H, 2 CH (benzonitrile)), 6.95 (d, *J* = 3.8 Hz, 1H, CH (thiophene)), 7.09 (s, 1H, CH (thiophene)), 7.22 (s, 1H, CH (Im)), 7.31 (m, 1H, CH (thiophene)), 7.36 (d, *J* = 9.1 Hz, 2H, 2 CH (benzonitrile)), 7.65 (s, 1H, CH (Im)), 7.70 (s, 1H, CH (Im)), 8.79 (s, 1H, CH (Im)); δ_C (125 MHz, MeOH-*d*₄) 34.7, 34.8, 45.5, 46.7, 50.3, 51.5, 100.7, 114.1, 119.6, 121.2, 126.2, 127.2, 128.3, 129.7, 133.2, 135.2, 138.2, 139.0, 139.5, 141.9, 152.0; HRMS (ESI) *m/z* calcd for [C₂₃H₂₅N₇O₂S₂ + H] 496.1589, obsd 496.1576; HPLC (I) *t*_R = 12.64 min (99.0%), (II) *t*_R = 18.84 min (98.2%).

[*N*-(Furan-2-ylmethyl), *N*-{2-[(4-Cyanophenyl)-(3-methyl-3*H*-imidazol-4-ylmethyl)-amino]-ethyl}] 1-Methyl-1*H*-imidazole-4-sulfonamide (1aj, 4.41)

Furan-2-carbaldehyde was reductively aminated with amine **9** according to general procedure C, on a 0.15 mmol scale. Purification by silica gel flash column chromatography (eluent CH₂Cl₂/MeOH/NH₄OH, 92:7:1) afforded 4-[[2-[(furan-2-ylmethyl)-amino]-ethyl]-(3-methyl-3*H*-imidazol-4-ylmethyl)-amino]-benzonitrile as a film (39 mg, 78%): δ_H (500 MHz, MeOH-*d*₄) 3.31 (obscured t, 2H, NHCH₂CH₂N), 3.84 (t, *J* = 7.4 Hz, 2H, NHCH₂CH₂N), 3.87 (s, 3H, CH₃ (Im)), 4.33 (s, 2H, CH₂-furan), 4.81 (s, 2H, CH₂Im), 6.48 (m, 1H, CH (furan)), 6.61 (d, *J* = 3.19 Hz, 1H, CH (furan)), 6.95 (d, *J* = 8.9 Hz, 2H, 2 CH (benzonitrile)), 7.18 (s, 1H, CH (Im)), 7.54 (d, *J* = 8.9 Hz, 2H, 2 CH (benzonitrile)), 7.60 (m, 1H, CH (furan)), 8.88 (s, 1H, CH (Im)); δ_C (125 MHz, MeOH-*d*₄) 32.8, 43.0, 43.1, 44.2, 46.0, 100.1, 110.7, 112.4, 113.0, 117.4, 119.0, 131.2, 133.5, 136.5, 144.5, 144.8, 149.7; LRMS (ESI) *m/z* 358.2 [C₁₉H₂₁N₅O + Na]. This secondary amine was reacted with 1-methyl-1*H*-imidazole-4-sulfonyl chloride according to general procedure A, on a 0.1 mmol scale. After workup, the crude material was purified by silica gel flash column chromatography (eluent CH₂Cl₂/MeOH/NH₄OH, 192:7:1) to furnish the title compound **1aj** as a white foam (43 mg, 90% 47.91818): δ_H (500 MHz, MeOH-*d*₄) 3.34 (t, *J* = 6.9 Hz, 2H, ((furan-3-ylmethyl)NCH₂CH₂N)), 3.46 (t, *J* = 6.9 Hz, 2H, ((furan-3-ylmethyl)NCH₂CH₂N)), 3.67 (s, 3H, CH₃ (Im)), 3.79 (s, 3H, CH₃ (Im)), 4.23 (s, 2H, CH₂-furan), 4.63 (s, 2H, CH₂Im), 6.18 (m, 1H, CH (furan)), 6.23 (m, 1H, CH (furan)), 6.73 (d, *J* = 9.1 Hz, 2H, 2 CH (benzonitrile)), 7.15 (s, 1H, CH (Im)), 7.29 (s, 1H, CH (furan)), 7.41 (d, *J* = 9.1 Hz, 2H, 2 CH (benzonitrile)), 7.59 (s, 1H, CH (Im)), 7.64 (s, 1H, CH (Im)), 8.79 (s, 1H, CH (Im)); δ_C (125 MHz, MeOH-*d*₄) 34.3, 45.4, 46.5, 47.1, 49.6 (obscured), 50.8, 100.4, 111.3, 111.7, 113.9, 119.3, 120.9, 126.8, 132.9, 134.8, 137.8, 139.1, 141.4, 144.4, 150.9, 151.8; HRMS (ESI) *m/z* calcd for [C₂₃H₂₅N₇O₃S + H] 480.1818, obsd 480.1833; HPLC (I) *t*_R = 12.51 min (100%).

[*N*-(Thiophen-2-ylmethyl), *N*-{2-[(4-Cyanophenyl)-(3-methyl-3*H*-imidazol-4-ylmethyl)-amino]-ethyl}] 1-Methyl-1*H*-imidazole-4-sulfonamide (1ak, 4.42)

Thiophene-2-carbaldehyde was reductively aminated with amine **9** (38 mg, 0.15 mmol) according to general procedure C, giving, after flash column chromatography (eluent CH₂Cl₂/MeOH/NH₄OH, 92:7:1), 4-((3-methyl-3*H*-imidazol-4-ylmethyl)-{2-[(thiophen-2-ylmethyl)-amino]-ethyl}-amino)-benzonitrile as a colorless film (38 mg, 72%): δ_H (500 MHz, MeOH-*d*₄) 3.37 (obscured t, 2H, NHCH₂CH₂N), 3.8–3.92 (m, 5H, NHCH₂CH₂N, CH₃ (Im)), 4.54 (s, 2H, CH₂-thiophene), 4.86 (s, 2H, CH₂Im), 6.87 (m, 1H, CH (thiophene)), 7.00 (d, *J* = 8.8 Hz, 2H, 2 CH (benzonitrile)), 7.13 (m, 1H, CH (thiophene)), 7.23 (s, 1H, CH (Im)), 7.34 (m, 1H, CH (thiophene)), 7.59 (d, *J* = 8.8 Hz, 2H, 2 CH (benzonitrile)), 8.93 (s, 1H, CH (Im)); δ_C (125 MHz, MeOH-*d*₄) 32.8, 42.9, 44.2, 45.0, 45.9, 100.2, 113.0, 117.4, 119.0, 127.3, 128.2, 130.6, 131.2, 131.5, 133.5, 136.6, 149.7; LRMS (ESI) *m/z* 374.2 [C₁₉H₂₁N₅S + Na]. This secondary amine (35 mg, 0.1 mmol) was reacted with 1-methyl-1*H*-imidazole-4-sulfonyl chloride according to general procedure A. The usual workup and purification by flash column chromatography (eluent CH₂Cl₂/MeOH/NH₄OH, 192:7:1) gave **1ak** as a glassy film (44 mg, 89%): δ_H (400 MHz, MeOH-*d*₄) 3.31 (t,

$J = 7.1$ Hz, 2H, ((thiophen-2-yl)NCH₂-CH₂N)), 3.47 (t, $J = 7.1$ Hz, 2H, ((thiophen-2-yl)NCH₂CH₂N)), 3.69 (s, 3H, CH₃ (Im)), 3.75 (s, 3H, CH₃ (Im)), 4.41 (s, 2H, CH₂-thiophene), 4.55 (s, 2H, CH₂Im), 6.61 (d, $J = 9.0$ Hz, 2H, 2 CH (benzonitrile)), 6.85 (m, 1H, CH (thiophene)), 6.89 (d, $J = 2.70$ Hz, 1H), 7.11 (s, 1H, CH (Im)), 7.29 (m, 1H, CH (thiophene)), 7.37 (d, $J = 9.0$ Hz, 2H, 2 CH (benzonitrile)), 7.67 (s, 1H, CH (Im)), 7.69 (s, 1H, CH (Im)), 8.78 (s, 1H, CH (Im)); δ_C (100 MHz, MeOH-*d*₄) 34.7, 34.8, 45.7, 46.6, 50.3 (obscured), 51.0, 100.9, 114.2, 119.6, 121.2, 126.5, 127.2, 128.5, 130.0, 133.2, 135.2, 138.2, 139.5, 140.7, 141.9, 152.0; HRMS (ESI) m/z calcd for [C₂₃H₂₅N₇O₂S₂ + H] 496.1589, obsd 496.1585; HPLC (I) $t_R = 12.90$ min (100%).

[*N*-(3,5-Dimethyl-isoxazol-4-ylmethyl), *N*-{2-[(4-Cyanophenyl)(3-methyl-3*H*-imidazol-4-ylmethyl)-amino]-ethyl}] 1-Methyl-1*H*-imidazole-4-sulfonamide (1a), 4.36)

Amine 9 was reacted with 1-methyl-1*H*-imidazole-4-sulfonyl chloride according to general procedure A, on a 0.15 mmol scale. Flash column chromatography of the crude material over silica gel (eluent CH₂Cl₂/MeOH/ NH₄OH, 92:7:1) afforded 1-methyl-1*H*-imidazole-4-sulfonic acid {2-[(4-cyano-phenyl)-(3-methyl-3*H*-imidazol-4-ylmethyl)-amino]-ethyl}-amide as a white powder (55 mg, 92%): δ_H (400 MHz, MeOH-*d*₄) 3.19 (t, $J = 6.3$ Hz, 2H, NHCH₂CH₂N), 3.64 (t, $J = 6.3$ Hz, 2H, NHCH₂CH₂N), 3.72 (s, 3H, CH₃ (Im)), 3.88 (s, 3H, CH₃ (Im)), 4.81 (s, 2H, CH₂Im), 6.89 (d, $J = 9.0$ Hz, 2H, 2 CH (benzonitrile)), 7.22 (s, 1H, CH (Im)), 7.50 (d, $J = 9.0$ Hz, 2H, 2 CH (benzonitrile)), 7.62 (s, 1H, CH (Im)), 7.71 (s, 1H, CH (Im)), 8.87 (s, 1H, CH (Im)); δ_C (100 MHz, MeOH-*d*₄) 33.8, 33.9, 40.7, 45.4, 50.9, 99.5, 113.5, 118.5, 120.5, 125.3, 132.3, 134.2, 137.2, 139.9, 140.7, 151.2; HRMS (ESI) m/z calcd for [C₁₈H₂₁N₇O₂S + H] 400.1556, obsd 400.1545. This secondary sulfonamide was then alkylated with 4-chloromethyl-3,5-dimethyl-isoxazole according to general procedure B, on a 0.1 mmol scale. After workup, purification was accomplished by silica gel flash column chromatography (eluent CH₂Cl₂/MeOH/NH₄OH, 192:7:1) to furnish the title compound 1a as a white foam (40 mg, 79%): δ_H (500 MHz, MeOH-*d*₄) 2.15 (s, 3H, CH₃ (isoxazole)), 2.20 (s, 3H, CH₃ (isoxazole)), 3.23 (t, $J = 6.7$ Hz, 2H, ((isoxazol-4-ylmethyl)NCH₂-CH₂N)), 3.53 (t, $J = 6.7$ Hz, 2H, ((isoxazol-4-ylmethyl)NCH₂-CH₂N)), 3.77 (s, 3H, CH₃ (Im)), 3.82 (s, 3H, CH₃ (Im)), 4.02 (s, 2H, CH₂-isoxazole), 4.56 (s, 2H, CH₂Im), 6.66 (d, $J = 8.7$ Hz, 2H, 2 CH (benzonitrile)), 7.17 (s, 1H, CH (Im)), 7.45 (d, $J = 8.7$ Hz, 2H, 2 CH (benzonitrile)), 7.74 (s, 1H, CH (Im)), 7.78 (s, 1H, CH (Im)), 8.85 (s, 1H, CH (Im)); δ_C (125 MHz, MeOH-*d*₄) 10.2, 10.9, 34.3, 34.4, 44.4, 45.0, 47.0, 51.2, 100.6, 110.7, 113.7, 119.3, 120.8, 127.1, 132.6, 134.9, 137.9, 138.2, 141.7, 151.4, 161.6, 169.6; HRMS (ESI) m/z calcd for [C₂₄H₂₈N₈O₃S H] 509.2083, obsd 509.2072; HPLC (I) $t_R = 12.27$ min (100%), (II) $t_R = 17.76$ min (100%).

[*N*-(2,4-Dimethyl-thiazol-5-ylmethyl), *N*-{2-[(4-Cyanophenyl)-(3-methyl-3*H*-imidazol-4-ylmethyl)-amino]-ethyl}] 1-Methyl-1*H*-imidazole-4-sulfonamide (1am), 4.40)

2,4-Dimethyl-thiazole-5-carbaldehyde was reductively aminated with amine 9 (38 mg, 0.15 mmol) according to general procedure C to give, after flash column chromatography (eluent CH₂Cl₂/MeOH/NH₄OH, 92:7:1), 4-[[2-[(2,4-dimethyl-thiazol-5-ylmethyl)-amino]-ethyl]- (3-methyl-3*H*-imidazol-4-ylmethyl)-amino]-benzonitrile as a glassy film (42 mg, 74%): δ_H (500 MHz, MeOH-*d*₄) 2.34 (s, 3H, CH₃ (thiazole)), 2.60 (s, 3H, CH₃ (thiazole)), 3.32 (t, $J = 7.06$ Hz, 2H, NHCH₂CH₂N), 3.83 (m, 5H, NHCH₂CH₂N, CH₃ (Im)), 4.39 (s, 2H, CH₂-thiazole), 4.78 (s, 2H, CH₂Im), 6.92 (d, $J = 9.0$ Hz, 2H, 2 CH (benzonitrile)), 7.14 (s, 1H, CH (Im)), 7.51 (d, $J = 9.0$ Hz, 2H, 2 CH (benzonitrile)), 8.85 (s, 1H, CH (Im)); LRMS (ESI) m/z 403.2 [C₂₀H₂₄N₆S + Na]. The secondary amine (38 mg, 0.1 mmol) was then treated with 1-methyl-1*H*-imidazole-4-sulfonyl chloride according to general procedure A. Workup and purification (flash column chromatography (eluent CH₂Cl₂/MeOH/NH₄OH, 192:7:1)) as usual yielded 1am as a white foam (47 mg, 90%): δ_H (500 MHz, MeOH-*d*₄) 2.21 (s, 3H, CH₃ (thiazole)), 2.55 (s, 3H, CH₃ (thiazole)), 3.39 (t, $J = 6.5$ Hz, 2H, ((thiazol-5-ylmethyl)-NCH₂CH₂N)), 3.64 (t, $J = 6.5$ Hz, 2H, ((thiazol-5-ylmethyl)-NCH₂CH₂N)), 3.77 (s, 3H,

CH₃ (Im)), 3.86 (s, 3H, CH₃ (Im)), 4.38 (s, 2H, CH₂-thiazole), 4.73 (s, 2H, CH₂Im), 6.71 (d, *J* = 9.1 Hz, 2H, 2 CH (benzonitrile)), 7.20 (s, 1H, CH (Im)), 7.46 (d, *J* = 9.1 Hz, 2H, 2 CH (benzonitrile)), 7.76 (s, 1H, CH (Im)), 7.79 (s, 1H, CH (Im)), 8.87 (s, 1H, CH (Im)); δ_C (125 MHz, MeOH-*d*₄) 14.8, 18.9, 34.7, 34.8, 45.9, 47.3, 47.6, 51.3, 100.8, 114.0, 119.6, 121.1, 127.5, 128.6, 133.2, 135.2, 138.3, 138.8, 142.0, 142.1, 150.9, 151.8; HRMS (ESI) *m/z* calcd for [C₂₄H₂₈N₈O₂S₂ + H] 525.1855, obsd 525.1828; HPLC (I) *t_R* = 12.14 min (96.61%), (II) *t_R* = 17.00 min (96.03%).

[*N*-(1,3,5-Trimethyl-1*H*-pyrazol-4-ylmethyl), *N*-{2-[(4-Cyanophenyl)-(3-methyl-3*H*-imidazol-4-ylmethyl)-amino]-ethyl}] 1-Methyl-1*H*-imidazole-4-sulfonamide (1an, 4.49)

Trimethyl-1*H*-pyrazole-4-carbaldehyde was reductively aminated with amine 9, according to general procedure C, on a 0.15 mmol scale. The crude material was chromatographed over silica gel (eluent CH₂Cl₂/MeOH/NH₄OH, 92:7:1) to give 4-((3-methyl-3*H*-imidazol-4-ylmethyl)-{2-[(1,3,5-trimethyl-1*H*-pyrazol-4-ylmethyl)-amino]-ethyl}-amino)-benzonitrile as a film (46 mg, 81%): δ_H (400 MHz, MeOH-*d*₄) 2.28 (s, 3H, CH₃ (pyrazole)), 2.34 (s, 3H, CH₃ (pyrazole)), 3.39 (t, *J* = 7.5 Hz, 2H, NHCH₂CH₂N), 3.75 (s, 3H, N-CH₃ (pyrazole)), 3.88–3.95 (m, 5H, NHCH₂CH₂N, CH₃ (Im)), 4.15 (s, 2H, CH₂-pyrazole), 4.88 (s, 2H, CH₂Im), 7.01 (d, *J* = 8.9 Hz, 2H, 2 CH (benzonitrile)), 7.22 (s, 1H, CH (Im)), 7.59 (d, *J* = 8.9 Hz, 2H, 2 CH (benzonitrile)), 8.94 (s, 1H, CH (Im)); δ_C (125 MHz, MeOH-*d*₄) 9.8, 11.4, 34.3, 36.1, 42.3, 44.7, 45.6, 47.5, 99.9, 108.3, 114.3, 118.8, 120.6, 132.8, 135.0, 138.0, 142.6, 148.5, 151.3; LRMS (ESI) *m/z* 400.2 [C₂₁H₂₇N₇ + Na]. This secondary amine (38 mg, 0.1 mmol) was then reacted with 1-methyl-1*H*-imidazole-4-sulfonyl chloride according to general procedure A. Workup then the usual purification (silica gel flash column chromatography (eluent CH₂Cl₂/MeOH/NH₄OH, 192:7:1)) furnished the title compound **1an** as a white foam (44 mg, 84%): δ_H (500 MHz, MeOH-*d*₄) 2.00 (s, 3H, CH₃ (pyrazole)), 2.06 (s, 3H, CH₃ (pyrazole)), 3.15 (t, *J* = 6.5 Hz, 2H, ((pyrazole-4-ylmethyl)-NCH₂CH₂N)), 3.44 (t, *J* = 6.5 Hz, 2H, ((pyrazole-4-ylmethyl)-NCH₂CH₂N)), 3.51 (s, 3H, N-CH₃ (pyrazole)), 3.73 (s, 3H, CH₃ (Im)), 3.78 (s, 3H, CH₃ (Im)), 3.92 (s, 2H, CH₂-pyrazole), 4.48 (s, 2H, CH₂Im), 6.50 (d, *J* = 8.9 Hz, 2H, 2 CH (benzonitrile)), 7.11 (s, 1H, CH (Im)), 7.39 (d, *J* = 8.9 Hz, 2H, 2 CH (benzonitrile)), 7.72 (s, 1H, CH (Im)), 7.75 (s, 1H, CH (Im)), 8.80 (s, 1H, CH (Im)); δ_C (125 MHz, MeOH-*d*₄) 9.5, 11.7, 34.3, 34.4, 36.0, 45.1, 45.4, 46.5, 51.2, 100.2, 111.8, 113.4, 119.2, 120.8, 127.1, 132.7, 134.8, 137.9, 138.1, 141.2, 141.7, 147.9, 151.4; HRMS (ESI) *m/z* calcd for [C₂₅H₃₁N₉O₂S + H] 522.2400, obsd 522.2377; HPLC (I) *t_R* = 12.49 min (95.83%), (II) *t_R* = 17.78 min (96.33%).

[*N*-(Cyclopropylmethyl), *N*-{2-[(4-Cyanophenyl)-(3-methyl-3*H*-imidazol-4-ylmethyl)-amino]-ethyl}] 1-Methyl-1*H*-imidazole-4-sulfonamide (1aw, 4.34)

First, cyclopropanecarbaldehyde was reductively aminated with amine 9 (38 mg, 0.15 mmol), according to general procedure C. Flash column chromatography (eluent CH₂Cl₂/MeOH/NH₄OH, 92:7:1) purified the material to give 4-[[2-(cyclopropylmethyl)-amino]-ethyl]-{3-methyl-3*H*-imidazol-4-ylmethyl)-amino]-benzonitrile as a colorless film (39 mg, 84%): δ_H (400 MHz, CDCl₃) 0.07 (m, 2H, 2 CH (cyclopropyl)), 0.46 (m, 2H, 2 CH (cyclopropyl)), 0.78 (m, 1H, CHCH₂NHCH₂CH₂N), 2.41 (m, 2H, CH₂-cyclopropyl), 2.75 (s, 2H, NHCH₂CH₂N), 3.50 (m, 2H, NHCH₂CH₂N), 3.55 (s, 3H, CH₃ (Im)), 4.88 (s, 2H, CH₂Im), 6.68 (d, *J* = 8.8 Hz, 2H, 2 CH (benzonitrile)), 6.86 (s, 1H, CH (Im)), 7.26 (s, 1H, CH (Im)), 7.46 (d, *J* = 8.8 Hz, 2H, 2 CH (benzonitrile); LRMS (ESI) *m/z* 332.2 [C₁₈H₂₃N₅ + Na]. This secondary amine was then reacted with 1-methyl-1*H*-imidazole-4-sulfonyl chloride according to general procedure A, on a 0.1 mmol scale. After workup, the crude material was purified by silica gel flash column chromatography (eluent CH₂Cl₂/MeOH/NH₄OH, 192:7:1) to furnish **1aw** as a white powder (39 mg, 86%): δ_H (500 MHz, MeOH-*d*₄) 0.14 (m, 2H, 2 CH (cyclopropyl)), 0.43 (m, 2H, 2 CH (cyclopropyl)), 0.84 (m, 1H, CHCH₂NCH₂CH₂N), 2.50 (d, *J* = 6.9 Hz, 2H, CH₂-cyclopropyl), 2.99 (t, *J* = 6.9 Hz, 2H,

((cyclopropylmethyl)NCH₂CH₂N), 3.73 (s, 3H, CH₃ (Im)), 3.81 (t, *J* = 6.9 Hz, 2H, ((cyclopropylmethyl)-NCH₂CH₂N)), 3.88 (s, 3H, CH₃ (Im)), 4.85 (s, 2H, CH₂Im), 6.97 (d, *J* = 9.1 Hz, 2H, 2 CH (benzonitrile)), 7.28 (s, 1H, CH (Im)), 7.62 (d, *J* = 9.1 Hz, 2H, 2 CH (benzonitrile)), 7.67 (s, 1H, CH (Im)), 7.71 (s, 1H, CH (Im)), 8.87 (s, 1H, CH (Im)); δ_C (125 MHz, MeOH-*d*₄) 4.6, 11.0, 34.3, 34.4, 45.8, 46.8, 51.6, 55.9, 100.4, 114.1, 119.3, 120.9, 126.5, 133.1, 134.9, 137.9, 139.5, 141.4, 151.9; HRMS (ESI) *m/z* calcd for [C₂₂H₂₇N₇O₂S + H] 454.2025, obsd 454.2009; HPLC (I) *t_R* = 12.55 min (99.05%), (II) *t_R* = 18.46 min (98.47%).

***tert*-Butyl 4-[[2-[benzyl-(1-methyl-1*H*-imidazole-4-sulfonyl)-amino]-ethyl]-(3-methyl-3*H*-imidazol-4-ylmethyl)-amino]-benzoate (10)**

tert-Butyl *p*-fluorobenzoate (750 mg, 3.93 mmol, 1 equiv) was dissolved in ethylenediamine (9; 4 mL, 59.8 mmol, 15.2 equiv) and heated to 120 °C for 24 h. All solvent was evaporated, and then the residue was dry-loaded onto silica gel and purified by flash column chromatography (eluent CH₂Cl₂/MeOH/NH₄OH, 92:7:1) to furnish *tert*-butyl 4-(2-amino-ethylamino)-benzoate as a white powder (891 mg, 96%): δ_H (400 MHz, CD₂Cl₂) 1.59 (s, 9H, CO₂-(CH₃)₃), 2.98 (t, *J* = 5.8 Hz, 2H, H₂NCH₂CH₂NH), 3.23 (q, *J* = 5.8 Hz, 2H, H₂NCH₂CH₂NH), 4.67 (br, 1H, H₂NCH₂CH₂NH), 6.62 (d, *J* = 8.6 Hz, 2H, 2 CH (Ar)), 7.81 (d, *J* = 8.6 Hz, 2H, 2 CH (Ar)); δ_C (125 MHz, CD₂Cl₂) 28.9, 41.7, 46.6, 80.3, 112.1, 120.9, 131.9, 152.9, 166.7; HRMS (EI+) *m/z* calcd for [C₁₃H₂₀N₂O₂] 236.1525, obsd 236.1527. *tert*-Butyl 4-(2-amino-ethylamino)-benzoate (700 mg, 3.03 mmol, 1 equiv) was then sulfonylated with 1-methyl-1*H*-imidazole-4-sulfonyl chloride according to general procedure A. The crude material was dry-loaded onto silica gel, and then purified by flash column chromatography (eluent CH₂-Cl₂/MeOH/NH₄OH, 192:7:1) to give *tert*-butyl 4-[2-(1-methyl-1*H*-imidazole-4-sulfonylamino)-ethylamino]-benzoate as a white powder (1.04 g, 90%): δ_H (500 MHz, CDCl₃) 1.56 (s, 9H, CO₂-(CH₃)₃), 3.17 (m, 2H, SO₂NHCH₂CH₂NH), 3.28 (m, 2H, SO₂NHCH₂CH₂NH), 3.67 (s, 3H, CH₃ (Im)), 6.51 (d, *J* = 8.5 Hz, 2H, 2 CH (Ar)), 7.46 (s, 1H, CH (Im)), 7.51 (s, 1H, CH (Im)), 7.75 (d, *J* = 8.5 Hz, 2H, 2 CH (Ar)); δ_C (125 MHz, MeOH-*d*₄) 28.7, 34.6, 42.4, 43.1, 80.8, 111.9, 120.5, 125.2, 131.8, 140.1, 140.3, 152.4, 167.4; HRMS (ESI+) *m/z* calcd for [C₁₇H₂₄N₄O₄S + H] 381.1597, obsd 381.1573. *tert*-Butyl 4-[2-(1-methyl-1*H*-imidazole-4-sulfonylamino)-ethylamino]-benzoate (610 mg, 1.63 mmol, 1 equiv) was then chemoselectively benzylated on the sulfonamide NH with benzyl bromide according to general procedure B. The crude material was then flash chromatographed over silica gel to furnish *tert*-butyl 4-[2-[benzyl-(1-methyl-1*H*-imidazole-4-sulfonyl)-amino]-ethylamino]-benzoate as a white solid (703 mg, 92%): δ_H (400 MHz, CDCl₃) 1.52 (s, 9H, CO₂-(CH₃)₃), 3.13 (t, *J* = 6.2 Hz, 2H, (Bn)NCH₂CH₂NH), 3.43 (t, *J* = 6.2 Hz, 2H, (Bn)NCH₂CH₂NH), 3.68 (s, 3H, CH₃ (Im)), 4.32 (s, 2H, CH₂Ph), 6.30 (d, *J* = 8.8 Hz, 2H, 2 CH (Ar)), 7.23–7.30 (m, 5H, 5 CH (Ph)), 7.42 (s, 1H, CH (Im)), 7.49 (s, 1H, CH (Im)), 7.70 (d, *J* = 8.8 Hz, 2H, 2 CH (Ar)); δ_C (500 MHz, CDCl₃) 28.1, 33.9, 41.6, 46.6, 52.6, 79.6, 111.1, 119.9, 124.4, 127.9, 128.3, 128.6, 131.1, 136.0, 139.0, 139.8, 151.1, 166.1; HRMS (ESI) *m/z* calcd for [C₂₄H₃₀N₄O₄S + H] 471.2066, obsd 471.2053. *tert*-Butyl 4-[2-[benzyl-(1-methyl-1*H*-imidazole-4-sulfonyl)-amino]-ethyl-amino]-benzoate (220 mg, 0.473 mmol, 1 equiv) was alkylated on the aniline NH with 5-chloromethyl-1-methyl-1*H*-imidazole 3 HCl³¹ according to general procedure E. The crude material was flash chromatographed over silica gel (eluent CH₂Cl₂/MeOH/NH₄OH, 192:7:1) to afford the title compound **11** as a colorless foam (200 mg, 76%): δ_H (500 MHz, CDCl₃) 1.53 (s, 9H, C(CH₃)₃), 3.09–3.15 (m, 2H, CH₂CH₂NSO₂), 3.29–3.34 (m, 2H, CH₂CH₂-NSO₂), 3.43 (s, 3H, CH₃), 3.73 (s, 3H, CH₃), 4.26 (s, 2H, CH₂Ph), 4.30 (s, 2H, CH₂Im), 6.35 (d, *J* = 9.0 Hz, 2H, 2 CH (Ar)), 6.69 (s, 1H, CH (Im)), 7.31–7.37 (m, 5H, 5 CH (Ph)), 7.39 (s, 1H, CH (Im)), 7.42 (s, 1H, CH (Im)), 7.46 (s, 1H, CH (Im)), 7.68 (d, *J* = 9.0 Hz, 2H, 2 CH (Ar)); δ_C (125 MHz, CDCl₃) 28.2, 31.6, 33.9, 44.1, 45.0, 49.7, 54.3, 79.8, 111.0, 120.0, 124.4, 127.5, 128.1, 128.6, 128.7, 128.9, 131.1, 136.2, 138.5, 139.0, 139.1, 150.3, 165.8; HRMS (ESI+)

m/z calcd for $[C_{29}H_{36}N_6O_4S + H]$ 565.2597, obsd 565.2576; HPLC (I) $t_R = 12.53$ min (100%), (II) $t_R = 18.77$ min (100%).

4-[[2-[Benzyl-(1-methyl-1*H*-imidazole-4-sulfonyl)-amino]-ethyl](3-methyl-3*H*-imidazol-4-ylmethyl)-amino]-benzoic Acid (**12**)

TFA (1.5 mL) was added to a solution of **11** (150 mg, 0.268 mmol, 1 equiv) in CH_2Cl_2 (1.5 mL), and the resulting mixture was stirred for 3 h at room temperature, after which time all solvents were evaporated. Residual TFA was removed by repeated coevaporation with a 2:1 mixture of $CHCl_3/MeOH$, then the residue was purified by silica gel flash column chromatography (eluent $CH_2Cl_2/MeOH/NH_4OH$, 25:7:1) to afford the title compound as a sticky foam (131 mg, 96%): δ_H (500 MHz, $MeOH-d_4$) 3.34–3.39 (m, 2H, $CH_2CH_2NSO_2$), 3.42–3.46 (m, 2H, $CH_2CH_2NSO_2$), 3.81 (s, 3H, CH_3), 3.84 (s, 3H, CH_3), 4.30 (s, 2H, CH_2Ph), 4.55 (s, 2H, CH_2Im), 6.53 (d, $J = 9.0$ Hz, 2H, 2 CH (Ar)), 7.15 (s, 1H, CH (Im)), 7.34–7.38 (m, 5H, 5 CH (Ph)), 7.76–7.79 (m, 3H, 2 CH (Ar), CH (Im)), 7.82 (s, 1H, CH (Im)), 8.87 (s, 1H, CH (Im)); δ_C (125 MHz, $MeOH-d_4$) 34.3, 34.4, 45.0, 46.5, 51.2, 55.2, 112.8, 119.3, 120.3, 126.8, 129.3, 129.9 (2 CH), 132.7, 133.1, 137.7, 137.9, 139.1, 141.5, 152.0, 170.1; HRMS (ESI+) m/z calcd for $[C_{25}H_{28}N_6O_4S + H]$ 509.1971, obsd 509.1953; HPLC (I) $t_R = 11.24$ min (100%), (II) $t_R = 15.21$ min (100%).

4-[[2-[Benzyl-(1-methyl-1*H*-imidazole-4-sulfonyl)-amino]-ethyl](1-methyl-1*H*-imidazol-4-ylmethyl)-amino]-benzamide (**13**)

To a solution of acid **12** (50 mg, 0.0984 mmol, 1 equiv), NH_4Cl (10.5 mg, 0.197 mmol, 2 equiv), and DIPEA (34 μL) in DMF (1 mL) was added HBTU (48.5 mg, 0.128 mmol, 1.3 equiv). The reaction mixture was stirred for 1 h, after which time TLC indicated the reaction was complete. Water (25 mL) was added, and then the crude product was extracted into EtOAc (5 \times 5 mL). The EtOAc extractions were combined, washed with water (3 \times 5 mL), brine (5 mL), dried (Na_2SO_4), filtered, and concentrated. The residue was dry-loaded onto silica gel, then flash chromatographed (eluent $CH_2Cl_2/MeOH/NH_4OH$, 92:7:1) to furnish primary amide **13** as a white powder (44 mg, 89%): δ_H (500 MHz, $CDCl_3$) 3.15 (m, 2H, (Bn) NCH_2CH_2N), 3.31 (m, 2H, (Bn) NCH_2CH_2N), 3.41 (s, 3H, CH_3 (Im)), 3.71 (s, 3H, CH_3 (Im)), 4.23 (s, 2H, CH_2Ph), 4.29 (s, 2H, CH_2Im), 6.02 (br, 2H, NH_2), 6.42 (d, $J = 9.0$ Hz, 2H, 2 CH (Ar)), 6.66 (s, 1H, CH (Im)), 7.29–7.34 (m, 6H, 5 CH (Ph), CH (Im)), 7.41 (s, 1H, CH (Im)), 7.45 (s, 1H, CH (Im)), 7.56 (d, $J = 9.0$ Hz, 2H, 2 CH (Ar)); δ_C (125 MHz, $CDCl_3$) 31.3, 33.7, 43.9, 44.8, 49.4, 50.2, 54.0, 111.1, 121.0, 124.2, 127.2, 127.9, 128.4, 128.6, 128.9, 136.0, 138.4, 138.8, 138.9, 149.8, 168.9; HRMS (ESI+) m/z calcd for $[C_{25}H_{29}N_7O_3S + H]$ 508.2137, obsd 508.2131; HPLC (I) $t_R = 11.72$ min (100%), (II) $t_R = 16.29$ min (100%).

[*N*-Benzyl, *N*-{2-[(biphenyl-4-yl)-(3-methyl-3*H*-imidazol-4-ylmethyl)-amino]-ethyl}] 1-methyl-1*H*-imidazole-4-sulfonamide (**14**)

Previously reported 1-*tert*-butoxycarbonylamino-{2-[biphenyl-4-yl-(3-methyl-3*H*-imidazol-4-ylmethyl)-amino]-ethane (compound **9a** in ref ³¹) (30 mg, 0.0739 mmol) was deprotected by stirring in a 1:1 mixture of TFA- CH_2Cl_2 (1 mL) for 30 min. After removal of all solvent in vacuo, the residue (23 mg, 0.0739 mmol) was sulfonylated with 1-methyl-1*H*-imidazole-4-sulfonyl chloride according to general procedure A, but with 5 equiv of DIPEA. After the usual workup, the residue was purified by silica gel flash column chromatography (eluent $CH_2Cl_2/MeOH/NH_4OH$, 92:7:1) to afford 1-methyl-1*H*-imidazole-4-sulfonic acid benzyl-[2-(biphenyl-4-ylamino)-ethyl]-amide as a colorless film (30 mg, 91%) Next, the secondary aniline of 1-methyl-1*H*-imidazole-4-sulfonic acid benzyl-[2-(biphenyl-4-ylamino)-ethyl]-amide (30 mg, 0.067 mmol, 1 equiv) was alkylated with the HCl salt of 5-chloromethyl-1-methyl-1*H*-imidazole³¹ according to general procedure E. After the usual workup, the crude material was dry-loaded onto silica gel and purified by flash column

chromatography (eluent CH₂Cl₂/MeOH/NH₄OH, 92:7:1) to give **14** as a glassy film (24 mg, 65%): δ_{H} (500 MHz, CDCl₃) 3.16 (m, 2H, (Bn)NCH₂-CH₂N), 3.33 (m, 2H, (Bn)NCH₂CH₂N), 3.44 (s, 3H, CH₃ (Im)), 3.75 (s, 3H, CH₃ (Im)), 4.27 (s, 2H, CH₂Ph), 4.38 (s, 2H, CH₂Im), 6.56 (d, $J = 9.0$ Hz, 2H, 2 CH (Ar)), 6.79 (s, 1H, CH (Im)), 7.34 – 7.51 (m, 15 H, 10 CH (Ph), 3 CH (Im), 2 CH (Ar)); δ_{C} (125 MHz, CDCl₃) 31.9, 34.2, 44.9, 45.4, 50.0, 54.5, 113.5, 124.6, 126.4, 126.5, 128.1, 128.3 (2), 128.9, 129.0, 129.2, 129.4, 130.5, 136.8, 138.8, 139.3, 139.9, 141.1, 147.2; HRMS (ESI+) m/z calcd for [C₃₀H₃₂N₆-O₂S + H] 541.2380, obsd 541.2386; HPLC (I) $t_{\text{R}} = 13.01$ min (100%), (II) $t_{\text{R}} = 20.24$ min (100%).

N-(2-*tert*-Butoxycarbonylaminoethyl) 1-Methyl-1*H*-imidazole-4-sulfonamide (15)

Mono-*N*-Boc-ethylenediamine (**6**; 5 g, 31.2 mmol, 1 equiv) was sulfonylated with 1-methyl-1*H*-imidazole-4-sulfonyl chloride (6.76 g, 37.4 mmol, 1.2 equiv), according to general procedure A. After 16 h, the solvent was reduced and then the reaction mixture was dry-loaded onto silica gel and purified by flash column chromatography (eluent CH₂Cl₂/MeOH/NH₄OH, 1092:7:1) to give the title compound as a white powder (9 g, 95%): δ_{H} (500 MHz, CD₂Cl₂) 1.37 (s, 9H, C(CH₃)₃), 2.99 (t, $J = 5.8$ Hz, 2H, CH₂NHSO₂), 3.11 (q, $J = 5.8$ Hz, 2H, CH₂NHBoc), 3.71 (s, 3H, CH₃), 5.53 (s, 1H, NHSO₂), 5.68 (s, 1H, NHBoc), 7.48 (s, 1H, Im), 7.56 (s, 1H, Im); δ_{C} (125 MHz, CD₂Cl₂) 27.6, 33.5, 39.8, 42.6, 78.9, 124.0, 127.2, 139.2, 156.1; HRMS (ESI+) m/z calcd for [C₁₁H₂₀N₄O₄S + H] 305.1284, obsd 305.1294.

[N-(2-*tert*-Butoxycarbonylaminoethyl), N-{N-(2-Pyrimidinyl)-piperidin-4-ylmethyl}] 1-Methyl-1*H*-imidazole-4-sulfonamide (16)

N-(2-*tert*-Butoxycarbonylaminoethyl) 1-methyl-1*H*-imidazole-4-sulfonamide (5.94 g, 19.5 mmol, 1 equiv) was chemoselectively alkylated on the sulfonamide NH with *N*-(2-pyrimidinyl)-piperidin-4-ylmethyl bromide (6 g, 23.4 mmol, 1.2 equiv), according to general procedure **B**, but the reaction was stirred for 4 d at room temperature. [*N*-(2-Pyrimidinyl)-piperidin-4-ylmethyl bromide was made from the reaction of *N*-(2-pyrimidinyl)-piperidin-4-ylmethyl alcohol (5 g, 25.9 mmol, 1 equiv) with PPh₃Br₂ (14.2 g, 33.7 mmol, 1.3 equiv) in CH₂Cl₂ (130 mL) at 0 °C to room temperature over 6 h. At this point, the reaction was complete. Water (100 mL) was added to quench, and then the CH₂Cl₂ layer was diluted further (500 mL total volume). The organic layer was collected, and the aqueous layer was extracted twice further (2 × 50 mL). The organic layers were collected, dried (Na₂SO₄), filtered, and concentrated. The residue was redissolved in CH₂Cl₂, dry-loaded onto silica gel, then purified by flash column chromatography (eluent Hex/EtOAc, 7:1) to furnish *N*-(2-pyrimidinyl)-piperidin-4-ylmethyl bromide as a white powder (6.04 g, 91%).] After workup, the crude material was dry-loaded onto silica gel and purified by silica gel flash column chromatography (eluent CH₂Cl₂/MeOH/NH₄OH, 192:7:1), affording the title compound as a white solid (8.81 g, 94%): δ_{H} (500 MHz, CDCl₃) 1.09 (qd, $J = 12.3, 4.0$ Hz, 2H, 2 CH (piperidinylmethyl)), 1.36 (s, 9H, C(CH₃)₃), 1.69–1.78 (m, 2H, 2 CH (piperidinylmethyl)), 1.84–1.92 (m, 1H, CH (piperidinylmethyl)), 2.77–2.83 (m, 2H, 2 CH (piperidinylmethyl)), 2.97 (br d, $J = 8.0$ Hz, 2H, 2 CH (piperidinylmethyl)), 3.25–3.34 (m, 4H, CH₂CH₂NHBoc), 3.67 (s, 3H, CH₃), 4.64–4.69 (m, 2H, 2 CH (piperidinylmethyl)), 5.53 (m, 1H, NHBoc), 6.34 (t, $J = 4.9$ Hz, 1H, CH (pyrimidine)), 7.36 (s, 1H, CH (Im)), 7.40 (s, 1H, CH (Im)), 8.20 (t, $J = 4.9$ Hz, 2H, 2 CH (pyrimidine)); δ_{C} (125 MHz, CDCl₃) 28.3, 29.4, 34.8, 35.4, 39.6, 43.4, 49.1, 55.2, 79.0, 109.2, 124.2, 138.9, 140.6, 155.9, 157.5, 161.4; HRMS (ESI+) m/z calcd for [C₂₁H₃₃N₇O₄S + H] 480.2393, obsd 480.2409.

[N-(2-Aminoethyl), N-{N-(2-Pyrimidinyl)-piperidin-4-ylmethyl}] 1-Methyl-1*H*-imidazole-4-sulfonamide (17)

To a cooled (0 °C), stirring solution of **16** (8.67 g, 18.1 mmol) in CH₂Cl₂ (47.5 mL) was added triisopropylsilane (TIPS; 2.5 mL), H₂O (2.5 mL) and TFA (47.5 mL). After 5 min, the

reaction was removed from the ice bath and allowed to stir for 1 h at room temperature, and then all solvents were evaporated. The residue was redissolved in CH₂Cl₂ and the minimal required volume of MeOH, then dry-loaded onto silica gel and purified by flash column chromatography (eluent CH₂Cl₂/MeOH/NH₄OH, 92:7:1) to give **17** as a white, sticky foam (7.2 g, 100%): δ_{H} (500 MHz, CDCl₃) 1.10 (qd, $J = 12.2$, 4.0 Hz, 2H, 2 CH (piperidinylmethyl)), 1.73–1.78 (m, 2H, 2 CH (piperidinylmethyl)), 1.87–1.95 (m, 1H, CH (piperidinyl)), 2.77–2.83 (m, 2H, 2 CH (piperidinylmethyl)), 2.92 (t, $J = 6.5$ Hz, 2H, CH₂NH₂), 3.00 (br d, $J = 7.5$ Hz, 2H, 2 CH (piperidinylmethyl)), 3.32 (t, $J = 6.4$ Hz, 2H, CH₂CH₂NH₂), 3.46–3.51 (br s, NH₂), 3.69 (s, 3H, CH₃ (Im)), 4.66–4.72 (m, 2H, 2 CH (piperidinylmethyl)), 6.38 (t, $J = 4.7$ Hz, 1H, CH (pyrimidine)), 7.40 (s, 1H, CH (Im)), 7.47 (s, 1H, CH (Im)), 8.22 (t, $J = 4.7$ Hz, 2H, 2 CH (pyrimidine)); δ_{C} (125 MHz, CDCl₃) 29.5, 33.8, 35.5, 40.1, 43.4, 52.5, 54.9, 109.2, 124.2, 139.0, 139.4, 158.5, 161.5; HRMS (ESI+) m/z calcd for [C₁₆H₂₅N₇O₂S + H] 380.1869, obsd 380.1886.

[*N*-{2-(2-Chloro-4-cyanophenyl)-aminoethyl}, *N*-{*N*-(2-Pyrimidinyl)-piperidin-4-ylmethyl}] 1-Methyl-1*H*-imidazole-4-sulfonamide (18a**)**

Compound **17** was reacted with 2-chloro-4-fluorobenzonitrile on a 0.338 mmol scale, according to general procedure D. After the usual workup, the crude material was purified by silica gel flash column chromatography (eluent CH₂Cl₂/MeOH/NH₄OH, 192:7:1) to give the title compound as a colorless, viscous oil (158 mg, 91%): δ_{H} (500 MHz, CDCl₃) 1.08 (qd, $J = 12.3$, 4.0 Hz, 2H, 2 CH (piperidinylmethyl)), 1.68–1.74 (m, 2H, 2 CH (piperidinylmethyl)), 1.77–1.86 (m, 1H, CH (piperidinylmethyl)), 2.72 (td, $J = 12.5$, 2.5 Hz, 2H, 2 CH (piperidinylmethyl)), 3.00 (br d, $J = 7.5$ Hz, 2H, 2 CH (piperidinylmethyl)), 3.48–3.55 (m, 4H, CH₂CH₂NHAr), 3.71 (m, 3H, CH₃ (Im)), 4.63–4.69 (m, 2H, 2 CH (piperidinylmethyl)), 5.77 (t, $J = 5.3$ Hz, 1H, CH₂NHAr), 6.40 (t, $J = 4.7$ Hz, 1H, CH (pyrimidine)), 6.66 (d, $J = 8.5$ Hz, 1H, CH (Ar)), 7.37 (dd, $J = 8.5$, 2.0 Hz, 1H, CH (Ar)), 7.43 (s, 1H, CH (Im)), 7.45 (d, $J = 2.0$ Hz, 1H, CH (Ar)), 7.46 (s, 1H, CH (Im)), 8.22 (t, $J = 4.7$ Hz, 2H, 2 CH (pyrimidine)); δ_{C} (125 MHz, CDCl₃) 29.6, 33.9, 36.0, 42.2, 43.4, 48.7, 56.1, 98.7, 109.4, 110.0, 118.6, 119.0, 124.4, 132.4, 132.5, 139.1, 139.5, 147.0, 157.5, 161.4; HRMS (ESI+) m/z calcd for [C₂₃H₂₇N₈O₂SCl + H] 515.1744, obsd 515.1754.

***N*-(2-(2-Cyanopyridin-5-ylamino)ethyl)-1-methyl-*N*-((1-(pyrimidin-2-yl)piperidin-4-yl)methyl)-1*H*-imidazole-4-sulfonamide (**18b**)**

Compound **17** was reacted with 2-cyano-5-fluoropyridine on a 0.791 mmol scale, according to general procedure D. After the usual workup, the crude material was purified by silica gel flash column chromatography (eluent CH₂Cl₂/MeOH/NH₄OH, 192:7:1) to give the title compound as a colorless, viscous oil (320 mg, 84%): δ_{H} (500 MHz, CDCl₃) 0.95 (qd, $J = 12.3$, 4.0 Hz, 2H, 2 CH (piperidinylmethyl)), 1.63–1.71 (m, 2H, 2 CH (piperidinylmethyl)), 1.74–1.83 (m, 1H, CH (piperidinylmethyl)), 2.72 (td, $J = 12.5$, 2.5 Hz, 2H, 2 CH (piperidinylmethyl)), 2.93 (br d, $J = 7.5$ Hz, 2H, 2 CH (piperidinylmethyl)), 3.23–3.27 (m, 2H, CH₂CH₂NHAr), 3.34–3.36 (m, 2H, CH₂CH₂NHAr), 3.65 (m, 3H, CH₃ (Im)), 4.55–4.59 (m, 2H, 2 CH (piperidinylmethyl)), 6.54 (m, 1H, CH₂NHAr), 6.96 (t, $J = 4.9$ Hz, 1H, CH (pyrimidine)), 7.04 (m, 1H, CH (Ar)), 7.62 (s, 1H, CH (Im)), 7.77–7.78 (m, 2H, CH (Im), CH (Ar)), 8.02 (m, 1H, CH (Ar)), 8.28 (t, $J = 4.9$ Hz, 2H, 2 CH (pyrimidine)); δ_{C} (125 MHz, DMSO-*d*₆) 28.96, 33.34, 34.88, 40.33, 41.20, 43.03, 47.87, 54.82, 109.46, 117.39, 118.92, 124.99, 129.69, 136.90, 137.56, 139.75, 146.98, 157.72, 161.02; HRMS (ESI+) m/z calcd for [C₂₂H₂₇N₉O₂S + H] 482.2087, obsd 482.2086.

[*N*-{2-(5-Bromopyridin-2-yl)-aminoethyl}, *N*-{*N*-(2-pyrimidinyl)-piperidin-4-ylmethyl}] 1-methyl-1*H*-imidazole-4-sulfonamide (18c**)**

Compound **17** was reacted with 5-bromo-2-fluoropyridine on a 0.512 mmol scale, according to general procedure D. After the usual workup, the crude material was purified by silica gel

flash column chromatography (eluent CH₂Cl₂/MeOH/NH₄OH, 192:7:1) to give the title compound as a colorless, viscous oil (200 mg, 73%): δ_{H} (500 MHz, CDCl₃) 1.11 (qd, $J = 12.3, 4.0$ Hz, 2H, 2 CH (piperidinylmethyl)), 1.72–1.78 (m, 2H, 2 CH (piperidinylmethyl)), 1.87–1.97 (m, 1H, CH (piperidinylmethyl)), 2.78 (td, $J = 12.8, 2.5$ Hz, 2H, 2 CH (piperidinylmethyl)), 3.03 (br d, $J = 8.0$ Hz, 2H, 2 CH (piperidinylmethyl)), 3.49–3.57 (m, 4H, CH₂CH₂-NHAr), 3.72 (m, 3H, CH₃ (Im)), 4.67–4.73 (m, 2 H, 2 CH (piperidinylmethyl)), 5.62 (t, $J = 5.3$ Hz, 1H, CH₂NHAr), 6.34 (dd, $J = 9.0$ Hz, 1H, CH (Ar)), 6.41 (t, $J = 4.9$ Hz, 1H, CH (pyrimidine)), 7.40 (dd, $J = 9.0, 2.5$ Hz, 1H, CH (Ar)), 7.42 (s, 1H, CH (Im)), 7.47 (s, 1H, CH (Im)), 8.05 (d, $J = 2.5$ Hz, 1H, CH (Ar)), 8.25 (t, $J = 4.9$ Hz, 2H, 2 CH (pyrimidine)); δ_{C} (125 MHz, CDCl₃) 29.7, 33.9, 35.6, 40.5, 43.6, 48.5, 55.0, 106.8, 109.3, 109.7, 124.4, 138.9, 139.3, 140.0, 148.4, 156.9, 157.6, 161.5; HRMS (ESI+) m/z calcd for [C₂₁H₂₇N₈O₂SBr + H] 535.1239, obsd 535.1259.

[N-{2-(5-Bromopyrimidin-2-yl)-aminoethyl}, N-(N-(2-Pyrimidinyl)-piperidin-4-ylmethyl)] 1-Methyl-1H-imidazole-4-sulfonamide (18d)

Compound **17** was reacted with 5-bromo-2-fluoropyrimidine on a 0.528 mmol scale, according to general procedure D. After the usual workup, the crude material was purified by silica gel flash column chromatography (eluent CH₂Cl₂/MeOH/NH₄OH, 192:7:1) to give the title compound as a white foam (255mg, 90%): δ_{H} (500 MHz, CDCl₃) 1.08 (qd, $J = 12.3, 4.0$ Hz, 2H, 2 CH (piperidinylmethyl)), 1.70–1.77 (m, 2H, 2 CH (piperidinylmethyl)), 1.83–1.92 (m, 1H, CH (piperidinylmethyl)), 2.78 (td, $J = 12.8, 2.5$ Hz, 2H, 2 CH (piperidinylmethyl)), 3.03 (br d, $J = 8.0$ Hz, 2H, 2 CH (piperidinylmethyl)), 3.43 (t, $J = 6.3$ Hz, 2H, CH₂CH₂NHAr), 3.57 (t, $J = 6.3$ Hz, 2H, CH₂CH₂NHAr), 3.68 (m, 3H, CH₃ (Im)), 4.60–4.66 (m, 2 H, 2 CH (piperidinylmethyl)), 6.39 (t, $J = 4.6$ Hz, 1H, CH (pyrimidine)), 7.40 (s, 1H, CH (Im)), 7.47 (s, 1H, CH (Im)), 8.19 (s, 2H, 2CH(Ar)), 8.21 (t, $J = 4.6$ Hz, 2H, 2CH (pyrimidine)); δ_{C} (125 MHz, CDCl₃) 29.5, 33.8, 35.5, 40.4, 43.6, 48.3, 55.0, 106.1, 109.3, 124.3, 139.1, 139.6, 157.6, 158.1, 160.3, 161.3; HRMS (ESI+) m/z calcd for [C₂₀H₂₆N₉O₂SBr + H] 536.1192, obsd 536.1213.

[N-{2-(3-Fluoro-4-cyanophenyl)-aminoethyl}, N-(N-(2-Pyrimidinyl)-piperidin-4-ylmethyl)] 1-Methyl-1H-imidazole-4-sulfonamide (18e)

Compound **17** was reacted with 2,4-difluorobenzonitrile on a 0.417 mmol scale, according to general procedure D, to give a separable mixture of the two expected isomers. After the usual workup, the crude material was purified by prepTLC (eluent CH₂Cl₂/MeOH/NH₄OH, 92:7:1) to give the title compound as a white foam (99 mg, 48%): δ_{H} (500 MHz, CDCl₃) 1.15 (qd, $J = 12.5, 4.0$ Hz, 2H, 2 CH (piperidinylmethyl)), 1.73–1.79 (m, 2H, 2 CH (piperidinylmethyl)), 1.87–1.95 (m, 1H, CH (piperidinylmethyl)), 2.80 (td, $J = 12.8, 2.5$ Hz, 2H, 2 CH (piperidinylmethyl)), 3.03 (br d, $J = 7.5$ Hz, 2H, 2 CH (piperidinylmethyl)), 3.36 (q, $J = 5.5$ Hz, 2H, CH₂CH₂NHAr), 3.65 (t, $J = 5.8$ Hz, 2H, CH₂CH₂NHAr), 3.77 (m, 3H, CH₃ (Im)), 4.70–4.75 (m, 2 H, 2 CH (piperidinylmethyl)), 6.10–6.13 (m, 1H, CH₂NHAr), 6.30 (dd, $J = 12.0, 2.0$ Hz, 1H, CH (Ar)), 6.39 (dd, $J = 8.8, 2.0$ Hz, 1H, CH (Ar)), 6.44 (t, $J = 4.9$ Hz, 1H, CH (pyrimidine)), 7.32 (dd, $J = 8.8, 7.3$ Hz, 1H, CH (Ar)), 7.47 (s, 1H, CH (Im)), 7.52 (s, 1H, CH (Im)), 8.27 (t, $J = 4.9$ Hz, 2H, CH (pyrimidine)); δ_{C} (125 MHz, CDCl₃) 29.5, 34.0, 35.5, 41.5, 43.5, 47.7, 54.4, 87.0 (d, $J_{\text{CF}} = 15.5$ Hz), 98.1 (d, $J_{\text{CF}} = 22.8$ Hz), 108.8 (br), 109.4, 115.7, 124.6, 133.9 (d, $J_{\text{CF}} = 2.75$ Hz), 139.0, 139.6, 153.4 (d, $J_{\text{CF}} = 10.9$ Hz), 157.6, 161.5, 165.0 (d, $J_{\text{CF}} = 252$ Hz); HRMS (ESI+) m/z calcd for [C₂₃H₂₇N₈O₂FS + H] 499.2040, obsd 499.2057.

[N-{2-(2-Fluoro-4-cyanophenyl)-aminoethyl}, N-(N-(2-pyrimidinyl)-piperidin-4-ylmethyl)] 1-Methyl-1H-imidazole-4-sulfonamide (18f)

Compound **17** was reacted with 3,4-difluorobenzonitrile on a 0.343 mmol scale, according to general procedure D. After the usual workup, the crude material was purified by silica gel

flash column chromatography (eluent CH₂Cl₂/MeOH/NH₄OH, 192:7:1) to give the title compound as a white foam (138 mg, 82%): δ_{H} (500 MHz, CDCl₃) 1.13 (qd, $J = 12.3$, 4.0 Hz, 2H, 2 CH (piperidinylmethyl)), 1.73–1.78 (m, 2H, 2 CH (piperidinylmethyl)), 1.83–1.91 (m, 1H, CH (piperidinylmethyl)), 2.78 (td, $J = 12.8$, 2.5 Hz, 2H, 2 CH (piperidinylmethyl)), 3.04 (br d, $J = 7.5$ Hz, 2H, 2 CH (piperidinylmethyl)), 3.51 (q, $J = 5.7$ Hz, 2H, CH₂CH₂NHAr), 3.59 (t, $J = 6.0$ Hz, 2H, CH₂CH₂NHAr), 3.75 (m, 3H, CH₃ (Im)), 4.69–4.75 (m, 2H, 2 CH (piperidinylmethyl)), 5.74–5.78 (m, 1H, CH₂NHAr), 6.43 (t, $J = 4.7$ Hz, 1H, CH (pyrimidine)), 6.68 (t, $J = 8.5$ Hz, 1H, CH (Ar)), 7.19 (dd, $J = 11.5$, 1.5 Hz, 1H, CH (Ar)), 7.31 (br dd, $J = 8.5$, 1.5 Hz, 1H, CH (Ar)), 7.44 (s, 1H, CH (Im)), 7.49 (s, 1H, CH (Im)), 8.27 (t, $J = 4.7$ Hz, 2H, 2 CH (pyrimidine)); δ_{C} (125 MHz, CDCl₃) 29.5, 33.9, 35.7, 41.6, 43.4, 48.3, 55.1, 97.4 (d, $J_{\text{CF}} = 9.13$ Hz), 109.4, 110.8 (d, $J_{\text{CF}} = 4.5$ Hz), 117.5 (d, $J_{\text{CF}} = 21.9$ Hz), 119.2 (d, $J_{\text{CF}} = 2.75$ Hz), 124.3, 130.1 (d, $J_{\text{CF}} = 2.75$ Hz), 139.1, 139.6, 140.5 (d, $J_{\text{CF}} = 11.9$ Hz), 149.8 (d, $J_{\text{CF}} = 241$ Hz), 157.6, 161.4; HRMS (ESI+) m/z calcd for [C₂₃H₂₇N₈O₂FS + H] 499.2040, obsd 499.2055.

[*N*-{2-(2,6-Difluoro-4-cyanophenyl)-aminoethyl}, *N*-{*N*-(2-Pyrimidinyl)-piperidin-4-ylmethyl}] 1-Methyl-1*H*-imidazole-4-sulfonamide (18g)

Compound **17** was reacted with 3,4,5-trifluorobenzonitrile on a 0.359 mmol scale, according to general procedure D. After the usual workup, the crude material was purified by silica gel flash column chromatography (eluent CH₂Cl₂/MeOH/NH₄OH, 192:7:1) to give the title compound as a white foam (179 mg, 97%): δ_{H} (500 MHz, CDCl₃) 1.09 (qd, $J = 12.3$, 4.0 Hz, 2H, 2 CH (piperidinylmethyl)), 1.68–1.75 (m, 2H, 2 CH (piperidinylmethyl)), 1.81–1.90 (m, 1H, CH (piperidinylmethyl)), 2.75 (td, $J = 12.5$, 2.5 Hz, 2H, 2 CH (piperidinylmethyl)), 2.98 (br d, $J = 7.0$ Hz, 2H, 2 CH (piperidinylmethyl)), 3.51 (t, $J = 5.8$ Hz, 2H, CH₂CH₂NHAr), 3.72 (m, 5H, CH₂CH₂-NHAr, CH₃ (Im)), 4.65–4.73 (m, 2H, 2 CH (piperidinylmethyl)), 5.67 (m, 1H, CH₂NHAr), 6.40 (t, $J = 4.9$ Hz, 1H, CH (pyrimidine)), 7.05 (dd, $J = 7.5$, 2.5 Hz, 2H, CH (Ar)), 7.43 (s, 1H, CH (Im)), 7.47 (s, 1H, CH (Im)), 8.23 (t, $J = 4.9$ Hz, 2H, 2CH (pyrimidine)); δ_{C} (125 MHz, CDCl₃) 29.6, 33.9, 35.7, 43.5, 43.7, 50.2, 55.4, 96.7 (t, $J_{\text{CF}} = 11.4$ Hz), 109.3, 115.8 (dd, $J_{\text{CF}} = 18.3$, 8.13 Hz), 117.9 (t, $J_{\text{CF}} = 3.19$ Hz), 124.4, 130.8 (t, $J_{\text{CF}} = 12.3$ Hz), 139.0, 139.7, 150.8 (dd, $J_{\text{CF}} = 241$, 10.0 Hz), 157.5, 161.4; HRMS (ESI+) m/z calcd for [C₂₃H₂₆N₈O₂F₂S + H] 517.1946, obsd 517.1953.

[*N*-{2-(2,3,5,6-Tetrafluoro-4-cyanophenyl)-aminoethyl}, *N*-{*N*-(2-Pyrimidinyl)-piperidin-4-ylmethyl}] 1-Methyl-1*H*-imidazole-4-sulfonamide (18h)

Compound **17** was reacted with 2-chloro-4-fluorobenzonitrile on a 0.338 mmol scale, according to general procedure D, although the reaction was complete within 12 h at room temperature. After the usual workup, the crude material was purified by silica gel flash column chromatography (eluent CH₂Cl₂/MeOH/NH₄OH, 192:7:1) to give the title compound as a white foam (158 mg, 85%): δ_{H} (500 MHz, CDCl₃) 1.13 (qd, $J = 12.2$, 4.0 Hz, 2H, 2 CH (piperidinylmethyl)), 1.72–1.79 (m, 2H, 2 CH (piperidinylmethyl)), 1.88–1.97 (m, 1H, CH (piperidinylmethyl)), 2.81 (td, $J = 12.8$, 2.5 Hz, 2H, 2 CH (piperidinylmethyl)), 2.97 (br d, $J = 7.0$ Hz, 2H, 2 CH (piperidinylmethyl)), 3.63 (t, $J = 5.0$ Hz, 2H, CH₂CH₂NHAr), 3.77 (s, 3H, CH₃ (Im)), 3.78–3.84 (m, 2H, CH₂-CH₂NHAr), 4.71–4.77 (m, 2H, 2CH (piperidinylmethyl)), 6.44 (t, $J = 4.8$ Hz, 1H, CH (pyrimidine)), 6.81–6.86 (m, 1H, CH₂NHAr), 7.47 (s, 1H, CH (Im)), 7.51 (s, 1H, CH (Im)), 8.27 (t, $J = 4.8$ Hz, 2H, CH (pyrimidine)); δ_{C} (125 MHz, CDCl₃) 29.7, 34.1, 35.9, 43.4, 43.5, 50.2, 55.0, 78.4 (t, $J_{\text{CF}} = 18.3$ Hz), 109.0 (m), 109.5, 124.7, 133.5 (m), 135.9 (dm), 139.0, 140.1, 148.1 (dm), 157.7, 161.6; HRMS (ESI+) m/z calcd for [C₂₃H₂₄N₈O₂F₄S + H] 553.1757, obsd 553.1774.

[*N*-{2-[(2-Chloro-4-cyanophenyl)-(3-methyl-3*H*-imidazol-4-ylmethyl)-amino]-ethyl}, *N*-{*N*-(2-Pyrimidinyl)-piperidin-4-ylmethyl}] 1-Methyl-1*H*-imidazole-4-sulfonamide (19a)

As per general procedure E with **18a** on a 0.068 mmol scale. After the usual workup, the crude material was purified by silica gel flash column chromatography (eluent CH₂Cl₂/MeOH/NH₄OH, 192:7:1) to afford the title compound as a white foam (37 mg, 90%): δ_{H} (500 MHz, CDCl₃) 1.04 (qd, $J = 12.2, 4.0$ Hz, 2H, 2 CH (piperidinylmethyl)), 1.63–1.68 (m, 2H, 2 CH (piperidinylmethyl)), 1.70–1.76 (m, 1H, CH (piperidinylmethyl)), 2.76 (td, $J = 12.5, 2.5$ Hz, 2H, 2 CH (piperidinylmethyl)), 2.94 (br d, $J = 7.0$ Hz, 2H, 2 CH (piperidinylmethyl)), 3.31–3.36 (m, 2H, SO₂NCH₂CH₂N), 3.39–3.44 (m, 2H, SO₂-NCH₂CH₂N), 3.51 (s, 3H, CH₃ (Im)), 3.73 (m, 3H, CH₃ (Im)), 4.41 (s, 2H, CH₂Im), 4.65–4.71 (m, 2 H, 2 CH (piperidinylmethyl)), 6.42 (t, $J = 4.9$ Hz, 1H, CH (pyrimidine)), 6.97 (s, 1H, CH (Im)), 7.23 (d, $J = 8.5$ Hz, 1H, CH (Ar)), 7.36 (s, 1H, CH (Im)), 7.41 (s, 1H, CH (Im)), 7.43 (s, 1H, CH (Im)), 7.48 (dd, $J = 8.5, 2.0$ Hz, 1H, CH (Ar)), 7.63 (d, $J = 2.0$ Hz, 1H, CH (Ar)), 8.26 (t, $J = 4.9$ Hz, 2H, 2 CH (pyrimidine)); δ_{C} (125 MHz, CDCl₃) 29.6, 31.7, 33.9, 36.0, 43.5, 45.7, 47.1, 50.7, 55.6, 107.1, 109.4, 117.6, 123.7, 124.1, 126.6, 129.0, 129.9, 131.4, 134.3, 138.9, 139.0, 139.7, 151.0, 157.6, 161.5; HRMS (ESI+) m/z calcd for [C₂₈H₃₃-N₁₀O₂SCl + H] 609.2275, obsd 609.2296; HPLC (I) $t_{\text{R}} = 12.90$ min (99.13%), (II) $t_{\text{R}} = 19.65$ min (98.61%).

***N*-(2-((2-Cyanopyridin-5-yl)((1-methyl-1*H*-imidazol-5-yl)methyl)-amino)ethyl)-1-methyl-*N*-((1-pyrimidin-2-yl)piperidin-4-yl)methyl)-1*H*-imidazole-4-sulfonamide (19b)**

As per general procedure E with **18b** on a 0.415 mmol scale. After the usual workup, the crude material was purified by silica gel flash column chromatography (eluent CH₂Cl₂/MeOH/NH₄OH, 192:7:1) to afford the title compound as a white foam (186 mg, 78%): δ_{H} (500 MHz, DMSO-*d*₆) 1.05–1.13 (m, 4H, 4 CH (piperidinylmethyl)), 1.69–1.74 (m, 1H, CH (piperidinylmethyl)), 2.79 (td, $J = 12.5, 2.5$ Hz, 2H, 2 CH (piperidinylmethyl)), 2.95 (br d, $J = 7.0$ Hz, 2H, 2 CH (piperidinylmethyl)), 3.28 (s, 3H, CH₃ (Im)), 3.34–3.39 (m, 2H, SO₂NCH₂CH₂N), 3.41–3.42 (m, 2H, SO₂NCH₂CH₂N), 3.68 (s, 3H, CH₃ (Im)), 4.38 (s, 2H, CH₂Im), 4.60–4.64 (m, 2 H, 2 CH (piperidinylmethyl)), 6.41 (t, $J = 4.8$ Hz, 1H, CH (pyrimidine)), 6.86 (s, 1H, CH (Ar)), 7.02 (s, 1H, CH (Im)), 7.20 (m, 1H, CH (Ar)), 7.41–7.50 (m, 2H, CH (Im), CH (Ar)), 7.65 (s, 1H, CH (Im)), 7.80 (s, 1H, CH (Im)), 8.26 (t, $J = 4.9$ Hz, 2H, 2 CH (pyrimidine)); δ_{C} (125 MHz, DMSO-*d*₆) 29.5, 32.0, 32.8, 34.0, 35.9, 43.5, 44.2, 48.9, 49.2, 49.4, 49.7, 53.2, 56.2, 109.5, 118.1, 120.8, 122.3, 124.6, 129.4, 135.8, 139.3, 145.5, 157.7, 161.4; HRMS (ESI+) m/z calcd for [C₂₇H₃₃N₁₁O₂S + H] 576.2618, obsd 576.2617.

[*N*-{2-[(5-Cyanopyridin-2-yl)-(3-methyl-3*H*-imidazol-4-ylmethyl)-amino]-ethyl}, *N*-{*N*-(2-Pyrimidinyl)-piperidin-4-ylmethyl}] 1-Methyl-1*H*-imidazole-4-sulfonamide (19c)

As per general procedure E with **18c** on a 0.178 mmol scale. After the usual workup, the crude material was purified by silica gel flash column chromatography (eluent CH₂Cl₂/MeOH/NH₄OH, 192:7:1) to furnish [*N*-{2-[(5-bromopyridin-2-yl)-(3-methyl-3*H*-imidazol-4-ylmethyl)amino]ethyl}, *N*-{*N*-(2-pyrimidinyl)-piperidin-4-ylmethyl}] 1-methyl-1*H*-imidazole-4-sulfonamide as a white foam (107 mg, 96%): δ_{H} (500 MHz, CDCl₃) 1.12 (qd, $J = 12.5, 4.0$ Hz, 2H, 2 CH (piperidinylmethyl)), 1.72–1.80 (m, 3H, 3 CH (piperidinylmethyl)), 2.84 (td, $J = 13.0, 2.5$ Hz, 2H, 2 CH (piperidinylmethyl)), 2.98 (br d, $J = 7.0$ Hz, 2H, 2 CH (piperidinylmethyl)), 3.14–3.18 (m, 2H, NSO₂CH₂CH₂N), 3.55 (s, 3H, CH₃ (Im)), 3.62–3.67 (m, 2H, NSO₂CH₂CH₂N), 3.73 (m, 3H, CH₃ (Im)), 4.69–4.78 (m, 2H, 2 CH (piperidinylmethyl)), 4.80 (s, 2H, CH₂Im), 6.43 (t, $J = 4.9$ Hz, 1H, CH (pyrimidine)), 6.69 (d, $J = 9.5$ Hz, 1H, CH (Ar)), 6.96 (s, 1H, CH (Im)), 7.38 (s, 1H, CH (Im)), 7.43 (s, 1H, CH (Im)), 7.46 (s, 1H, CH (Im)), 7.55 (dd, $J = 9.0, 2.5$ Hz, 1H, CH (Ar)), 8.15 (d, $J = 2.5$ Hz, 1H, CH (Ar)), 8.27 (t, $J = 4.9$ Hz, 2H, 2 CH (pyrimidine)); δ_{C} (125 MHz, CDCl₃) 29.6, 31.8, 33.9, 35.6, 41.0, 43.5, 46.2, 47.0, 55.9, 107.1, 107.6, 109.3, 124.2, 128.2, 129.1, 138.8,

138.9, 139.3, 140.1, 148.2, 155.9, 157.6, 161.5; HRMS (ESI+) m/z calcd for $[C_{26}H_{33}N_{10}O_2SBr + H]$ 629.1770, obsd 629.1780; HPLC (I) $t_R = 12.78$ min (100%), + (II) $t_R = 18.88$ min (100%). The aryl bromide was then converted to the corresponding aryl nitrile on a 0.115 mmol scale, according to general procedure F. After workup, the crude material was dry-loaded onto silica gel, and purified by flash column chromatography (eluent $CH_2Cl_2/MeOH/NH_4OH$, 192:7:1) to give **19c** as a white foam (51 mg, 77%): δ_H (500 MHz, $CDCl_3$) 1.11 (qd, $J = 12.5, 4.0$ Hz, 2H, 2 CH (piperidinylmethyl)), 1.67–1.77 (m, 3H, 3 CH (piperidinylmethyl)), 2.78–2.87 (m, 2H, 2 CH (piperidinylmethyl)), 2.93 (br d, $J = 7.0$ Hz, 2H, 2 CH (piperidinylmethyl)), 3.15–3.22 (m, 2H, $SO_2NCH_2CH_2N$), 3.54 (s, 3H, CH_3 (Im)), 3.69–3.78 (m, 5H, $SO_2NCH_2CH_2N$, CH_3 (Im)), 4.68–4.76 (m, 2H, 2 CH (piperidinylmethyl)), 4.91 (s, 2H, CH_2 Im), 6.43 (t, $J = 4.9$ Hz, 1H, CH (pyrimidine)), 6.85 (d, $J = 9.5$ Hz, 1H, CH (Ar)), 6.97 (s, 1H, CH (Im)), 7.39 (s, 1H, CH (Im)), 7.42 (s, 1H, CH (Im)), 7.43 (s, 1H, CH (Im)), 7.66 (dd, $J = 9.0, 2.5$ Hz, 1H, CH (Ar)), 8.27 (t, $J = 4.9$ Hz, 2H, 2 CH (pyrimidine)), 8.41 (d, $J = 2.5$ Hz, 1H, CH (Ar)); δ_C (125 MHz, $CDCl_3$) 29.7, 31.9, 34.0, 35.7, 41.0 (br), 43.6, 46.3, 47.1, 56.0, 97.1, 106.1, 109.4, 118.3, 124.3, 127.3, 129.7, 139.0, 139.2, 139.4, 140.3, 152.4, 157.6, 158.5, 161.6; HRMS (ESI+) m/z calcd for $[C_{27}H_{33}N_{11}O_2S + H]$ 576.2618, obsd 576.2628; HPLC (I) $t_R = 12.43$ min (100%), (II) $t_R = 17.87$ min (100%).

[*N*-{2-[(5-Cyanopyrimidin-2-yl)-(3-methyl-3*H*-imidazol-4-ylmethyl)-amino]-ethyl}, *N*-{*N*-(2-Pyrimidinyl)-piperidin-4-ylmethyl}] 1-Methyl-1*H*-imidazole-4-sulfonamide (19d**)**

As per general procedure E with **18d** on a 0.187 mmol scale to afford [*N*-{2-[(5-bromopyrimidin-2-yl)-(3-methyl-3*H*-imidazol-4-ylmethyl)amino]ethyl}, *N*-{*N*-(2-pyrimidinyl)-piperidin-4-ylmethyl}] 1-methyl-1*H*-imidazole-4-sulfonamide as a white foam (109 mg, 93%): δ_H (500 MHz, $CDCl_3$) 1.17 (qd, $J = 12.2, 4.0$ Hz, 2H, 2 CH (piperidinylmethyl)), 1.78–1.84 (m, 2H, 2 CH (piperidinylmethyl)), 1.92–1.99 (m, 1H, CH (piperidinylmethyl)), 2.82 (td, $J = 12.8, 2.5$ Hz, 2H, 2 CH (piperidinylmethyl)), 3.10 (br d, $J = 7.5$ Hz, 2H, 2 CH (piperidinylmethyl)), 3.19–3.23 (m, 2H, $SO_2NCH_2-CH_2N$), 3.58 (s, 3H, CH_3 (Im)), 3.71–3.75 (m, 5H, $SO_2NCH_2-CH_2N$, CH_3 (Im)), 4.71–4.77 (m, 2H, 2 CH (piperidinylmethyl)), 4.89 (s, 2H, CH_2 Im), 6.43 (t, $J = 4.9$ Hz, 1H, CH (pyrimidine)), 7.05 (s, 1H, CH (Im)), 7.42 (s, 1H, CH (Im)), 7.43 (s, 1H, CH (Im)), 7.46 (s, 1H, CH (Im)), 8.28 (t, $J = 4.9$ Hz, 2H, 2 CH (pyrimidine)) 8.30 (s, 2H, 2 CH (Ar)); δ_C (125 MHz, $CDCl_3$) 29.7, 31.9, 33.9, 35.6, 40.7, 43.7, 46.0, 46.2, 55.8, 106.4, 109.3, 124.4, 128.1, 129.5, 138.5, 138.9, 139.3, 157.6, 158.0, 159.3, 161.6; HRMS (ESI) m/z calcd for $[C_{25}H_{32}N_{11}O_2SBr + H]$ 630.1723, obsd 630.1748; +HPLC (I) $t_R = 13.05$ min (100%), (II) $t_R = 19.52$ min (100%). The aryl bromide was then converted to the corresponding aryl nitrile on a 0.127 mmol scale, according to general procedure F. After workup, the crude material was dry-loaded onto silica gel and purified by flash column chromatography (eluent $CH_2Cl_2/MeOH/NH_4OH$, 192:7:1) to give **19d** as a white foam (50 mg, 69%): δ_H (500 MHz, $CDCl_3$) 1.16 (qd, $J = 12.2, 4.0$ Hz, 2H, 2 CH (piperidinylmethyl)), 1.75–1.82 (m, 2H, 2 CH (piperidinylmethyl)), 1.86–1.94 (m, 1H, CH (piperidinylmethyl)), 2.80 (td, $J = 12.8, 2.5$ Hz, 2H, 2 CH (piperidinylmethyl)), 3.07 (br d, $J = 7.5$ Hz, 2H, 2CH (piperidinylmethyl)), 3.26–3.30 (m, 2H, $SO_2NCH_2-CH_2N$), 3.58 (s, 3H, CH_3 (Im)), 3.74 (s, 3H, CH_3 (Im)), 3.83–3.87 (m, 2H, $SO_2NCH_2-CH_2N$), 4.70–4.76 (m, 2H, 2 CH (piperidinylmethyl)), 4.99 (s, 2H, CH_2 Im), 6.44 (t, $J = 4.8$ Hz, 1H, pyrimidine), 7.07 (s, 1H, CH (Im)), 7.39–7.44, (s, 3H, 3 CH (Im)), 8.28 (t, $J = 4.9$ Hz, 2H, 2 CH (pyrimidine)), 8.54 (br s, 2H, 2 CH (Ar)); δ_C (125 MHz, $CDCl_3$) 29.7, 32.0, 34.0, 35.8, 40.9, 43.7, 46.3, 46.5, 55.9, 96.8, 109.5, 116.2, 124.5, 127.2, 129.8, 138.8, 139.0, 139.3, 157.7, 160.6, 161.0, 161.6; HRMS (ESI+) m/z calcd for $[C_{26}H_{32}N_{12}O_2S + H]$ 577.2570, obsd 577.2569; HPLC (I) $t_R = 12.45$ min (100%), (II) $t_R = 17.94$ min (100%).

[*N*-{2-[(3-Fluoro-4-cyanophenyl)-(3-methyl-3*H*-imidazol-4-ylmethyl)-amino]-ethyl}, *N*-{*N*-(2-Pyrimidinyl)-piperidin-4-ylmethyl}] 1-Methyl-1*H*-imidazole-4-sulfonamide (19e)

As per general procedure E with **18e** on a 0.0683 mmol scale. After the usual workup, the crude material was purified by silica gel flash column chromatography (eluent CH₂Cl₂/MeOH/NH₄OH, 192:7:1) to furnish **19e** as a white foam (36 mg, 89%): δ_{H} (500 MHz, CDCl₃) 1.10 (qd, $J = 12.2, 4.0$ Hz, 2H, 2 CH (piperidinylmethyl)), 1.60–1.67 (m, 1H, CH (piperidinylmethyl)), 1.69–1.75 (m, 2H, 2 CH (piperidinylmethyl)), 2.80 (td, $J = 12.8, 2.5$ Hz, 2H, 2 CH (piperidinylmethyl)), 2.95 (br d, $J = 7.5$ Hz, 2H, 2 CH (piperidinylmethyl)), 3.20–3.24 (m, 2H, SO₂NCH₂CH₂N), 3.56 (s, 3H, CH₃ (Im)), 3.62–3.66 (m, 2H, SO₂NCH₂CH₂N), 3.72 (m, 3H, CH₃ (Im)), 4.52 (s, 2H, CH₂Im), 4.67–4.73 (m, 2H, 2 CH (piperidinylmethyl)), 6.43 (t, $J = 4.7$ Hz, 1H, CH (pyrimidine)), 6.60 (dd, $J = 13.0, 2.5$ Hz, 1H, CH (Ar)), 6.67 (dd, $J = 9.0, 2.5$ Hz, 1H, CH (Ar)), 6.87 (s, 1H, CH (Im)), 7.37–7.40 (m, 2H, CH (Im), CH (Ar)), 7.43 (s, 1H, CH (Im)), 7.48 (s, 1H, CH (Im)), 8.26 (t, $J = 4.7$ Hz, 2H, 2 CH (pyrimidine)); δ_{C} (125 MHz, CDCl₃) 29.5, 31.7, 34.0, 35.9, 43.5, 44.5, 46.5, 49.3, 56.3, 88.1 (d, $J_{\text{CF}} = 15.5$ Hz), 99.3 (d, $J_{\text{CF}} = 24.6$ Hz), 108.4 (d, $J_{\text{CF}} = 1.9$ Hz), 109.5, 115.2, 124.4, 126.3, 129.1, 134.3 (d, $J_{\text{CF}} = 2.75$ Hz), 139.0, 139.1, 139.2, 152.7 (d, $J_{\text{CF}} = 10.9$ Hz), 157.6, 161.5, 164.9 (d, $J_{\text{CF}} = 252$ Hz); HRMS (ESI+) m/z calcd for [C₂₈H₃₃N₁₀O₂SF + H] 593.2571, obsd 593.2588; HPLC (I) $t_{\text{R}} = 12.54$ min (98.51%), (II) $t_{\text{R}} = 18.51$ min (98.09%).

[*N*-{2-[(2-Fluoro-4-cyanophenyl)-(3-methyl-3*H*-imidazol-4-ylmethyl)-amino]-ethyl}, *N*-{*N*-(2-Pyrimidinyl)-piperidin-4-ylmethyl}] 1-Methyl-1*H*-imidazole-4-sulfonamide (19f)

As per general procedure E with **18f** on a 0.060 mmol scale. After the usual workup, the crude material was purified by silica gel flash column chromatography (eluent CH₂Cl₂/MeOH/NH₄OH, 192:7:1) to afford **19f** as a white foam (33 mg, 93%): δ_{H} (500 MHz, CDCl₃) 1.09 (qd, $J = 12.3, 4.0$ Hz, 2H, 2 CH (piperidinylmethyl)), 1.70–1.78 (m, 3H, 3 CH (piperidinylmethyl)), 2.76–2.83 (m, 2H, 2 CH (piperidinylmethyl)), 2.95 (br d, $J = 7.0$ Hz, 2H, 2 CH (piperidinylmethyl)), 3.31 (br t, $J = 7.5$ Hz, 2H, SO₂NCH₂CH₂N), 3.53 (br t, $J = 7.5$ Hz, 2H, SO₂NCH₂CH₂N), 3.58 (m, 3H, CH₃ (Im)), 3.73 (m, 3H, CH₃ (Im)), 4.50 (s, 2H, CH₂Im), 4.67–4.73 (m, 2H, 2 CH (piperidinylmethyl)), 6.43 (t, $J = 4.7$ Hz, 1H, CH (pyrimidine)), 6.93 (s, 1H, CH (Im)), 7.06 (t, $J = 8.8$ Hz, 1H, CH (Ar)), 7.28 (dd, $J = 13.0, 1.8$ Hz, 1H, CH (Ar)), 7.31 (br dd, $J = 8.5, 1.8$ Hz, 1H, CH (Ar)), 7.37 (s, 1H, CH (Im)), 7.41 (s, 1H, CH (Im)), 7.48 (s, 1H, CH (Im)), 8.26 (t, $J = 4.7$ Hz, 2H, 2 CH (pyrimidine)); δ_{C} (125 MHz, CDCl₃) 29.6, 31.8, 34.0, 35.9, 43.5, 45.9, 47.5, 50.5, 55.8, 103.0 (d, $J_{\text{CF}} = 10$ Hz), 109.4, 118.2 (d, $J_{\text{CF}} = 1.8$ Hz), 119.5 (d, $J_{\text{CF}} = 4.6$ Hz), 120.2 (d, $J_{\text{CF}} = 25.5$ Hz), 124.2, 126.9, 129.3, 129.5 (d, $J_{\text{CF}} = 2.8$ Hz), 138.9, 139.0, 139.6, 141.5 (d, $J_{\text{CF}} = 8.1$ Hz), 152.9 (d, $J_{\text{CF}} = 244$ Hz), 157.6, 161.5; HRMS (ESI+) m/z calcd for [C₂₈H₃₃N₁₀O₂-FS + H] 593.2571, obsd 593.2568; HPLC (I) $t_{\text{R}} = 12.75$ min (100%), (II) $t_{\text{R}} = 19.09$ (99.22%).

[*N*-{2-[(2,6-Difluoro-4-cyanophenyl)-(3-methyl-3*H*-imidazol-4-ylmethyl)-amino]-ethyl}, *N*-{*N*-(2-Pyrimidinyl)-piperidin-4-ylmethyl}] 1-Methyl-1*H*-imidazole-4-sulfonamide (19g)

As per general procedure E with **18g** on a 0.068 mmol scale. After the usual workup, the crude material was purified by silica gel flash column chromatography (eluent CH₂Cl₂/MeOH/NH₄OH, 192:7:1) to yield **19g** as a white foam (40 mg, 97%): δ_{H} (500 MHz, CDCl₃) 1.06 (qd, $J = 12.3, 4.0$ Hz, 2H, 2 CH (piperidinylmethyl)), 1.67–1.77 (m, 3H, 3 CH (piperidinylmethyl)), 2.78 (td, $J = 12.8, 2.5$ Hz, 2H, 2 CH (piperidinylmethyl)), 2.96 (br d, $J = 6.5$ Hz, 2H, 2 CH (piperidinylmethyl)), 3.26–3.30 (m, 2H, SO₂NCH₂CH₂N), 3.39–3.43 (m, 2H, SO₂NCH₂CH₂N), 3.57 (s, 3H, CH₃ (Im)), 3.73 (s, 3H, CH₃ (Im)), 4.38 (s, 2H, CH₂Im), 4.66–4.73 (m, 2H, 2 CH (piperidinylmethyl)), 6.42 (t, $J = 4.9$ Hz, 1H, CH (pyrimidine)), 6.92 (s, 1H, CH (Im)), 7.12–7.17 (m, 2H, 2 CH (Ar)), 7.35 (s, 1H, CH (Im)), 7.40 (s, 1H, CH (Im)), 7.42 (s, 1H, CH (Im)), 8.26 (t, $J = 4.9$ Hz, 2H, 2 CH (pyrimidine)); δ_{C} (125 MHz, CDCl₃) 29.6, 31.4, 33.9, 36.0, 43.5, 46.3 (t, $J_{\text{CF}} = 4.5$ Hz), 47.8, 51.9 (t, $J_{\text{CF}} = 2.6$ Hz), 55.6, 106.9 (t, $J_{\text{CF}} = 11.9$ Hz), 109.4, 116.6 (m), 116.6 (t, $J_{\text{CF}} = 2.8$ Hz), 124.1,

126.9, 129.9, 131.1 (t, $J = 13.3$ Hz), 138.9, 139.2, 139.7, 157.6, 158.3 (dd, $J_{CF} = 249, 8.3$ Hz), 161.5; HRMS (ESI+) m/z calcd for $[C_{28}H_{32}N_{10}O_2F_2S + H]$ 611.2477, obsd 611.2494; + HPLC (I) $t_R = 12.93$ min (100%), (II) $t_R = 19.59$ min (100%).

[*N*-{2-[(2,3,5,6-Tetrafluoro-4-cyanophenyl)-(3-methyl-3*H*-imidazol-4-ylmethyl)-amino]-ethyl}, *N*-{*N*-(2-Pyrimidinyl)-piperidin-4-ylmethyl}] 1-Methyl-1*H*-imidazole-4-sulfonamide (19h)

As per general procedure **E** with **18h** on a 0.0688 mmol scale. After the usual workup, the crude material was purified by silica gel flash column chromatography (eluent $CH_2Cl_2/MeOH/NH_4OH$, 192:7:1) to afford **19h** as a white foam (28 mg, 63%): δ_H (500 MHz, $CDCl_3$) 1.08 (qd, $J = 12.2, 4.0$ Hz, 2H, 2 CH (piperidinylmethyl)), 1.69–1.81 (m, 3H, 3 CH (piperidinylmethyl)), 2.80 (td, $J = 12.8, 2.5$ Hz, 2H, 2 CH (piperidinylmethyl)), 2.96 (br d, $J = 7.5$ Hz, 2H, 2 CH (piperidinylmethyl)), 3.34–3.40 (m, 2H, $SO_2NCH_2CH_2N$), 3.51–3.56 (m, 2H, $SO_2NCH_2CH_2N$), 3.57 (s, 3H, CH_3 (Im)), 3.74 (s, 3H, CH_3 (Im)), 4.53 (s, 2H, CH_2 Im), 4.68–4.74 (m, 2 H, 2 CH (piperidinylmethyl)), 6.43 (t, $J = 4.7$ Hz, 1H, CH (pyrimidine)), 6.98 (s, 1H, CH (Im)), 7.38 (s, 1H, CH (Im)), 7.41–7.46 (m, 2H, 2 CH (Im)), 8.27 (t, $J = 4.7$ Hz, 2H, CH (pyrimidine)); δ_C (125 MHz, $CDCl_3$) 29.6, 31.5, 33.9, 36.0, 43.5, 46.2, 47.9, 51.9 (m), 55.7, 86.9 (t, $J_{CF} = 17.4$ Hz), 107.8 (m), 109.5, 124.2, 126.2, 130.2, 133.9 (m), 139.0, 139.4, 139.6, 142.1 (dm), 147.8 (dm), 157.6, 161.5; HRMS (ESI+) m/z calcd for $[C_{28}H_{30}N_{10}O_2F_4S + H]$ 647.2288, obsd 647.2314; HPLC (I) $t_R = 12.74$ min (98.92%), (II) $t_R = 19.07$ min (98.14%).

***N*-(2-Aminoethyl)-*N*-(cyclohexylmethyl)pyridine-2-sulfonamide (21)**

Mono-*N*-Boc-ethylenediamine (**6**; 860 mg, 5.37 mmol, 1 equiv) was reacted with pyridine-2-sulfonyl chloride according to general procedure A. After workup, the crude material was dry-loaded onto silica gel and purified by flash column chromatography (eluent $CH_2Cl_2/MeOH/NH_4OH$, 92:7:1) to afford *tert*-butyl 2-(pyridine-2-sulfonamido)ethylcarbamate as a white powder (1.26 g, 80%): δ_H (400 MHz, $DMSO-d_6$) 0.89 (s, 9H, $C(CH_3)_3$), 2.04 (m, 2H, $SO_2NHCH_2CH_2NHBoc$), 2.86 (m, 2H, $SO_2NHCH_2CH_2NHBoc$), 6.30 (br, 1H, NH_{SO_2}), 7.21 (m, 1H, CH (Py)), 7.414 (m, 1H, $NHBoc$), 7.47 (m, 1H, CH (Py)), 7.63 (m, 1H, CH (Py)), 8.27 (m, 1H, CH (Py)); δ_C (125 MHz, $DMSO-d_6$) 28.0, 39.9, 42.5, 77.6, 121.4, 126.8, 138.5, 149.8, 155.3, 157.7; HRMS (ESI+) m/z calcd for $[C_{12}H_{19}N_3O_4S + H]$ 302.1175, obsd 302.1174. The sulfonamide NH of *tert*-butyl 2-(pyridine-2-sulfonamido)ethylcarbamate (1.1 g, 3.65 mmol, 1 equiv) was then chemoselectively alkylated with cyclohexylmethyl bromide (840 mg, 4.75 mmol, 1.3 equiv) according to general procedure **B**, but the reaction was stirred for 4 days at room temperature. After workup, the crude material was dry-loaded onto silica gel and purified by flash column chromatography (eluent $CH_2Cl_2/MeOH/NH_4OH$, 92:7:1) to furnish *tert*-butyl 2-(*N*-(cyclohexylmethyl)pyridine-2-sulfonamido)ethylcarbamate in quantitative yield (1.53 g) as a white solid: δ_H (500 MHz, $DMSO-d_6$) 0.77–0.83 (m, 2H, 2 CH (cyclohexylmethyl)), 1.09–1.19 (m, 3H, 3 CH (cyclohexylmethyl)), 1.36 (s, 9H, $C(CH_3)_3$), 1.54–1.65 (m, 6H, 6 CH (cyclohexylmethyl)), 3.03–3.07 (m, 4H, $SO_2NCH_2CH_2-NHBoc$, NCH_2CH (cyclohexylmethyl)), 3.24 (t, $J = 7.0$ Hz, 2H, $SO_2NCH_2CH_2NHBoc$), 6.79 (br, 1H, $NHBoc$), 7.67 (m, 1H, CH (Py)), 7.92 (m, 1H, CH (Py)), 8.09 (m, 1H, CH (Py)), 8.72 (m, 1H, CH (Py)); δ_C (125 MHz, $DMSO-d_6$) 25.1, 25.8, 28.0, 29.9, 35.6, 39.9, 48.4, 55.4, 77.6, 122.1, 127.0, 138.6, 150.0, 155.3, 157.1; HRMS (ESI+) m/z calcd for $[C_{19}H_{31}N_3O_4S + H]$ 398.2114, obsd 398.2113. *tert*-Butyl 2-(*N*-(cyclohexylmethyl)pyridine-2-sulfonamido)ethylcarbamate (1.28 g, 3.22 mmol, 1 equiv) was dissolved in propan-2-ol (15 mL). Upon complete dissolution of the solid, 4 M HCl (15 mL) was added, and the reaction was stirred for one hour. All solvents were then evaporated. The residue was redissolved in CH_2Cl_2 (250 mL) and carefully washed with saturated $NaHCO_3$ (25 mL \times 3), dried (Na_2SO_4), filtered, and concentrated to afford *N*-(2-aminoethyl)-*N*-(cyclohexylmethyl)pyridine-2-sulfonamide (**21**) as a viscous oil (945 mg, 97%): δ_H (500 MHz, $DMSO-d_6$) 0.78–0.84 (m,

2H, 2 CH (cyclohexylmethyl)), 1.09–1.17 (m, 3H, 3 CH (cyclohexylmethyl)), 1.57–1.68 (m, 6H, 6 CH (cyclohexylmethyl)), 2.75 (t, $J = 7.0$ Hz, 2H, NCH_2CH (cyclohexylmethyl)), 3.04 (t, $J = 7.4$ Hz, 2H, $\text{SO}_2\text{NCH}_2\text{CH}_2\text{NH}_2$), 3.34 (t, $J = 7.4$ Hz, 2H, $\text{SO}_2\text{NCH}_2\text{CH}_2\text{NH}_2$), 5.15 (br, 2H, NH_2), 7.68 (m, 1H, CH (Py)), 7.93 (m, 1H, CH (Py)), 8.10 (m, 1H, CH (Py)), 8.73 (m, 1H, CH (Py)); δ_{C} (125 MHz, DMSO) 25.1, 25.8, 29.9, 35.7, 49.4, 55.5, 66.2, 122.2, 127.1, 138.7, 150.0, 157.1; HRMS (ESI+) m/z calcd for $[\text{C}_{14}\text{H}_{23}\text{N}_3\text{O}_2\text{S} + \text{H}]$ 298.1589, obsd 298.1589.

(2-((4-Cyanophenyl)((1-methyl-1*H*-imidazol-5-yl)methyl)amino)ethyl)-*N*-(cyclohexylmethyl)pyridine-2-sulfonamide (21a)

The primary amine of *N*-(2-aminoethyl)-*N*-(cyclohexylmethyl)-pyridine-2-sulfonamide (**21**) was arylated with *p*-fluorobenzonitrile on a 0.336 mmol scale, according to general procedure **D**. After workup and purification by silica gel flash column chromatography (eluent $\text{CH}_2\text{Cl}_2/\text{MeOH}/\text{NH}_4\text{OH}$, 192:7:1), *N*-(2-(4-cyanophenylamino)ethyl)-*N*-(cyclohexylmethyl)-pyridine-2-sulfonamide was obtained as a colorless gum (119 mg, 89%): δ_{H} (500 MHz, DMSO- d_6) 0.77–0.83 (m, 2H, 2 CH (cyclohexylmethyl)), 1.09 (br, 3H, 3 CH (cyclohexyl)), 1.48–1.63 (m, 6H, 6 CH (cyclohexylmethyl)), 3.06 (d, $J = 6.4$ Hz, 2H, NCH_2CH (cyclohexylmethyl)), 3.28–3.38 (m, 4H, $\text{SO}_2\text{NCH}_2\text{CH}_2\text{NHAr}$), 6.61 (d, $J = 8.5$ Hz, 2H, 2 CH (Ar)), 6.70 (t, $J = 6.4$ Hz, 1H, NH), 7.45 (d, $J = 8.5$ Hz, 2H, 2 CH (Ar)), 7.66 (m, 1H, CH (Py)), 7.94 (m, 1H, CH (Py)), 8.07 (m, 1H, CH (Py)), 8.73 (m, 1H, CH (Py)); δ_{C} (125 MHz, DMSO) 25.1, 25.8, 29.9, 35.8, 41.5, 47.7, 55.6, 95.9, 111.6, 120.3, 122.2, 127.1, 133.3, 138.6, 150.1, 151.6, 157.0; HRMS (ESI+) m/z calcd for $[\text{C}_{21}\text{H}_{26}\text{N}_4\text{O}_2\text{S} + \text{H}]$ 399.1855, obsd 399.1857. *N*-(2-(4-Cyanophenylamino)ethyl)-*N*-(cyclohexylmethyl)pyridine-2-sulfonamide was then alkylated with 5-chloromethyl-1*H*-imidazole-3 HCl according to general procedure **E** on a 0.117 mmol scale. After workup and chromatography over silica gel (eluent $\text{CH}_2\text{Cl}_2/\text{MeOH}/\text{NH}_4\text{OH}$, 192:7:1), the title compound *N*-(2-((4-cyanophenyl)((1-methyl-1*H*-imidazol-5-yl)methyl)amino)ethyl)-*N*-(cyclohexylmethyl)-pyridine-2-sulfonamide (**21a**) was furnished as a glassy film (46 mg, 80%): δ_{H} (500 MHz, CDCl_3) 0.84–0.78 (m, 2H, 2 CH (cyclohexylmethyl)), 1.06–1.14 (m, 3H, 3 CH (cyclohexylmethyl)), 1.35–1.27 (m, 1H, CH (cyclohexylmethyl)), 1.66–1.59 (m, 5H, 5 CH (cyclohexylmethyl)), 2.95 (d, $J = 7.0$ Hz, 2H, NCH_2CH (cyclohexyl)), 3.36 (t, $J = 7.9$ Hz, 2H, $\text{SO}_2\text{NCH}_2\text{CH}_2\text{N}$), 3.61 (s, 3H, CH_3 (Im)), 3.65 (t, $J = 7.9$ Hz, 2H, $\text{SO}_2\text{NCH}_2\text{CH}_2\text{N}$), 4.55 (s, 2H, CH_2 Im), 6.85 (d, $J = 9.0$ Hz, 2H, 2 CH (Ar)), 6.88 (s, 1H, CH (Im)), 7.47–7.44 (m, 3H, 2 CH (Ar), CH (Im)), 7.71 (s, 1H, CH (Py)), 7.91–7.86 (m, 2H, 2 CH (Py)), 8.61 (m, 1H, CH (Py)); δ_{C} (125 MHz, CDCl_3) 25.6, 26.2, 30.6, 32.0, 36.9, 44.3, 46.8, 49.4, 57.1, 99.5, 112.3, 119.9, 122.5, 126.6, 127.2, 127.7, 133.8, 137.9, 138.7, 149.9, 150.4, 157.5; HRMS (ESI+) m/z calcd for $[\text{C}_{26}\text{H}_{32}\text{N}_6\text{O}_2\text{S} + \text{H}]$ 493.2386, obsd 493.2364.

***N*-(2-((4-Cyano-2-fluorophenyl)((1-methyl-1*H*-imidazol-5-yl)-methyl)amino)ethyl)-*N*-(cyclohexylmethyl)pyridine-2-sulfonamide (21b)**

The primary amine of *N*-(2-aminoethyl)-*N*-(cyclohexylmethyl)pyridine-2-sulfonamide (**21**) was arylated with 3,4-difluorobenzonitrile on a 0.337 mmol scale, according to general procedure **D**. After workup and purification by silica gel flash column chromatography (eluent $\text{CH}_2\text{Cl}_2/\text{MeOH}/\text{NH}_4\text{OH}$, 192:7:1), *N*-(2-(4-cyano-2-fluorophenylamino)ethyl)-*N*-(cyclohexylmethyl)pyridine-2-sulfonamide was obtained as a white foam (111 mg, 79%): δ_{H} (500 MHz, DMSO- d_6) 0.83–0.77 (m, 2H, 2 CH (cyclohexylmethyl)), 1.09 (br, 3H, 3 CH (cyclohexylmethyl)), 1.62–1.51 (m, 6H, 6 CH (cyclohexylmethyl)), 3.06 (d, $J = 7.5$ Hz, 2H, NCH_2CH (cyclohexyl)), 3.42–3.34 (m, 4H, $\text{SO}_2\text{NCH}_2\text{CH}_2\text{N}$), 6.54 (br, 1H, NHAr), 6.80 (t, $J = 8.5$ Hz, 1H, CH (Ar)), 7.45 (dd, $J = 11.5, 1.5$ Hz, 1H, CH (Ar)), 7.53 (dd, $J = 8.5, 1.5$ Hz, 1H, CH (Ar)), 7.66 (m, 1H, CH (Py)), 7.93 (m, 1H, CH (Py)), 8.07 (m, 1H, CH (Py)), 8.71 (m, 1H, CH (Py)); δ_{C} (125 MHz, DMSO- d_6) 25.1, 25.9, 30.0, 35.7, 37.1, 41.3, 47.5, 55.5, 61.8, 94.4, 122.2, 127.1, 130.4, 138.7, 140.7, 142.5, 150.1, 156.9, 179.7; HRMS (ESI

+) m/z calcd for $[C_{21}H_{25}FN_4O_2S + H]$ 417.1760, obsd 417.1749. *N*-(2-(4-Cyano-2-fluorophenylamino)ethyl)-*N*-(cyclohexylmethyl)pyridine-2-sulfonamide was then alkylated with 5-chloromethyl-1*H*-imidazole·HCl according to general procedure E on a 0.216 mmol scale. After workup and chromatography over silica gel (eluent $CH_2Cl_2/MeOH/NH_4OH$, 192:7:1), the title compound *N*-(2-((4-cyano-2-fluorophenyl)((1-methyl-1*H*-imidazol-5-yl)methyl)amino)ethyl)-*N*-(cyclohexylmethyl)-pyridine-2-sulfonamide was afforded as a white foam (90 mg, 81%): δ_H (500 MHz, $CDCl_3$) 0.68–0.75 (m, 2H, 2 CH (cyclohexylmethyl)), 1.03 (br, 3H, 3 CH (cyclohexylmethyl)), 1.23–1.32 (m, 1H, CH (cyclohexylmethyl)), 1.50–1.60 (m, 5H, 5 CH (cyclohexylmethyl)), 2.80 (s, 2H, NCH_2CH (cyclohexylmethyl)), 3.34–3.47 (m, 4H, $SO_2NCH_2CH_2N$), 3.54 (s, 3H, CH_3 (Im)), 4.46 (s, 2H, CH_2 Im), 6.61 (br, 1H, CH (Ar)), 6.95 (s, 1H, CH (Im)), 7.11 (m, 1H, CH (Ar)), 7.26 (br, 1H, CH (Ar)), 7.53 (m, 2H, CH (Py), CH (Im)) 7.65 (br, 1H, CH (Py)), 8.26 (m, 1H, CH (Py)), 8.69 (m, 1H, CH (Py)); δ_C (125 MHz, $CDCl_3$) 25.5, 26.1, 30.5, 31.3, 31.8, 36.6, 45.7, 47.3, 50.4, 56.4, 102.9, 118.1, 119.5, 120.2, 122.4, 126.5, 128.7, 129.3, 138.8, 141.3, 149.8, 153.9, 157.6, 162.4; HRMS (ESI+) m/z calcd for $[C_{26}H_{31}FN_6O_2S + H]$ 511.2291, obsd 511.2265; + HPLC (I) t_R = 18.69 min (99.3%), (II) t_R = 36.03 min (99.7%).

***N*-(2-((5-Cyanopyridin-2-yl)((1-methyl-1*H*-imidazol-5-yl)-methyl)amino)ethyl)-*N*-(cyclohexylmethyl)pyridine-2-sulfonamide (21c)**

The primary amine of *N*-(2-aminoethyl)-*N*-(cyclohexylmethyl)pyridine-2-sulfonamide (**21**) was arylated with 5-cyano-2-fluoropyridine on a 0.350 mmol scale, according to general procedure D. After workup and purification by silica gel flash column chromatography (eluent $CH_2Cl_2/MeOH/NH_4OH$, 192:7:1), *N*-(2-(5-cyanopyridin-2-ylamino)ethyl)-*N*-(cyclohexylmethyl)pyridine-2-sulfonamide was obtained as a colorless gum (115 mg, 82%): δ_H (500 MHz, $DMSO-d_6$) 0.78–0.82 (m, 2H, 2 CH (cyclohexylmethyl)), 1.09 (br, 3H, 3 CH (cyclohexylmethyl)), 1.57–1.63 (m, 6H, 6 CH (cyclohexylmethyl)), 3.06 (d, J = 7.5 Hz, 2H, NCH_2CH (cyclohexylmethyl)), 3.37–3.47 (m, 4H, $SO_2-NCH_2CH_2N$), 6.50 (t, J = 8.5 Hz, NH), 6.87 (d, J = 9.0 Hz, 1H, CH (Ar)), 7.61–7.66 (m, 3H, 2 CH (Ar), CH (Py)), 7.92 (d, J = 7.5 Hz, 1H, CH (Py)), 8.06 (m, 1H, CH (Py)), 8.36 (m, 1H, CH (Ar)), 8.71 (m, 1H, CH (Py)); δ_C (125 MHz, $DMSO-d_6$) 25.1, 25.8, 30.0, 35.6, 47.7, 54.7, 55.5, 69.3, 94.7, 108.7, 118.7, 122.1, 126.9, 138.5, 150.0, 152.8, 157.0, 159.6; HRMS (ESI+) m/z calcd for $[C_{20}H_{25}N_5O_2S + H]$ 400.1807, obsd 400.1795. *N*-(2-(5-Cyanopyridin-2-ylamino)ethyl)-*N*-(cyclohexylmethyl)pyridine-2-sulfonamide was then alkylated with 5-chloromethyl-1*H*-imidazole·HCl according to general procedure E on a 0.240 mmol scale. After workup and chromatography over silica gel (eluent $CH_2Cl_2/MeOH/NH_4OH$, 192:7:1), the title compound *N*-(2-((5-cyanopyridin-2-yl)((1-methyl-1*H*-imidazol-5-yl)methyl)-amino)ethyl)-*N*-(cyclohexylmethyl)pyridine-2-sulfonamide was afforded as a white foam (110 mg, 93%): δ_H (500 MHz, $CDCl_3$) 0.75–0.83 (m, 2H, 2 CH (cyclohexylmethyl)), 1.07–1.16 (m, 3H, 3 CH (cyclohexylmethyl)), 1.33–1.43 (m, 1H, CH (cyclohexylmethyl)), 1.59–1.65 (m, 5H, 5 CH (cyclohexylmethyl)), 2.94 (d, J = 7.0 Hz, 2H, NCH_2CH (cyclohexylmethyl)), 3.28 (t, J = 8.1 Hz, 2H, $SO_2NCH_2CH_2N$), 3.55 (s, 3H, CH_3 (Im)), 3.70 (t, J = 8.1 Hz, 2H, $SO_2NCH_2CH_2N$), 4.89 (s, 2H, CH_2 Im), 6.81 (d, J = 9.0 Hz, 1H, CH (Ar)), 6.97 (s, 1H, CH (Im)), 7.45 (m, 1H, CH (Im)), 7.57 (s, 1H, CH (Ar)), 7.64 (m, 1H, CH (Ar)), 7.89–7.85 (m, 2H, 2 CH (Py)), 8.39–8.38 (m, 1H, CH (Ar)), 8.60 (m, 1H, CH (Py)); δ_C (125 MHz, $CDCl_3$) 25.6, 26.2, 30.5, 32.0, 36.6, 40.9, 47.2, 56.8, 97.1, 105.9, 118.2, 122.5, 126.6, 127.4, 128.8, 137.9, 138.9, 140.2, 149.9, 152.3, 157.5, 158.4, 162.4; HRMS (ESI+) m/z calcd for $[C_{25}H_{31}N_7O_2S + H]$ 494.2338, obsd 494.2313; HPLC + (I) t_R = 18.15 min (99.5%), (II) t_R = 34.66 min (97.4%).

In Vitro and Whole Cell Inhibition Assays of Protein Prenylation

In vitro inhibition assays for FTase and GGTase-I were conducted by measuring the incorporation of $[^3H]FPP$ and $[^3H]GGPP$ into recombinant H-Ras-CVLS and H-Ras-CVLL,

respectively, as previously described.³⁶ The in vivo inhibition of farnesylation and geranylgeranylation was determined based on the level of inhibition by synthetic compounds of H-Ras and Rap1A processing, respectively.³⁷ Briefly, oncogenic H-Ras-transformed NIH3T3 cells were treated with various concentrations of inhibitors, and the cell lysates were isolated and proteins separated on a 12.5% SDS-PAGE gel. The separated proteins were transferred to nitrocellulose and immunoblotted using an anti-Ras antibody (Y13–258) or an anti-Rap1A antibody (SantaCruz Biotechnology, Santa Cruz, CA), respectively. Antibody reactions were visualized using either peroxidase-conjugated goat antirat IgG or goat antirabbit IgG (Jackson ImmunoResearch, West Grove, PA) and an enhanced chemiluminescence detection system.

Acknowledgments

Financial support for this work was provided by the National Institutes of Health (CA67771 & GM52382) and the Medicines for Malaria Venture (MMV). We also thank Vijay M. Shahani for additional assistance in the flexible ligand GOLD docking experiments.

References

1. Basso AD, Kirschmeier P, Bishop WR. Lipid posttranslational modifications. Farnesyltransferase inhibitors. *J. Lipid Res* 2006;47:15–31. [PubMed: 16278491]
2. Bell I. Inhibitors of farnesyltransferase: a rational approach to cancer chemotherapy? *J. Med. Chem* 2004;47:1869–1878. [PubMed: 15055985]
3. Doll RJ, Kirschmeier P, Bishop WR. Farnesyltransferase inhibitors as anticancer agents: critical crossroads. *Curr. Opin. Drug Discovery Dev* 2004;7:478–486.
4. Shields JM, Pruitt K, McFall A, Shaub A, Der CJ. Understanding Ras: “It ain't over 'til it's over”. *Trends Cell Biol* 2000;10:147–154. [PubMed: 10740269]
5. Bos JL. Ras oncogenes in human cancer: A review. *Cancer Res* 1989;49:4682–4689. [PubMed: 2547513]
6. Clark, GJ.; Der, CJ. Ras proto-oncogene activation in human malignancy. In: Garrett, CT.; Sell, S., editors. *Cellular Cancer Markers*. Humana Press; Totowa, NJ: 1995. p. 17-52.
7. Willumsen BM, Norris K, Papageorge AG, Hubbert NL, Lowy DR. Harvey murine sarcoma virus p21 Ras protein: biological and biochemical significance of the cysteine nearest the carboxy terminus. *EMBO J* 1984;3:2581–2585. [PubMed: 6096132]
8. Casey PJ, Solski PA, Der C, Buss JE. p21 Ras is modified by a farnesyl isoprenoid. *Proc. Natl. Acad. Sci. U.S.A* 1989;86:8323–8327. [PubMed: 2682646]
9. Sousa SF, Fernandes PA, Ramos MJ. Farnesyltransferase inhibitors: a detailed chemical view on an elusive biological problem. *Curr. Med. Chem* 2008;15:1478–1492. [PubMed: 18537624]
10. Asoh K, Kohchi M, Hyoudoh I, Ohtsuka T, Masubuchi M, Kawasaki K, Ebiike H, Shiratori Y, Fukami TA, Kondoh O, Tsukaguchi T, Ishii N, Aoki Y, Shimma N, Sakaitani M. Synthesis and structure-activity relationships of novel benzofuran farnesyltransferase inhibitors. *Bioorg. Med. Chem. Lett* 2009;19:1753–1757. [PubMed: 19217288]
11. Lethu S, Ginisty M, Bosc D, Joelle D. Discovery of a new class of protein farnesyltransferase inhibitors in the arylthiophene series. *J. Med. Chem* 2009;55:6205–6208. [PubMed: 19772293]
12. Bell IM. Inhibitors of protein prenylation 2000. *Exp. Opin. Ther. Patents* 2000;10:1813–1831.
13. Venet M, End D, Angibaud P. Farnesyl Protein Transferase Inhibitor ZARNESTRA R115777–History of a Discovery. *Curr. Top. Med. Chem* 2003;3:1095–1102. [PubMed: 12769710]
14. Rao S, Cunningham D, de Gramont A, Shceithauer W, Smakal M, Humblet Y, Kourteva G, Iveson T, Andre T, Dostalova J, Illes A, Belly R, Perez-Ruixo JJ, Park YC, Palmer PA. Phase III double-blind placebo-controlled study of farnesyl transferase inhibitor R115777 in patients with refractory advanced colorectal cancer. *J. Clin. Oncol* 2004;22:3950–3957. [PubMed: 15459217]
15. Macdonald JS, McCoy S, Whitehead RP, Iqbal S, Wade JL III, Giguere JK, Abbruzzese JL. A phase II study of farnesyl transferase inhibitor R115777 in pancreatic cancer: a Southwest oncology group (SWOG 9924) study. *Invest. New Drugs* 2005;23:485–487. [PubMed: 16133800]

16. Sparano JA, Moulder S, Kazi A,A, Coppola D, Negassa A,A, Vahdat L, Li T, Pellegrino C, Fineberg S, Munster P, Malafa M, Lee D, Hoschander S, Hopkins U, Hershman D, Wright JJ, Kleer C, Merajver S, Sebti SM. Phase II trial of tipifarnib plus neoadjuvant doxorubicin-cyclophosphamide in patients with clinical stage IIB–IIIC breast cancer. *Clin. Cancer Res* 2009;15:2942–2948. [PubMed: 19351752]
17. Sparano JA, Moulder S, Kazi A, Vahdat L, Li T, Pellegrino C, Munster P, Malafa M, Lee D, Hoschander S, Hopkins U, Hershman D, Wright JJ, Sebti SM. Targeted inhibition of farnesyltransferase in locally advanced breast cancer: a phase I and II trial of tipifarnib plus dose-dense doxorubicin and cyclophosphamide. *J. Clin. Oncol* 2006;24:3013–3018. [PubMed: 16769985]
18. Falsetti SC, Wang DA, Peng H, Carrico D, Cox AD, Der CJ, Hamilton AD, Sebti SM. Geranylgeranyltransferase I inhibitors target RalB to inhibit anchorage-dependent growth and induce apoptosis and RalA to inhibit anchorage-independent growth. *Mol. Cell. Biol* 2007;27:8003–8014. [PubMed: 17875936]
19. Prendergast GC, Rane N. Farnesyltransferase Inhibitors: Mechanism and Applications. *Expert Opin. Invest. Drugs* 2001;10:2105–2116.
20. Liu A-X, Du W, Liu J-P, Jessell TM, Prendergast GC. RhoB Alteration Is Necessary for Apoptotic and Antineoplastic Responses to Farnesyltransferase Inhibitors. *Mol. Cell. Biol* 2000;20:6105–6113. [PubMed: 10913192]
21. Chen Z, Sun J, Pradines A, Favre G, Adnane J, Sebti SM. Both Farnesylated and Geranylgeranylated RhoB Inhibit Malignant Transformation and Suppress Human Tumor Growth in Nude Mice. *J. Biol. Chem* 2000;275:17974–17978. [PubMed: 10770919]
22. Casey PJ. Biochemistry of Protein Prenylation. *Lipid Res* 1992;33:1731–1740.
23. Zhang FL, Casey PJ. Protein Prenylation: Molecular Mechanisms and Functional Consequences. *Annu. Rev. Biochem* 1996;65:241–269. [PubMed: 8811180]
24. Der CJ, Cox AD. Isoprenoid Modification and Plasma-Membrane Association: Critical Factors for Ras Oncogenicity. *Cancer Cells* 1991;3:331–340. [PubMed: 1751286]
25. Qian Y, Blaskovich MA, Saleem M, Seong CM, Wathen SP, Hamilton AD, Sebti SM. Design and structural requirements of potent peptidomimetic inhibitors of p21ras farnesyltransferase. *J. Biol. Chem* 1994;269:12410–12413. [PubMed: 8175645]
26. Qian Y, Marugan JJ, Fossum RD, Vogt A, Sebti SM, Hamilton AD. Probing the hydrophobic pocket of farnesyltransferase: aromatic substitution of CAAX peptidomimetics leads to highly potent inhibitors. *Bioorg. Med. Chem* 1999;7:3011–3024. [PubMed: 10658608]
27. Ohkanda J, Lockman JW, Kothare MA, Qian Y, Blaskovich MA, Sebti SM, Hamilton AD. Design and synthesis of potent nonpeptidic farnesyltransferase inhibitors based on a terphenyl scaffold. *J. Med. Chem* 2002;45:177–188. [PubMed: 11754590]
28. Ohkanda J, Strickland CL, Blaskovich MA, Carrico D, Lockman JW, Vogt A, Bucher CJ, Sun J, Qian Y, Knowles D, Pusateri EE, Sebti SM, Hamilton AD. Structure-based design of imidazole-containing peptidomimetic inhibitors of protein farnesyltransferase. *Org. Biomol. Chem* 2006;4:482–492. [PubMed: 16446806]
29. (a) Glenn MP, Chang SY, Hucke O, Verlinde CL, Rivas K, Hornéey C, Yokoyama K, Buckner FS, Pendyala PR, Chakrabarti D, Gelb M, Van Voorhis WC, Sebti SM, Hamilton AD. Structurally simple farnesyltransferase inhibitors arrest the growth of malaria parasites. *Angew. Chem., Int. Ed* 2005;44:4903–4906. (b) Glenn MP, Chang SY, Hornéey C, Rivas K, Yokoyama K, Pusateri EE, Fletcher S, Cummings CG, Buckner FS, Pendyala PR, Chakrabarti D, Sebti SM, Gelb M, Van Voorhis WC, Hamilton AD. Structurally simple, potent, Plasmodium selective farnesyltransferase inhibitors that arrest the growth of malaria parasites. *J. Med. Chem* 2006;49:5710–5727. [PubMed: 16970397]
30. Fletcher S, Cummings CG, Rivas K, Katt WP, Hornéey C, Buckner FS, Chakrabarti D, Sebti SM, Gelb MH, Van Voorhis WC, Hamilton AD. Potent, Plasmodium-selective farnesyltransferase inhibitors that arrest the growth of malaria parasites: structure-activity relationships of ethylenediamine-analogue scaffolds and homology model validation. *J. Med. Chem* 2008;51:5176–5197. [PubMed: 18686940]

31. Eastman RT, White J, Hucke O, Bauer K, Yokoyama K, Nallan L, Chakrabarti D, Verlinde CL, Gelb MH, Rathod PK, Van Voorhis WC. Resistance to a protein farnesyltransferase inhibitor in *Plasmodium falciparum*. *J. Biol. Chem* 2005;280:13554–13559. [PubMed: 15661734]
32. Jones G, Willett P, Glen RC, Leach AR, Taylor R. Development and validation of a genetic algorithm for flexible docking. *J. Mol. Biol* 1997;267:727–748. [PubMed: 9126849]
33. Hunt JT, Ding CZ, Batorsky R, Bednarz M, Bhide R, Cho Y, Chong S, Chao S, Gullo-Brown J, Guo P, Kim SH, Lee FY, Leftheris K, Miller A, Mitt T, Patel M, Penhallow BA, Ricca C, Rose WC, Schmidt R, Slusarchyk WA, Vite G, Manne V. Discovery of (R)-7-cyano-2,3,4,5-tetrahydro-1-(1*H*-imidazol-4-ylmethyl)-3-(phenylmethyl)-4-(2-thienylsulfonyl)-1*H*-1,4-benzodiazepine (BMS-214662), a farnesyltransferase inhibitor with potent preclinical antitumor activity. *J. Med. Chem* 2000;43:3587–3595. [PubMed: 11020273]
34. Lombardo LJ, Camuso A, Clark J, Fager K, Gullo-Brown J, Hunt JT, Inigo I, Kan D, Kolowitz B, Lee F, McGlinchey K, Qian L, Ricca C, Rovnyak G, Traeger S, Tokarski J, Williams DK, Wu LI, Zhao Y, Manne V, Bhide RS. Design, synthesis and structure-activity relationships of tetrahydroquinoline-based farnesyltransferase inhibitors. *Bioorg. Med. Chem. Lett* 2005;15:1895–1899. [PubMed: 15780629]
35. Long SB, Hancock PJ, Kral AM, Hellinga HW, Beese LS. The crystal structure of human protein farnesyltransferase reveals the basis for inhibition by CaaX tetrapeptides and their mimetics. *Proc. Natl. Acad. Sci. U.S.A* 2001;98:12948–12953. [PubMed: 11687658]
36. Reid TS, Beese LS. Crystal structures of the anticancer clinical candidates R115777 (Tipifarnib) and BMS-214662 complexed with protein farnesyltransferase suggest a mechanism of FTI selectivity. *Biochemistry* 2004;43:6877–6884. [PubMed: 15170324]
37. Delano, WL. The PyMOL Molecular Graphics System. DeLano Scientific; San Carlos, CA: 2002.
38. Hast MA, Fletcher S, Cummings CG, Pusateri EE, Blaskovich MA, Rivas K, Gelb MH, Van Voorhis WC, Sebti SM, Hamilton AD, Beese LS. Structural basis for binding and selectivity of antimalarial and anticancer ethylenediamine inhibitors to protein farnesyltransferase. *Chem Biol* 2009;16:181–192. [PubMed: 19246009]
39. Vogt A, Qian Y, McGuire TF, Hamilton AD, Sebti SM. Protein geranylgeranylation, not farnesylation, is required for G1 to S phase transition in mouse fibroblasts. *Oncogene* 1996;13:1991–1999. [PubMed: 8934546]
40. Sun J, Qian Y, Hamilton AD, Sebti SM. Both farnesyltransferase and geranylgeranyltransferase I inhibitors are required for inhibition of oncogenic K-Ras prenylation but each alone is sufficient to suppress human tumor growth in nude mouse xenografts. *Oncogene* 1998;16:1467–1473. [PubMed: 9525745]

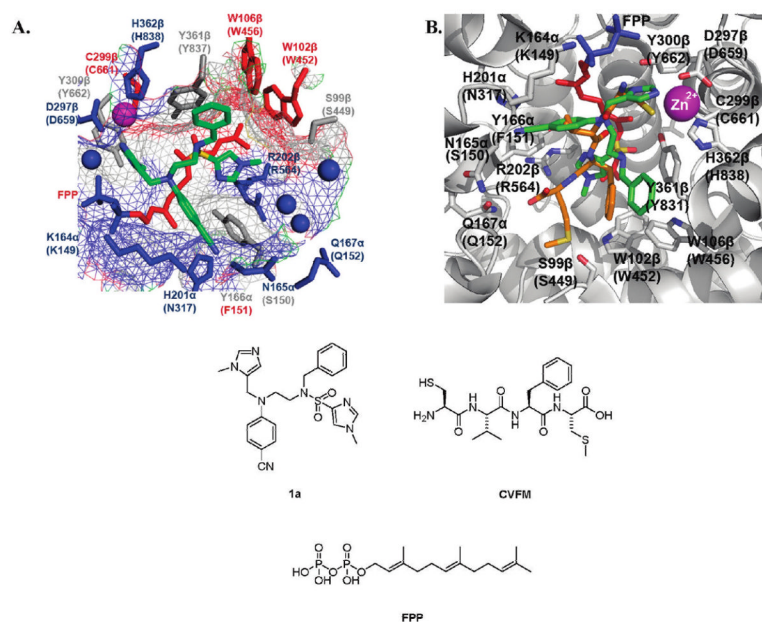


Figure 1. One high scoring active site conformation of inhibitor **1a** (green) as identified by flexible ligand GOLD³² docking experiments (A) using a Connolly analytical surface graphical representation developed in PyMOL,³⁷ red hydrophobic to blue hydrophilic, and (B) using a “cartoon” graphical representation developed in PyMOL³⁷ and overlaid with the peptide inhibitor CVFVM (orange) from the rFTase crystal structure. Binding surface of rat FTase (PDB ID: 1JCR³⁵), values in parentheses refer to corresponding residues in *P/FTase*;³¹ small molecules colored by atom type: FPP colored red (farnesyl) and blue (pyrophosphate); blue spheres = water molecules; purple sphere = zinc ion.

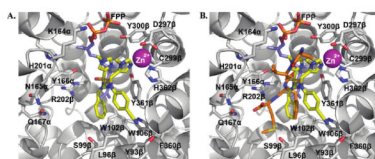


Figure 2. (A) Co-crystal structure of inhibitor **1a** (yellow, and colored by atom type) and FPP bound to rFTase (PDB ID: 3E32),³⁸ and (B) co-crystal structure of FPP and inhibitor **1a** overlaid with the tetrapeptide inhibitor CVFM (orange, and colored by atom type) from PDB ID: 1JCR.³⁵

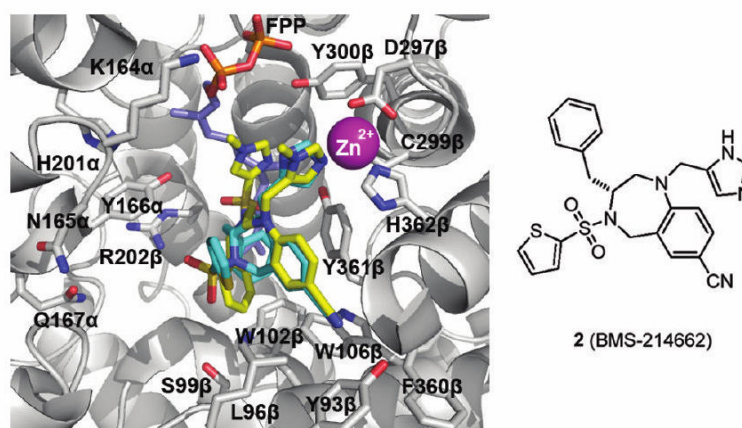
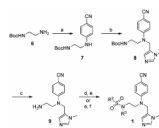
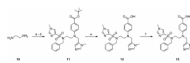


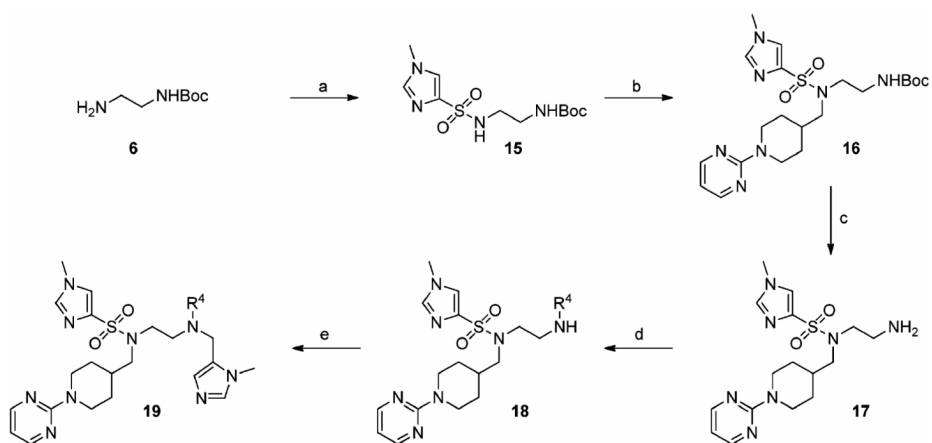
Figure 3. Overlay of the crystal structures of the ternary complexes of **1a**³⁸ (yellow, colored by atom type) and **2**³⁶ (cyan, colored by atom type) with FPP in rFTase.

**Scheme 1a.**

^a (a) *para*-Fluorobenzonitrile, DIPEA, DMSO, 120 °C, 48 h, 89%; (b) (1) LDA, THF, -78 °C, 30 min, (2) 5-chloromethyl-1-methyl-1*H*-imidazole · HCl,²⁹ NaH, -78 °C, 1 h, 52% (98% brsm); (c) TFA-CH₂-Cl₂, 1:1, rt, 30min, 99%; (d) (1) R²CHO, AcOH, 4 Å MS, MeOH, rt, 30min, (2) NaCNBH₃, rt, 16 h, 72–84%; (e) R²SO₂Cl, DIPEA, CH₃CN, 0 °C → rt, 16 h, 82–93%; ((f) R³Br, Cs₂CO₃, DMF, rt, 16 h, 79–82%.

**Scheme 2a.**

^a (a) *tert*-Butyl *para*-fluorobenzoate, DMSO, 120 °C, 24 h, 96%; (b) 1-methyl-1*H*-imidazole-4-sulfonyl chloride, DIPEA, CH₃CN, 0 °C → rt, 12 h, 90%; (c) BnBr, Cs₂CO₃, DMF, rt, 16 h, 92%; (d) (1) NaH, DMF, 0 °C, 30 min, (2) 5-chloromethyl-1-methyl-1*H*-imidazole · HCl,^{29b} 0 °C → rt, 3 h, 76%; (e) TFA-CH₂Cl₂, 1:1, 3 h, rt, 96%; (f) NH₄Cl, HBTU, DIPEA, DMF, rt, 16 h, 89%.

**Scheme 3a.**

^a (a) 1-Methyl-1*H*-imidazole-4-sulfonyl chloride, DIPEA, CH_3CN , $0\text{ }^\circ\text{C} \rightarrow \text{rt}$, 16 h, 95%; (b) 4-bromomethyl-*N*-(2-pyrimidinyl)-piperidine, Cs_2CO_3 , DMF, rt , 4 d, 94%; (c) TFA- CH_2Cl_2 -TIPS- H_2O , 47.5:47.5:2.5:2.5, rt , 1 h, 100%; (d) R^4F , DIPEA, DMSO, $120\text{ }^\circ\text{C}$, 24–48 h, 48–97%; (e) (1) NaH, $0\text{ }^\circ\text{C}$, 30 min, (2) 5-chloromethyl-1-methyl-1*H*-imidazole 3 HCl, ^{29b} $0\text{ }^\circ\text{C} \rightarrow \text{rt}$, 2–3h, 63–96%.

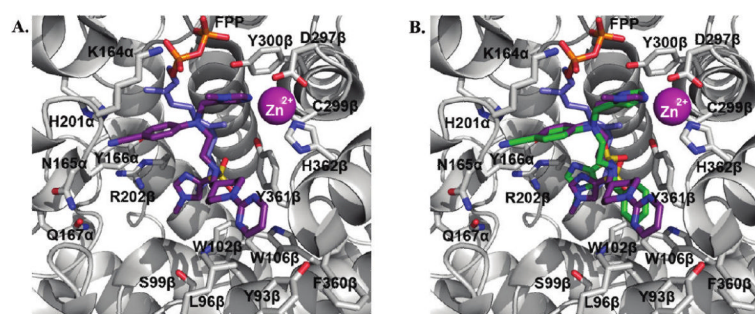


Figure 4. One high scoring rFTase active site conformation of inhibitor **1az** (purple, colored by atom type) as identified by flexible ligand GOLD³² docking experiments (A) in isolation and (B) overlaid with the high scoring active site conformation of inhibitor **1a** (green, colored by atom type) that was presented in Figure 1B. The co-substrate FPP was included in the docking experiments as this forms part of the binding surface.

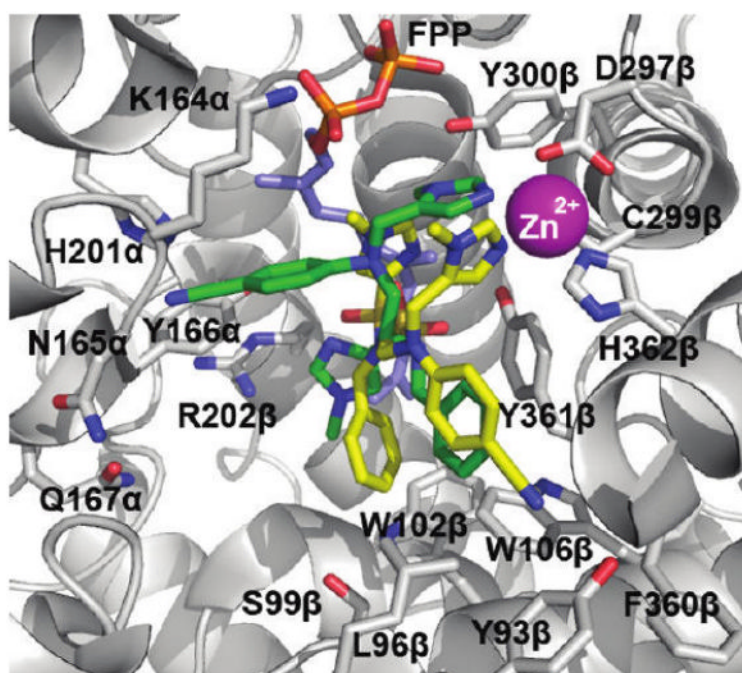
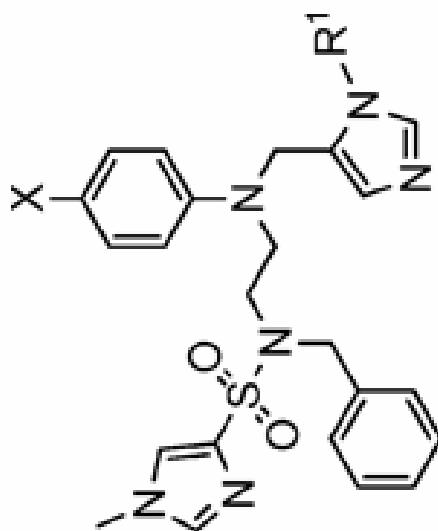


Figure 5. Overlay of the co-crystal structure of **1a** (yellow, colored by atom type; PDB ID: 3E32³⁸) and FPP with a high scoring (low energy) GOLD docked pose of **1a** (green, colored by atom type) in the active site of rFTase.

Table 1

Enzyme Inhibition and Whole Cell Data of a Focused Set of Ethylenediamine-Based PfFTase Inhibitors



no.	X	R ¹	IC ₅₀ (nM) ^a			processing IC ₅₀ (μM) ^c		
			hFTase	GGTase-I	selectivity ^b	H-Ras	Rap1A	
3 (FTI-2581)	H	H	6300 ± 360	> 10000	1.6	> 10	> 10	> 10
4 (FTI-2584)	Br	H	730 ± 20	4400	6.0	5.7 ± 1.2	> 10	> 10
5 (FTI-2586)	Br	Me	79 ± 30	530 ± 170	6.7	1.6 ± 1.3	> 10	> 10
1a (FTI-2585)	CN	Me	56 ± 29	2700 ± 2200	48	1.9 ± 1.2	> 10	> 10

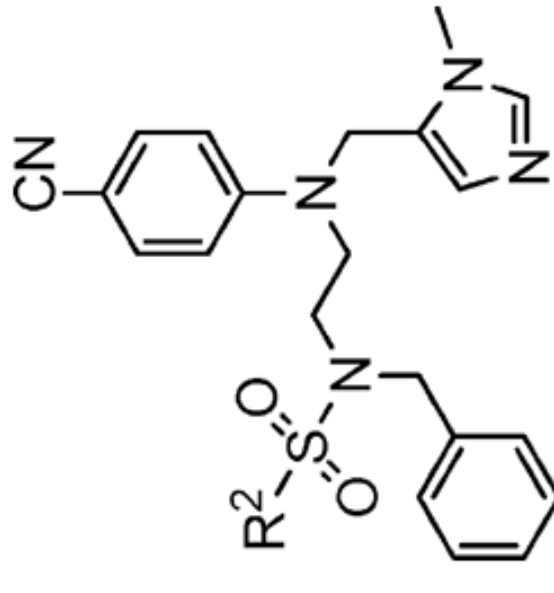
^aIC₅₀ = inhibitor concentration required to achieve 50% inhibition of h FTase or GGTase-I in vitro.

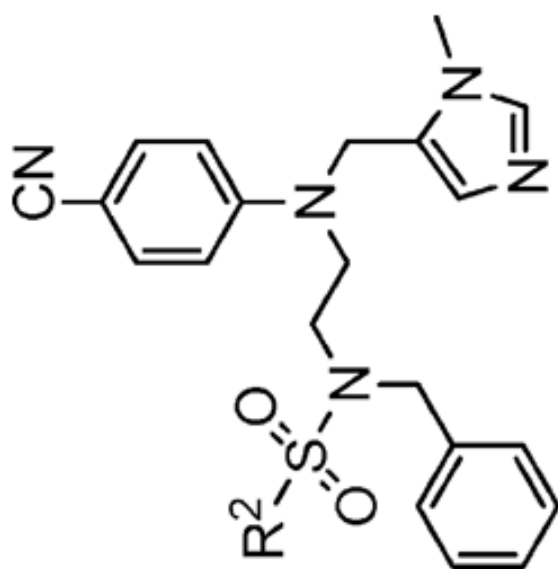
^bRatio of GGTase-I to FTase IC₅₀s.


^cProcessing IC₅₀ = inhibitor concentration required to achieve 50% inhibition of farnesylation of H-Ras or geranylgeranylation of Rap1A in whole cells. In all cases, IC₅₀ data represents the average of three independent assays (*n* = 3), unless otherwise stated, and errors are given as standard deviations.

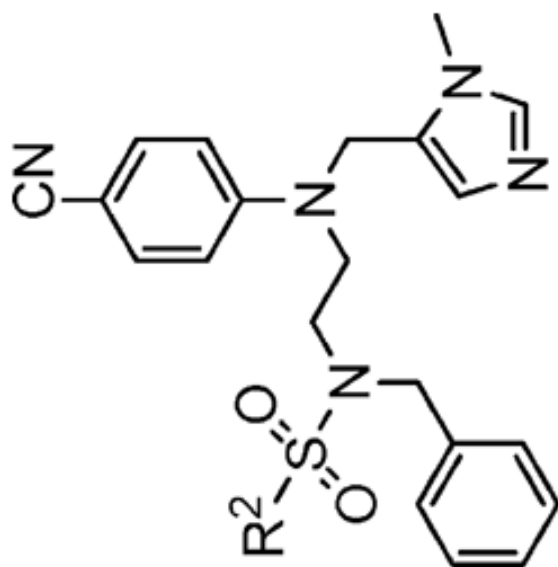
Table 2

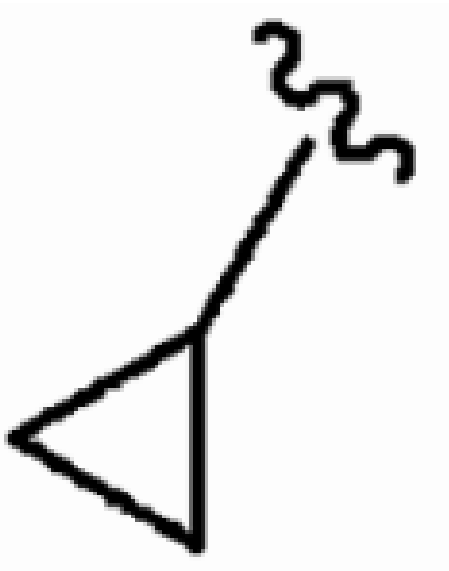
Enzyme Inhibition and Whole Cell Data of Ethylenediamine-Based FTIs Exhibiting a Range of R²-Sulfonyl Groups

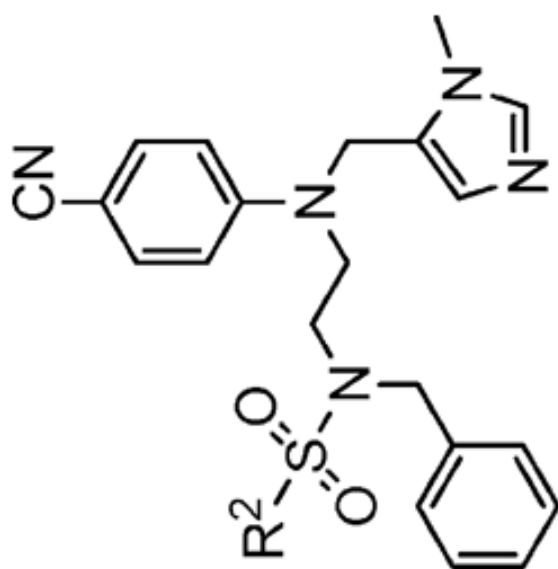
Number	Compound	IC ₅₀ (nM)		Selectivity		Processing IC ₅₀ (μM)	
		hFTase	GGTase-I	H-Ras	Rap1A	H-Ras	Rap1A
1a (FTI-2585)		56 ± 29	2700 ± 2200	48	1.9 ± 1.2	>10	>10



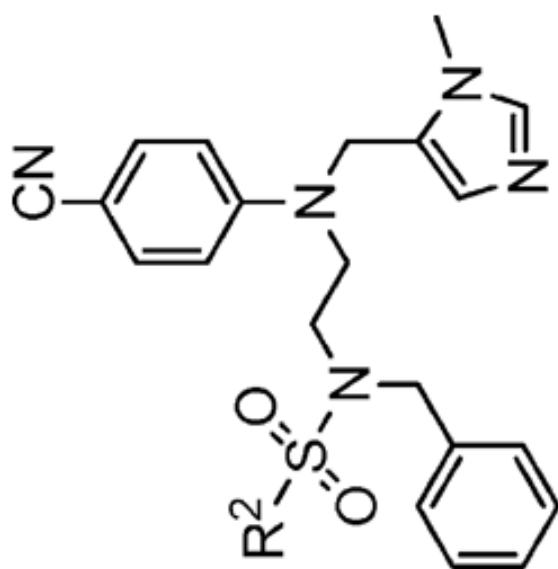
Number	Compound	IC ₅₀ (nM)		Selectivity	Processing IC ₅₀ (μM)	
		hFTase	GGTase-I		H-Ras	Rap1A
1b (FTI-2640)		48 ± 35	4100 ± 1700	85	0.07	>10



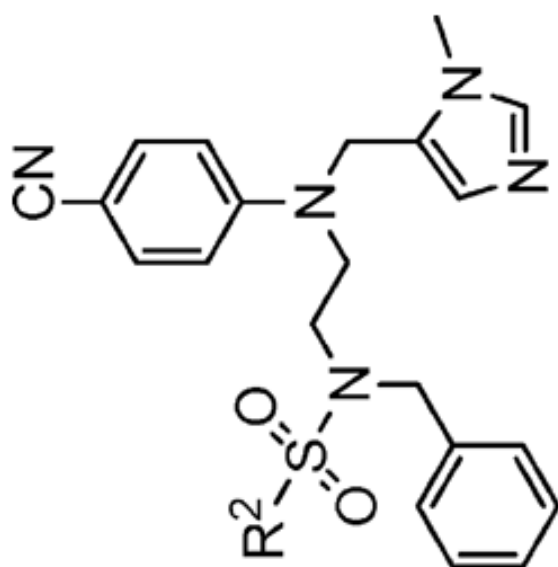
Number	Compound	IC ₅₀ (nM)		Selectivity	Processing IC ₅₀ (μM)	
		hFTase	GGTase-I		H-Ras	Rap1A
Ic (FTI-2644)		85 ± 0.7	5500 ± 2700	65	ND ^a	ND



Number	Compound	IC ₅₀ (nM)			Selectivity	Processing IC ₅₀ (μM)	
		hFTase	GGTase-I	H-Ras		Rap1A	
1d (FTI-2592)		41 ± 26	310 ± 50	7.6	0.3 ± 0.1	>10	
1e (FTI-2589)		50 ± 13	10,000	200	0.5 ± 0.2	>10	
1f (FTI-2587)		25 ± 20	820 ± 240	113	0.09 ± 0.06	>10	



Number	Compound	IC ₅₀ (nM)		Selectivity	Processing IC ₅₀ (μM)	
		hFTase	GGTase-I		H-Ras	Rap1A
I _g (FTI-2590)		30 ± 14	10,000	333	0.6 ± 0.3	>10



Number	Compound	IC ₅₀ (nM)		Selectivity	Processing IC ₅₀ (μM)	
		hFTase	GGTase-I		H-Ras	Rap1A
1h (FTI-2591)		160 ± 110	10,000	63	1.5 ± 0.3	>10

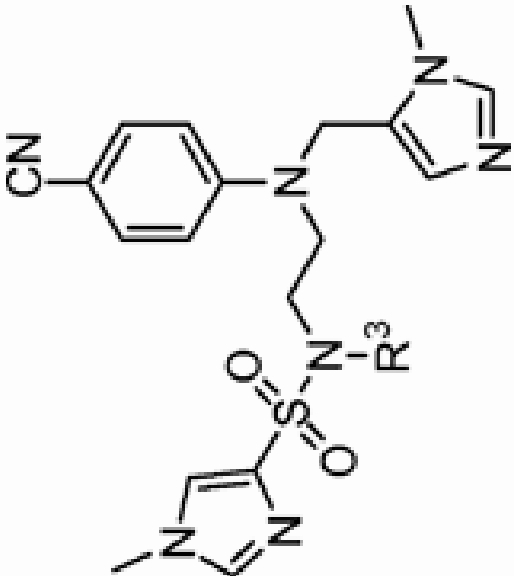
ND = not determined.

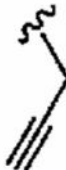

NIH-PA Author Manuscript

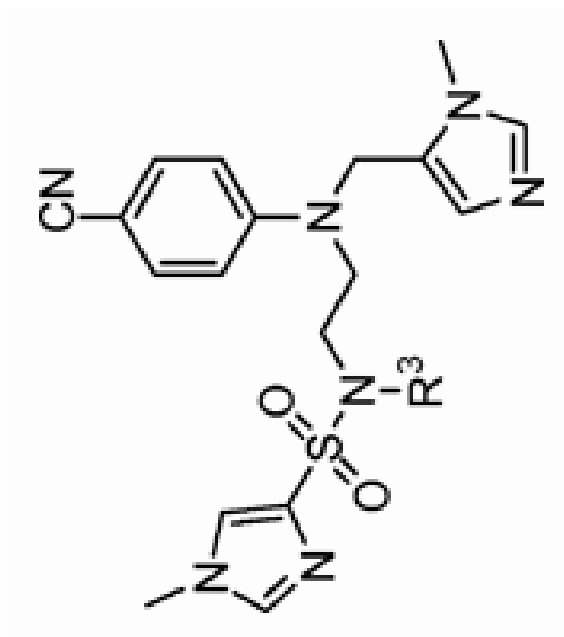
NIH-PA Author Manuscript

NIH-PA Author Manuscript

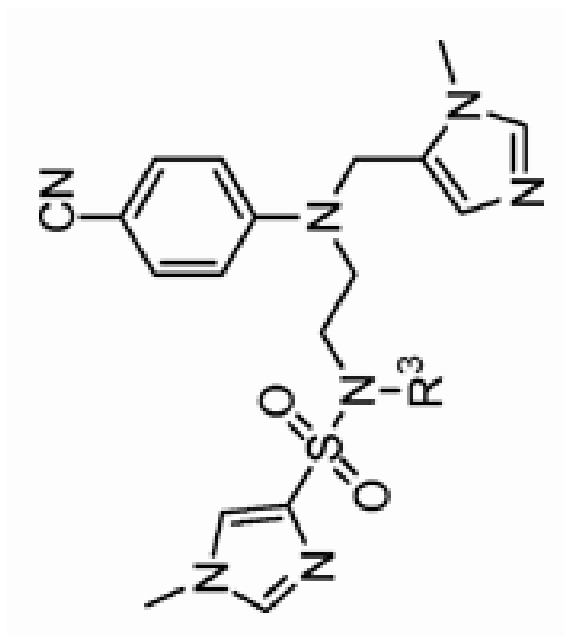
Table 3
Enzyme Inhibition and Whole Cell Data of Ethylenediamine-Based FTIs Exhibiting a Range of R³ Sulfonamides



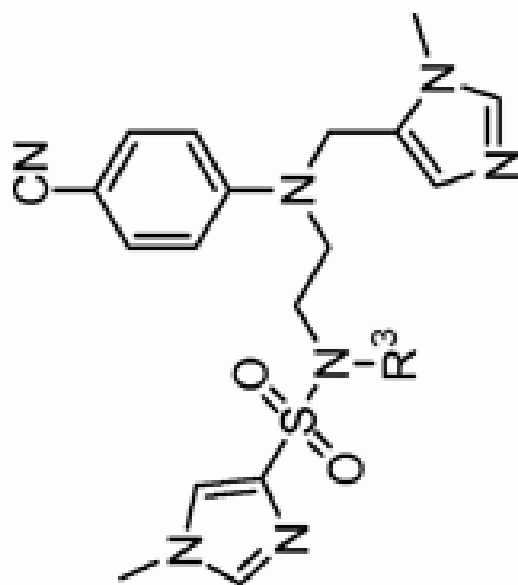
Number	Compound R ³	IC ₅₀ (nM)		Selectivity	Processing IC ₅₀ (nM)	
		hFTase	GGTase-I		H-Ras	Rap1A
1a (FTI-2630)		720 ± 200	>10,000	>14	6 (n = 2)	>10
1b (FTI-2600)		54 ± 30	>10,000	>14	>10	>10



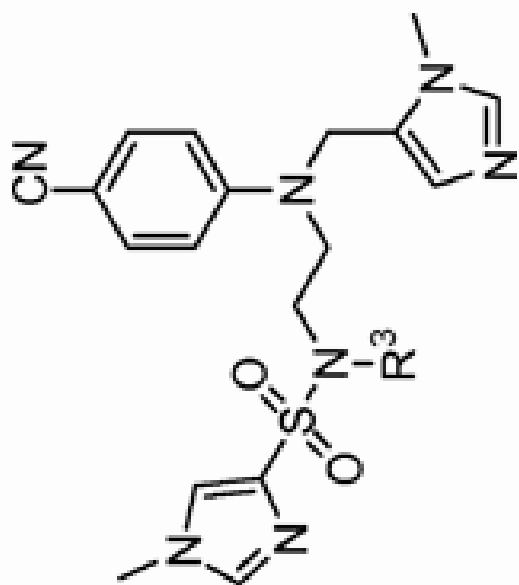
Number	Compound	IC ₅₀ (nM)			Selectivity	Processing IC ₅₀ (μM)	
		hFTase	GGTase-I	H-Ras		Rap1A	
1ac (FTI-2506)		114 ± 80	600 ± 300	5.3	>10	>10	



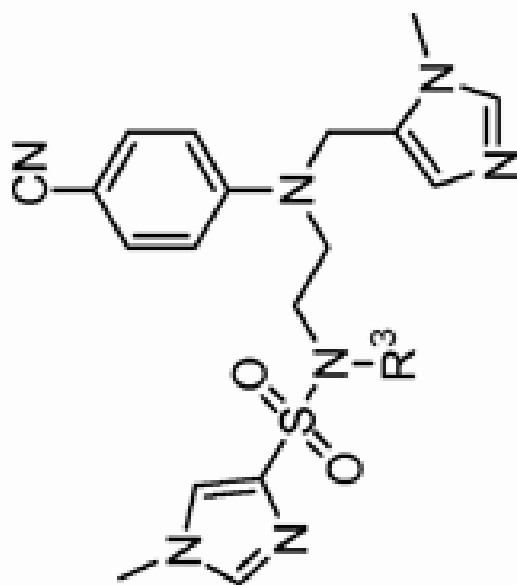
Number	Compound	IC ₅₀ (nM)			Selectivity	Processing IC ₅₀ (μM)	
		hFTase	GGTase-I	H-Ras		Rap1A	
1ad (FTI-2611)		180 ± 100	5500 ± 1900	31	5.7 ± 1.5	>10	
1ae (FTI-2607)		1400 ± 900	>10,000	7.1	>10	>10	



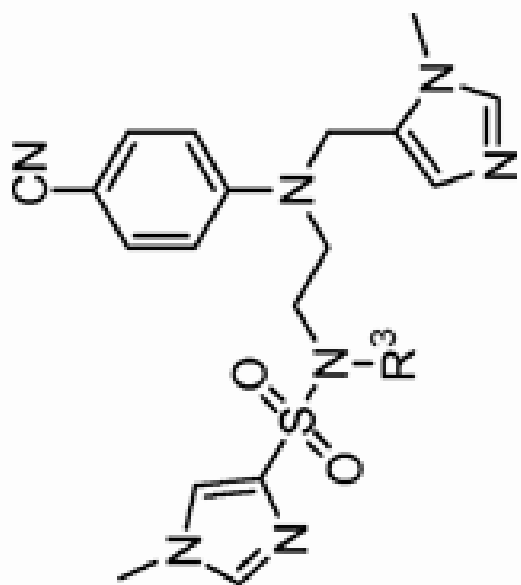
Number	Compound R ³	IC ₅₀ (nM)			Processing IC ₅₀ (μM)		
		hFTase	GGTase-I	Selectivity	H-Ras	Rap1A	
1a (FTI-2585)		56 ± 29	2700 ± 2200	48	1.9 ± 1.2	>10	>10
1af (FTI-2601)		72 ± 20	>10,000	>139	>10	>10	>10
1ag (FTI-2602)		30 ± 33	510 ± 270	17	4.3 ± 1.5	>10	>10
1ah (FTI-2635)		320 ± 190	6100 ± 1600	19	0.65 (n=2)	>10	>10



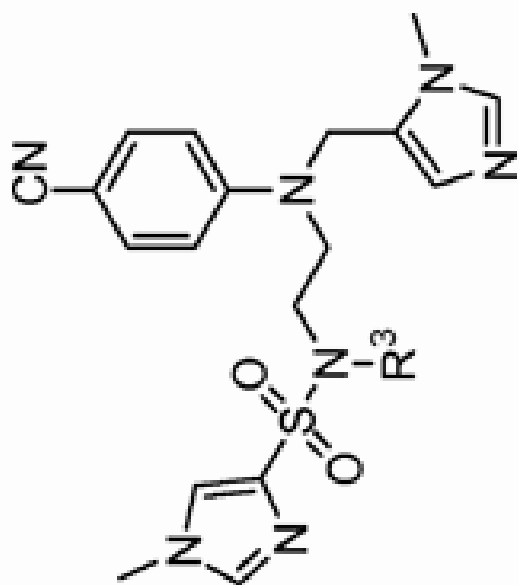
Number	Compound R ³	IC ₅₀ (nM)			Selectivity	Processing IC ₅₀ (μM)	
		hFTase	GGTase-I	H-Ras		Rap1A	
1ai (FTI-2536)		67 ± 38	940 ± 20	14	0.4 (n = 2)	>10	
1aj (FTI-2538)		870 ± 120	13,400 (n = 2)	15	0.8 (n = 2)	>10	
1ak (FTI-2639)		2300 ± 1500	5900 ± 3000	2.6	0.4 (n = 2)	>10	



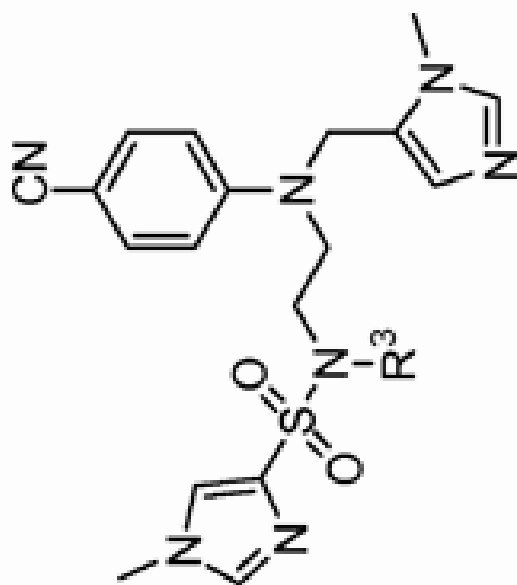
Number	Compound	IC ₅₀ (nM)			Selectivity	Processing IC ₅₀ (μM)	
		hFTase	GGTase-I	H-Ras		Rap1A	
1a (FTI-2533)		510 ± 460	1360 ± 740	2.7	>10	>10	
1am (FTI-2637)		6200 ± 920	>10,000	>1.6	>10	>10	



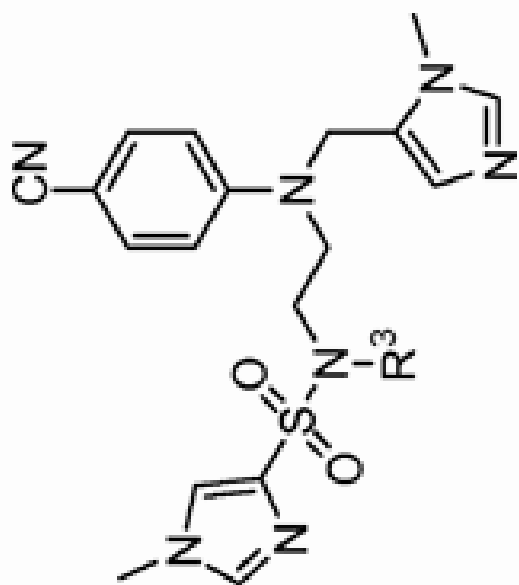
Number	Compound	IC ₅₀ (nM)			Selectivity	Processing IC ₅₀ (μM)	
		hFTase	GGTase-I	H-Ras		Rap1A	
1an (FTI-2542)		5300 ± 1700	>10,000	>1.9	ND	ND	ND
1ao (FTI-2614)		51 ± 26	780 ± 320	15	1 ± 0	>10	>10



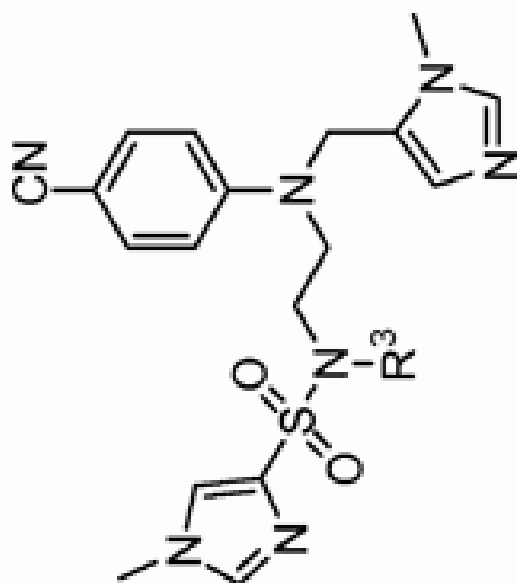
Number	Compound	IC ₅₀ (nM)			Selectivity	Processing IC ₅₀ (μM)	
		hFTase	GGTase-I	H-Ras		Rap1A	
1ap (FTI-2615)		54 ± 30	630 ± 240	12	0.3 ± 0.2	>10	
1aq (FTI-2623)		370 ± 210	580 ± 200	1.6	2 ± 1	>10	
1ar (FTI-2624)		78 ± 12	ND	-	5 ± 3	>10	



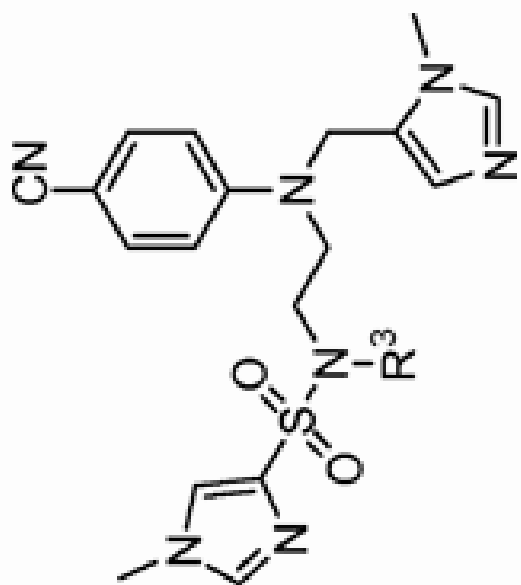
Number	Compound	IC ₅₀ (nM)			Selectivity	Processing IC ₅₀ (μM)	
		hFTase	GGTase-I	H-Ras		Rap1A	
1 _{as} (FTI-2625)		370 ± 370	6500 ± 2900	18	>10	>10	



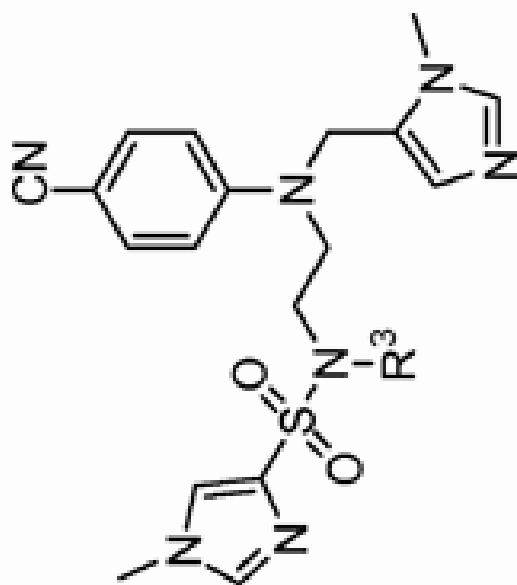
Number	Compound	IC ₅₀ (nM)			Selectivity	Processing IC ₅₀ (μM)	
		hFTase	GGTase-I	H-Ras		Rap1A	
1at (FTI-2610)		230 ± 150	550 ± 120	2.4	3 ± 0	>10	
1au (FTI-2612)		1700 ± 900	7300 ± 2200	4.3	5 ± 1	>10	



Number	Compound	IC ₅₀ (nM)			Selectivity	Processing IC ₅₀ (μM)	
		hFTase	GGTase-I	H-Ras		Rap1A	
1av (FTI-2715)		390 ± 100	5800 ± 3500	15	4 ± 1	>10	
1aw (FTI-2631)		590 ± 300	>10,000	>17	>10	>10	



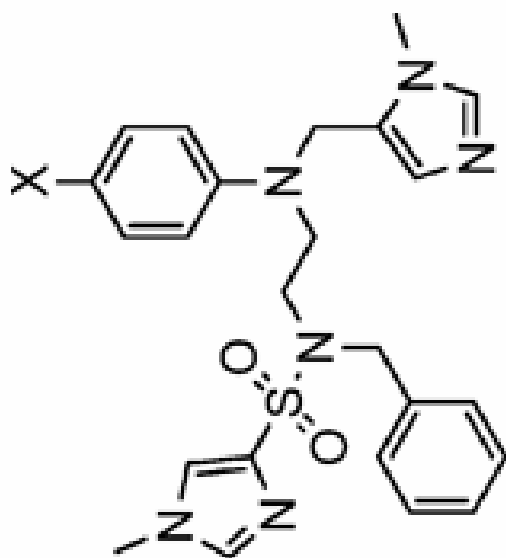
Number	Compound	IC ₅₀ (nM)			Selectivity	Processing IC ₅₀ (μM)	
		hFTase	GGTase-I	H-Ras		Rap1A	
1ax (FTI-2602)		60 ± 10	530 ± 120	8.8	0.1 ± 0.07	>10	
1ay (FTI-2670)		3700 ± 790	>10,000	>2.7	>2	>2	



Number	Compound	IC ₅₀ (nM)			Processing IC ₅₀ (μM)		
		hFTase	GGTase-I	Selectivity	H-Ras	Rap1A	
1az (FTI-2722)		510 ± 62	>10,000	>20	>10	>10	

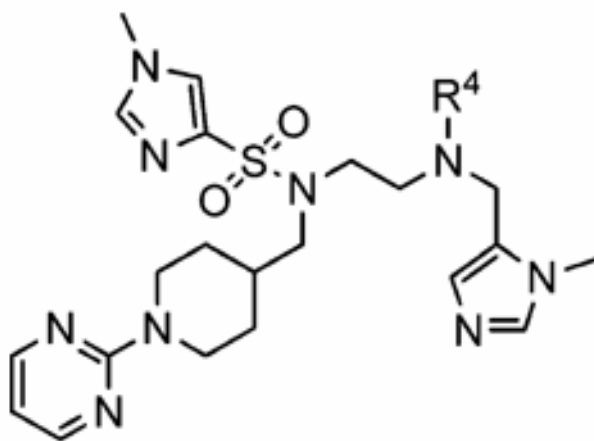
Table 4

Enzyme Inhibition and Whole Cell Data of Ethylenediamine-Based FTIs Exhibiting a Range of *para*-Substituted Anilines

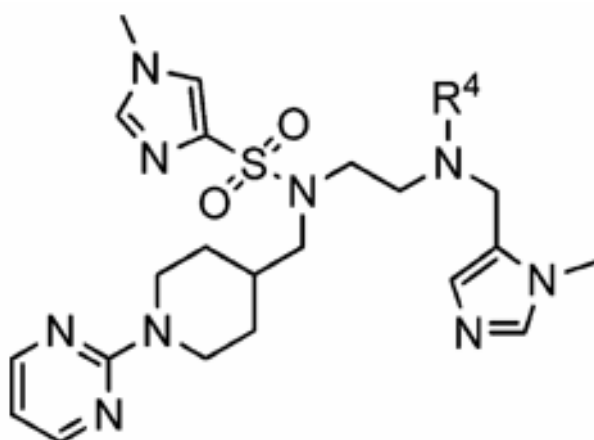


no.	compd	X	IC ₅₀ (nM)			selectivity	processing IC ₅₀ (nM)	
			hFTase	GG'Tase-I	Rap1A		H-Ras	Rap1A
4	(FTI-2586)	Br	79 ± 30	530 ± 170	6.7	1.6 ± 1.3	>10	
1a	(FTI-2585)	CN	56 ± 29	2700 ± 2200	48	1.9 ± 1.2	>10	
11	(FTI-2720)	CO ₂ tBu	5400 (n = 2)	4900 (n = 2)	0.9	ND	ND	
12	(FTI-2721)	COOH	> 10000	> 10000	–	ND	ND	
13	(FTI-2728)	CONH ₂	5300 (n = 2)	> 10000	> 2	ND	ND	
14	(FTI-2727)	Ph	6850 (n = 2)	5000 ± 2600	0.7	ND	ND	

Table 5

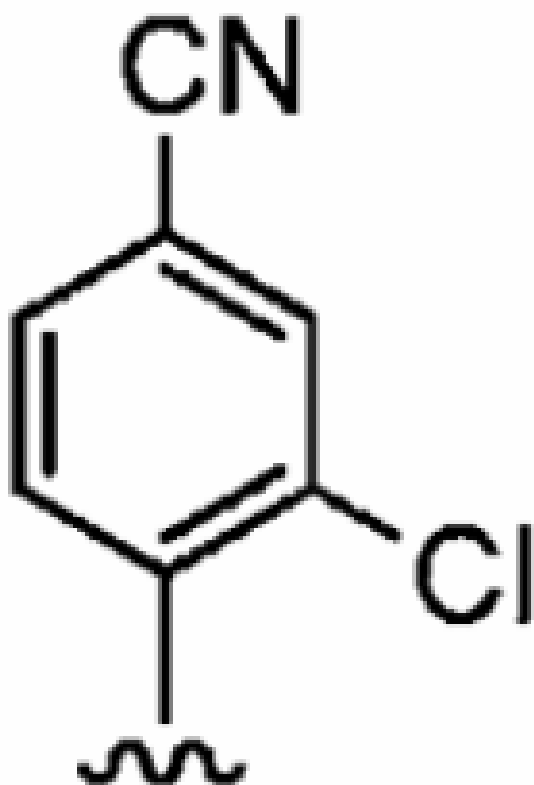
Enzyme Inhibition and Whole Cell Data of Ethylenediamine-Based FTIs Exhibiting a Range of R⁴ Anilines

Number	Compound R ⁴	IC ₅₀ (nM)		Selectivity
		hFTase	GGTase-I	
1az (FTI-2722)		510 ± 62	>10,000	>20



Number	Compound R ⁴	IC ₅₀ (nM)		Selectivity
		hFTase	GGTase-I	

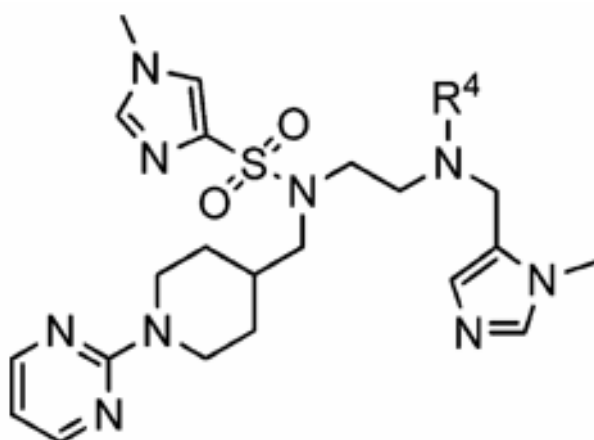
19a
(FTI-2718)



550 ± 110

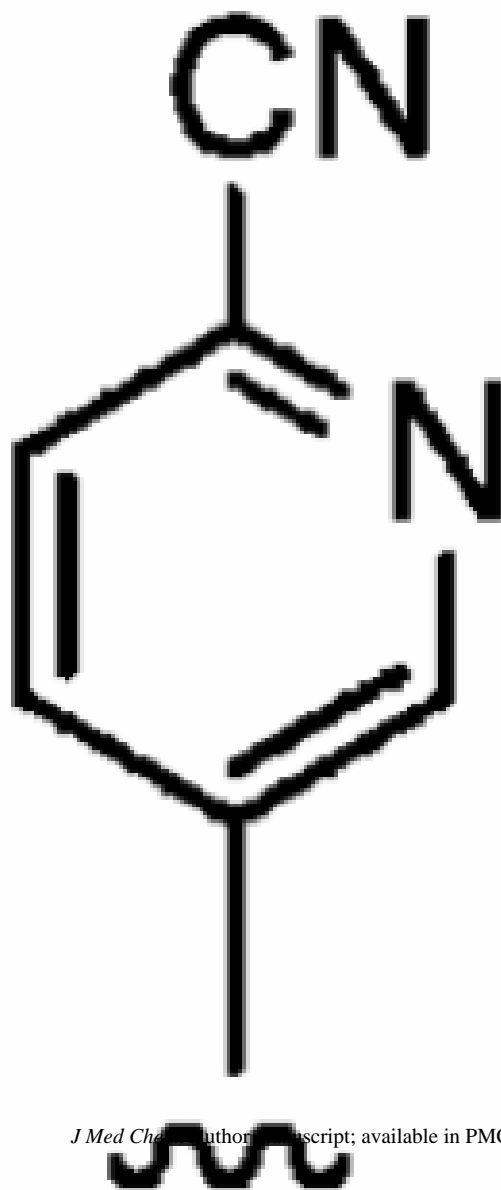
>10,000

>18



Number	Compound R ⁴	IC ₅₀ (nM)		Selectivity
		hFTase	GGTase-I	

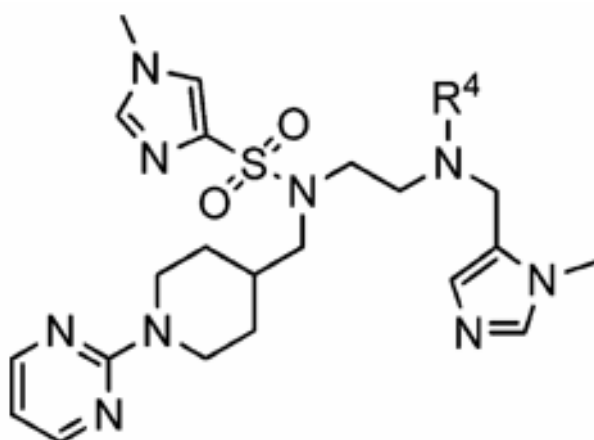
19b
(FTI-2733)



520 ± 320

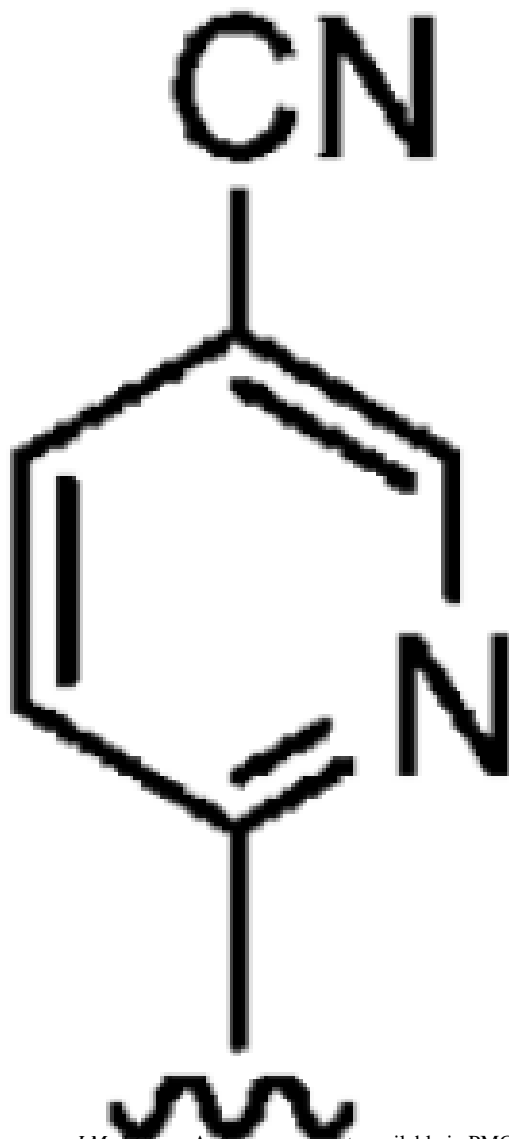
>10,000

>19

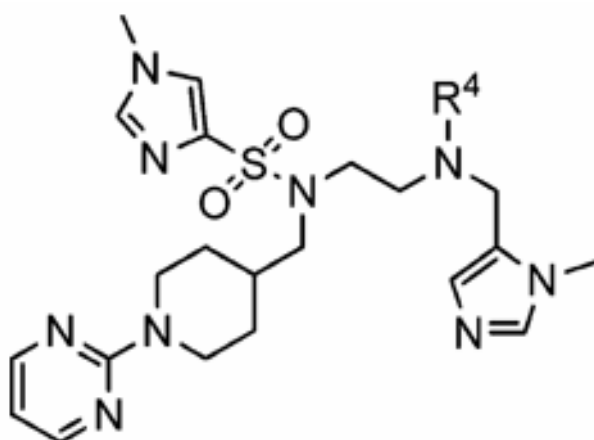


Number	Compound R ⁴	IC ₅₀ (nM)		Selectivity
		hFTase	GGTase-I	

19c
(FTI-2707)

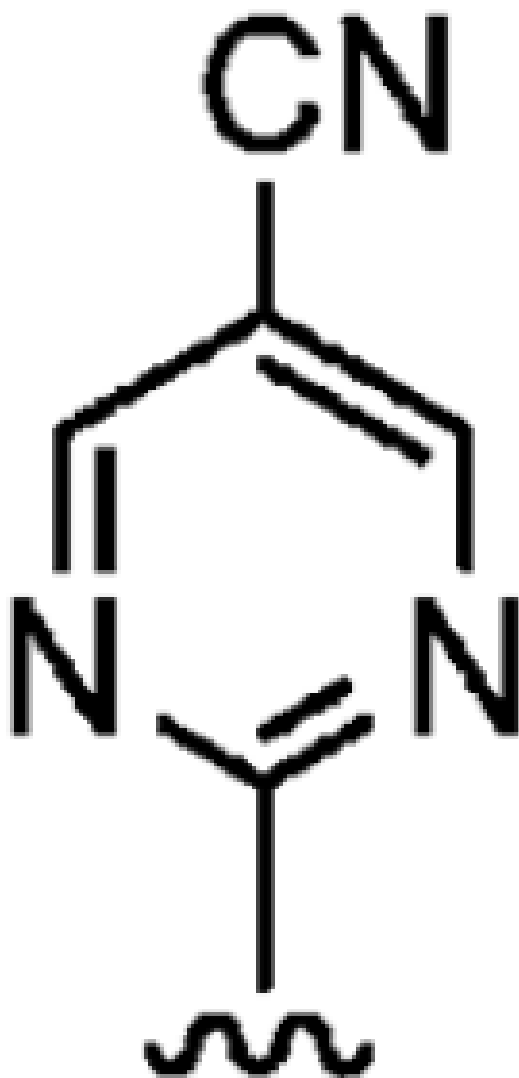


110 ± 26 >10,000 >91



Number	Compound R ⁴	IC ₅₀ (nM)		Selectivity
		hFTase	GGTase-I	

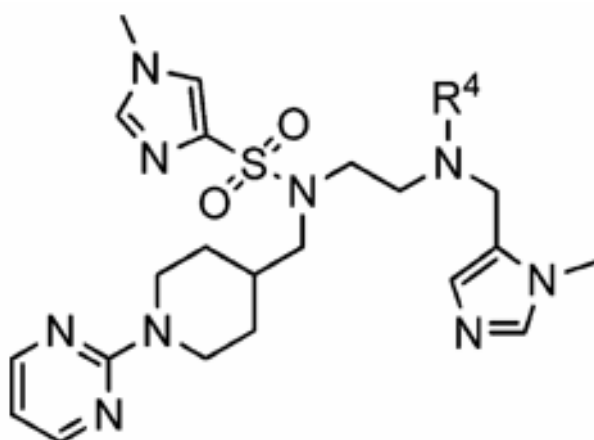
19d
(FTI-2709)



620 ± 100

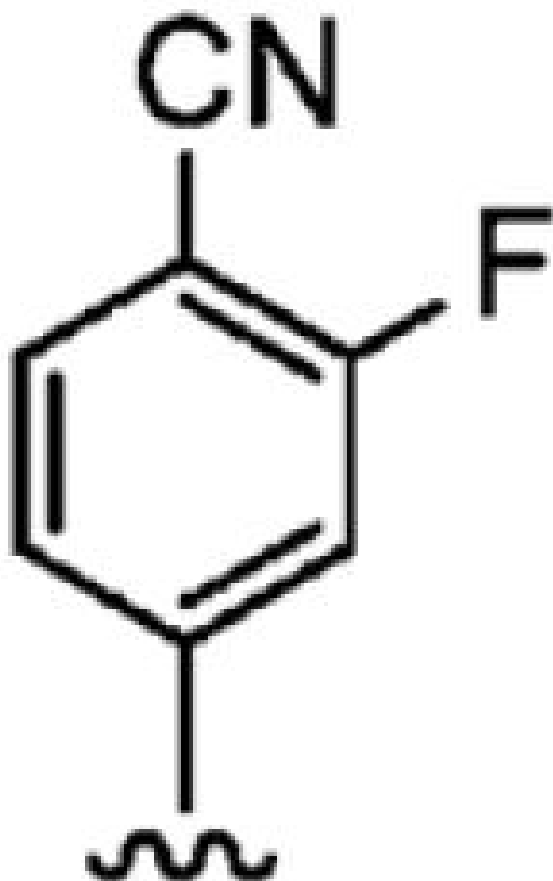
>10,000

>16

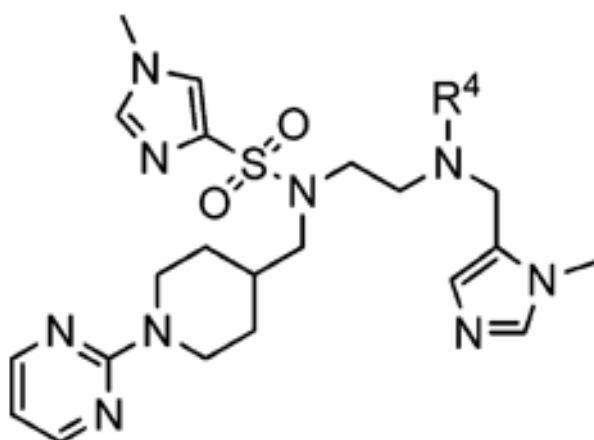


Number	Compound R ⁴	IC ₅₀ (nM)		Selectivity
		hFTase	GGTase-I	

19e
(FTI-2712)

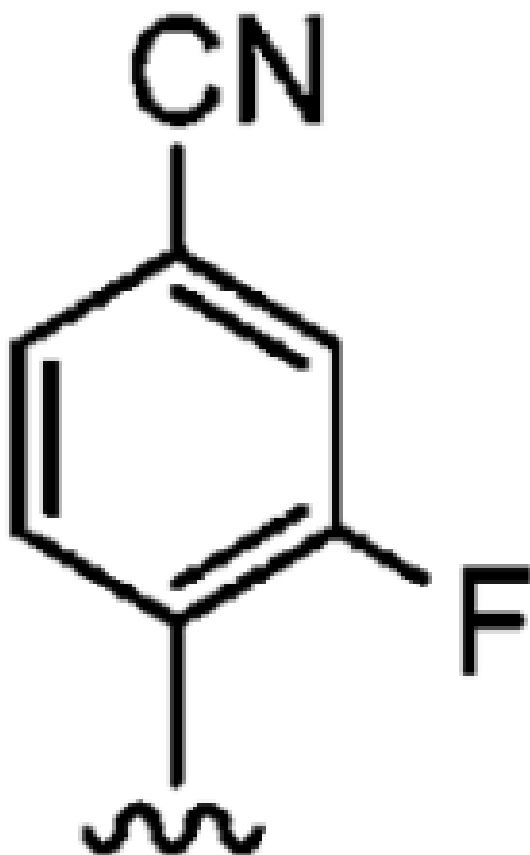


230 ± 110 9400 (n = 2) 41



Number	Compound R ⁴	IC ₅₀ (nM)		Selectivity
		hFTase	GGTase-I	

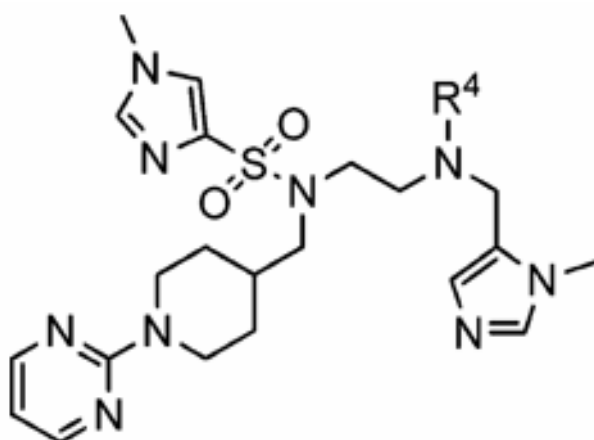
19f
(FTI-2713)



64 ± 8.6

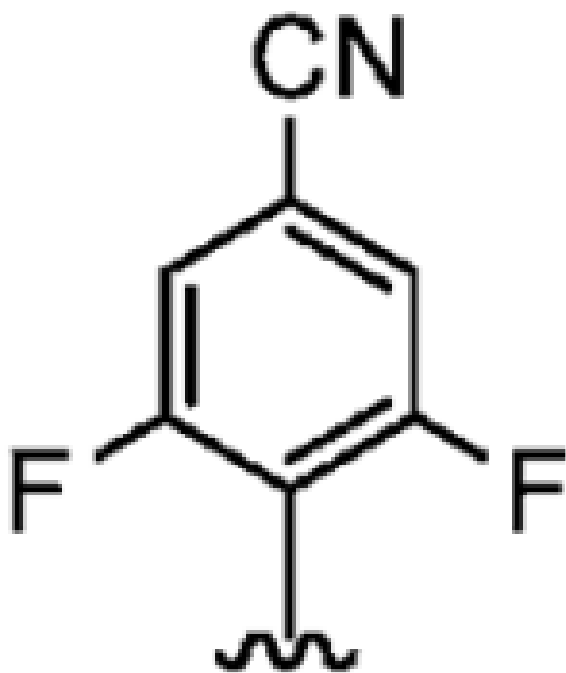
>10,000

>156



Number	Compound R ⁴	IC ₅₀ (nM)		Selectivity
		hFTase	GGTase-I	

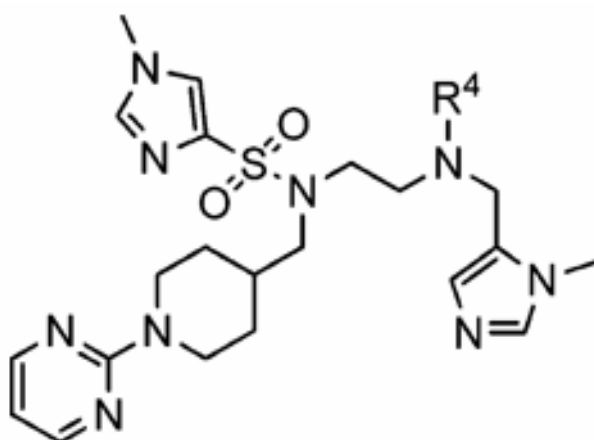
19g
(FTI-2715)



290 ± 180

>10,000

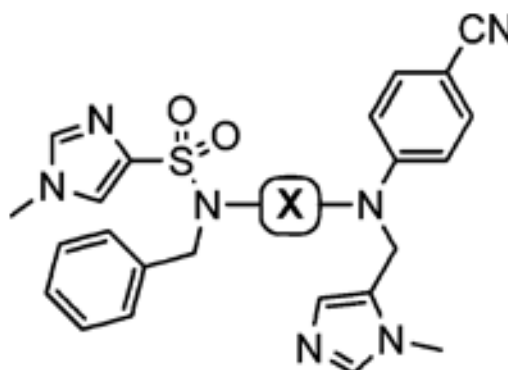
>34



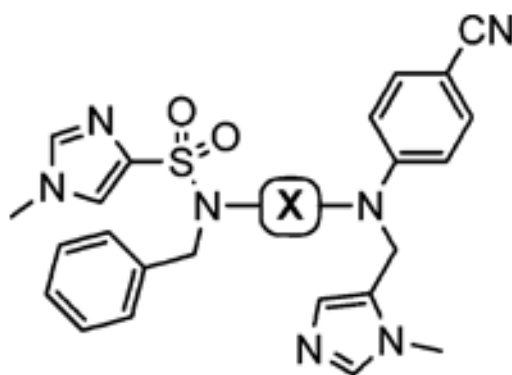
Number	Compound R ⁴	IC ₅₀ (nM)		Selectivity
		hFTase	GGTase-I	
19h (FTI-2719)		490 ± 70	8750 ± 750	18

Table 6

Enzyme Inhibition Data of FTIs Exhibiting a Range of Ethylenediamine-Analogue Scaffolds



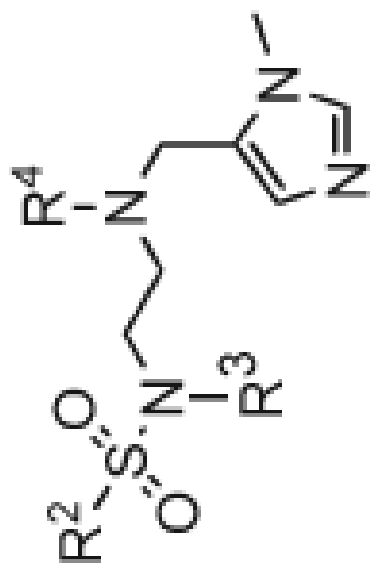
Number	Compound R ⁴	IC ₅₀ (nM)		Selectivity
		hFTase	GGTase-I	
1a		56 ± 29	2700 ± 2200	48
20a		420 ± 210	4600 (n = 2)	11
20b		1000 ± 350	>10,000	>10



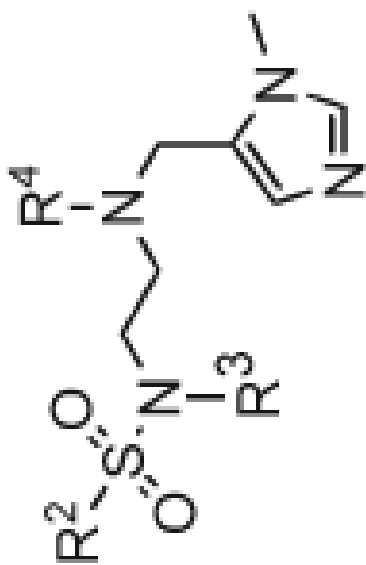
Number	Compound R ⁴	IC ₅₀ (nM)		Selectivity
		hFTase	GGTase-I	
20c		450 ± 70	9150 (n = 2)	20
20d		650 ± 220	>10,000	>15
20e		380 ± 100	7050 (n = 2)	19

Table 7

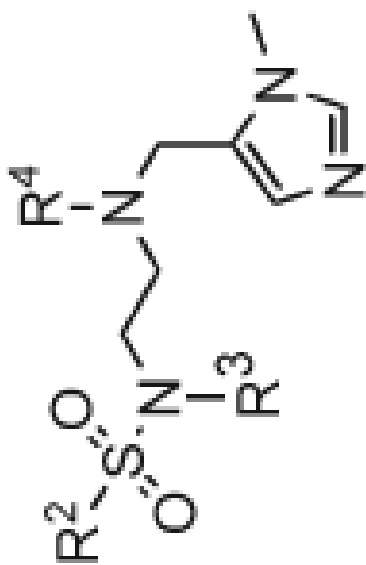
, Ethylenediamine-Based FTIs



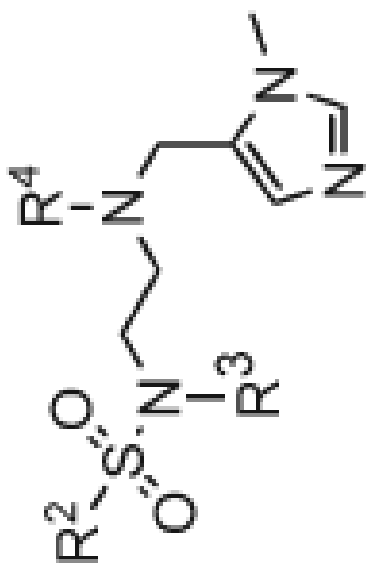
R ³	R ⁴	IC ₅₀ (nM)		Selectivity	Processing IC ₅₀ (μM)	
		hFTase	GGTase-I		H-Ras	Rap1A
		56 ± 29	2700 ± 2200	48	1.9 ± 1.2	>10



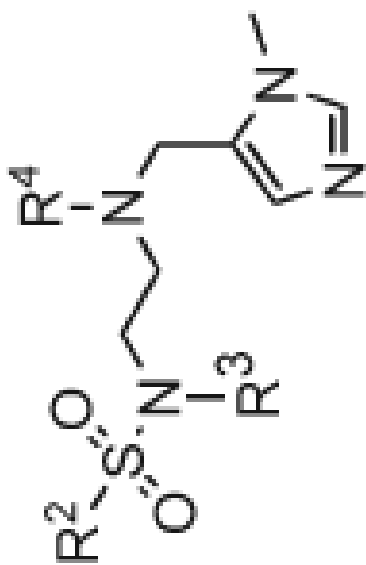
R ³	R ⁴	IC ₅₀ (nM)		Selectivity	Processing IC ₅₀ (μM)	
		hFTase	GGTase-I		H-Ras	Rap1A
		60 ± 10	530 ± 120	8.8	0.1 ± 0.07	>10



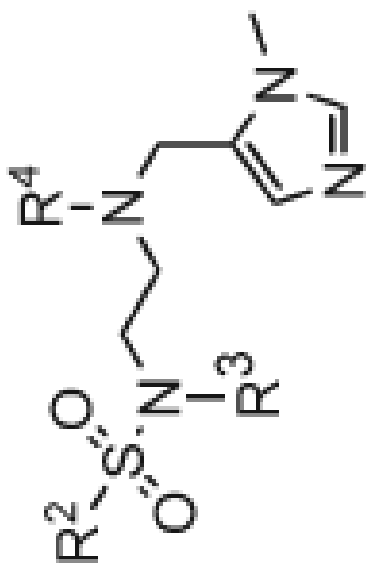
R ³	R ⁴	IC ₅₀ (nM)		Selectivity	Processing IC ₅₀ (μM)	
		hFTase	GGTase-I		H-Ras	Rap1A
		25 ± 20	820 ± 240	33	0.09 ± 0.06	>10



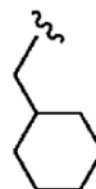
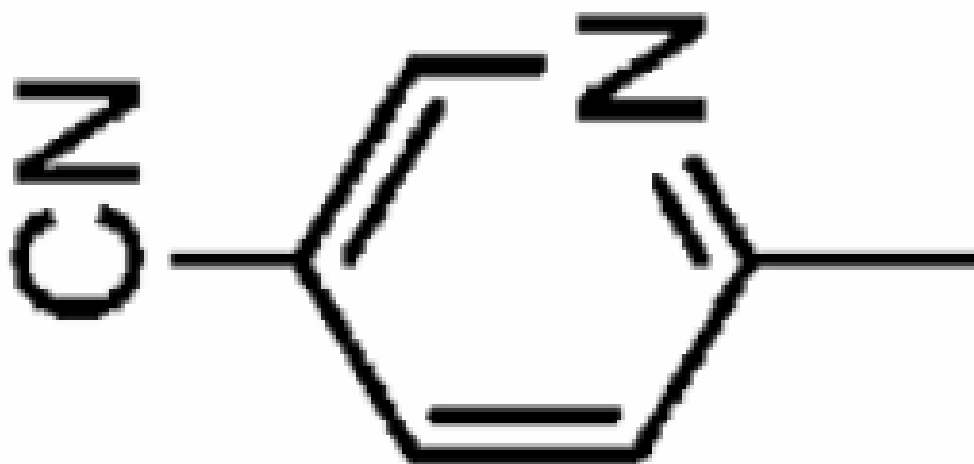
R ³	R ⁴	IC ₅₀ (nM)		Selectivity	Processing IC ₅₀ (μM)	
		hFTase	GGTase-I		H-Ras	Rep1A
		400 ± 160	610 ± 160	1.5	0.268 ± 0.212	6.2 ± 1.2



R ³	IC ₅₀ (nM)		Selectivity	Processing IC ₅₀ (μM)	
	hFTase	GGTase-I		H-Ras	Rap1A
	250 ± 190	520 ± 90	2.1	0.0887 ± 0.0258	2.7 ± 1.5



R ³	R ⁴	IC ₅₀ (nM)		Selectivity	Processing IC ₅₀ (μM)	
		hFTase	GGTase-I		H-Ras	Rap1A



350 ± 170 690 ± 92 2 0.288 ± 0.251 19